

Ex LIBRIS
UNIVERSITATIS
ALBERTAENSIS



THE UNIVERSITY OF ALBERTA

ULTRA-THIN FILMS

by



HARI KRISHNA CHAURASIA

A THESIS

SUBMITTED TO THE FACULTY OF GRADUATE STUDIES AND RESEARCH
IN PARTIAL FULFILMENT OF THE REQUIREMENTS FOR THE DEGREE
OF DOCTOR OF PHILOSOPHY

DEPARTMENT OF ELECTRICAL ENGINEERING

EDMONTON, ALBERTA

FALL 1974

ABSTRACT

A quartz crystal microbalance employing a water cooled, AT-cut, 5 MHz quartz crystal in a tunnel diode oscillator circuit is used to monitor the thickness of ultra-thin ($< 50 \text{ \AA}$), highly conducting films of gold, deposited by a new technique. The oscillator frequency is stable within 5 Hz over extended periods of several hours, equivalent to an error of less than $\pm 0.25 \text{ \AA}$ from this source. Relaxation effects during post deposition crystal cooling are observed.

It is shown that the resistivity of ultra-thin ($< 50 \text{ \AA}$) films can be determined conveniently and accurately by microwave measurements. Study of the effects of annealing are also facilitated.

The phenomenon of island formation during the initial stages of film growth has so far precluded the possibility of obtaining continuous films below a thickness of about 300 \AA . By depositing on 3 to 10 \AA thick platinum nucleating layers on air cleaved mica substrates, gold films between 5 and 40 \AA thick are found highly conducting. Comparison with earlier theoretical studies indicates totally diffuse scattering at film boundaries and a surface roughness parameter of less than 3 \AA . The effect of aging on resistivity indicates low temperature interdiffusion in platinum and gold; while the effect of annealing further confirms a high degree of continuity of Au-Pt composite films. The results are interpreted to indicate substantial inhibition of island formation.

An application of gold films in mercury detection is

investigated. Optimum gold films on glass for this purpose are shown to be of pure gold evaporated by an electron beam heated source, having a thickness in the region of 100 \AA and annealed at $\sim 175^\circ\text{C}$. Such films on glass wool have a possible application in personnel protection, mercury pollution elimination, and recovery of mercury from fossil fuels. Thin films of gold on glass are shown capable of providing a method for accelerating recovery of victims of some forms of mercury poisoning.

I am indebted to Mr. A. Rutledge for his inspired support during every phase of this work but none more helpfully.

The support of the active staff of the departmental workshop under the able supervision of Mr. J. Egan and Mr. E. Leachman made a sizable proportion of this project possible. I am particularly eager to express my thanks to Messrs. G. Hill, R.B. Cook, R.W. Arnold and J. Arnold.

To Mr. C.H.B. Walker and Mr. J.M. Rutherford I am grateful for many hours of discussion and help. I am also indebted to the reviewers of our papers and one patent for learned criticisms which helped in giving a right direction to my work. I wish to express my thanks and appreciation to Mrs. R.E. Rutherford for her expert and patient typing of several manuscripts of papers as also this thesis.

I owe special thanks and gratitude to those who bravely braved the saddest life of a university professor's wife for the rather pecuniary and frustrating assistance with a graduate student; she has been an unfailing source of encouragement and moral support. Finally, I am forever in the debt of my parents whose sacrifices and generosity made me achieve all my academic ambitions.

ACKNOWLEDGMENT

I wish to thank Dr. W.A.G. Voss, my thesis supervisor and a long time friend, for his invaluable help and encouragement. The assistance of Dr. R.P.W. Lawson, Mr. R.A. Schmaus, and Mr. J.J. George is gratefully acknowledged. To Dr. E.E. Daniel and Mr. B. Munson of the Department of Pharmacology and to Dr. H.D. Baillie of the Crumpsall Hospital, Manchester, U.K. I am very thankful for guidance in the work on mercury.

I am indebted to Mr. A. Huizinga; his inspired support during every phase of this work has been immeasurably helpful .

The support of the entire staff of the departmental workshop under the able supervision of Mr. E. Buck and Mr. K. Doerrbecker made a sizable proportion of this project possible. I am particularly eager to express my thanks to Messrs. G. Fij, H.R. Gans, B.W. Arnold and P. Arnold.

To Mr. C.M.B. Walker and Mr. D.M. Kembhavi I am grateful for many hours of discussion and help. I am also indebted to the reviewers of our papers and one patent for learned criticism which helped in giving a right direction to many ideas. I wish to express my thanks and appreciation to Mrs. M.K. Munteer for her expert and patient typing of several manuscripts of papers as also this thesis.

I owe special thanks and gratitude to Meena who bravely traded the sedate life of a university professor's wife for the rather pecuniary and frustrating existence with a graduate student; she has been an unfailing source of encouragement and moral support. Finally, I am forever in the debt of my parents whose sacrifices amidst poverty made me achieve all my academic ambitions.

TABLE OF CONTENTS

CHAPTER		PAGE
I	INTRODUCTION	1
II	FILM DEPOSITION METHODS	8
	2.1 Vacuum Deposition System	8
	2.2 Planetary Target System	11
	2.3 Film Configuration	15
	2.3.1 Films for resistivity measurements. .	15
	2.3.2 Films for mercury detection	15
	2.4 Substrates	18
	2.4.1 Mica substrates for ultra-thin films.	18
	2.4.2 Glass substrates for deposition of films for mercury detection	20
	2.5 Electron Beam (e-beam) Evaporator	21
	2.6 Film Deposition Procedure	22
	2.7 Annealing	24
III	THICKNESS MONITORING WITH A QUARTZ CRYSTAL MICROBALANCE	26
	3.1 Design Considerations	26
	3.2 System Description	28
	3.3 Performance of the Thickness Monitoring System	35
	3.3.1 Charge effects	35
	3.3.2 Temperature rise due to radiation from the source	37
	3.3.3 Post deposition relaxation effects .	43
	3.4 Discussion	50

IV	MEASUREMENT OF THE RESISTIVITY OF ULTRA-THIN FILMS	52
	4.1 Introduction	52
	4.2 Experimental Results	55
	4.3 Discussion	61
V	RESISTIVITY OF GOLD FILMS ON PLATINUM NUCLEATING SURFACES	67
	5.1 Problems in the Analysis of Composite Films	67
	5.2 Results and Discussion	69
VI	EXPERIMENTS ON MERCURY DETECTION	82
	6.1 Introduction	82
	6.1.1 Environmental mercury and its effects	82
	6.1.2 Mercury detection	85
	6.2 Experimental Methods	87
	6.2.1 Films for mercury detection and the film holder	87
	6.2.2 System description	89
	6.2.3 Standard samples	95
	6.2.4 Decay of 0.1 μg Hg/5ml solution with time	96
	6.2.5 Summary of precautions	98
	6.2.6 Extraction of mercury from weak aqueous solution of HgCl_2	100
	6.3 Results	101

6.4	Discussion	107
6.4.1	Composite Au-Pt and Au-Ag films	107
6.4.1.1	Diffusion processes	108
6.4.1.2	Effects of annealing on mechanical properties of thin films	109
6.4.1.3	Effect of annealing on the sensitivity of composite films	110
6.4.1.4	Effect of annealing on the resistance of composite films	110
6.4.2	Effect of annealing on pure gold films	111
6.4.2.1	Resistance of pure gold films	111
6.4.2.2	Relative sensitivity of pure gold films	111
6.4.3	Adsorption of mercury from aqueous solutions	112
6.4.4	Gold coated glass wool	113
VII	CONCLUSION AND SUGGESTIONS FOR FURTHER WORK	114
7.1	Conclusion	114
7.2	Suggestions for further work	116
7.2.1	Work on ultra-thin films	116
7.2.2	Mercury detection experiments	118
REFERENCES	120

LIST OF TABLES

Table	Description	Page
I	Comparison of $R_S(\text{d.c.})$ and $R_S(\mu)$ of 10.8 \AA Films	79
II	Comparison of $R_S(\text{d.c.})$ and $R_S(\mu)$ of a 21.7 \AA Film; Results for Imperfect Mica Cleavages	80
III	Resistance Change of Gold Films due to Mercury Adsorption From Aqueous Solutions	101

LIST OF FIGURES

Figure		Page
2.1	Vacuum Deposition System	9,10
2.2	Design Procedure for Planetary Target System	13
2.3	Photograph of the Planetary Target System Assembly around Thickness Monitoring System, Various Masks are also shown	14
2.4	Configuration of Films for Resistivity Measurements	16
2.5(a)	Mask for Film Deposition	16
2.5(b)	Mask for D.C. Contact Deposition	16
2.6	Configuration of the Films for Mercury Detection	17
2.7	Deviation from Vertical of Evaporant Flux Beam due to Improperly Focused e-Beam	23
2.8(a)	Shape of the Melt of a Full Crucible Charge	23
2.8(b)	Shape of the Melt of a Small Crucible Charge	23
3.1	Tunnel Diode Oscillator Circuit	29
3.2	Schematic Diagram of Thickness Monitoring System	29
3.3	Circuit Diagram of Digital-to-Analog Convertor for 3-digit, 4-bit BCD Output	31
3.4	Meechum Bridge Oscillator Circuit	32
3.5	Comparison of Frequency Stabilities of	

	Tunnel Diode and Meechum Bridge Oscillator Circuits	33
3.6	Water Cooled Crystal Mount	34
3.7(a)	Photograph Showing Crystal Mounting (Vacuum Side)	36
3.7(b)	Photograph of Top-Plate Assembly showing Crystal Cooling, Oscillator Connection and other Feedthroughs	36
3.8	Capacitance Probe Arrangement for Monitoring Charge Build-up During e-Beam Evaporation	38
3.9	Charge vs. Time for Stray Electrons from e-Beam Evaporator	39
3.10	Charge vs. Time During e-Beam Evaporation of Silver	40
3.11	Charge vs. Time During e-Beam Evaporation of Gold	41
3.12	Charge vs. Time During e-Beam Evaporation of Platinum	42
3.13	Thermocouple Placement for Crystal Temperature Measurement	44
3.14	Thermocouple Voltage vs. Time During Silver Deposition	45
3.15	Thermocouple Voltage vs. Time During Gold Deposition	46
3.16	Thermocouple Voltage vs. Time During Platinum Deposition	47

3.17	Post-Deposition Crystal Frequency vs. Time	48
3.18	Crystal Frequency vs. Time for Prolonged Platinum Deposition	49
4.1	Thin Film Holder for X-Band Waveguide	54
4.2	Photograph of the Waveguide Film Holder and Short Circuit Arrangement	57
4.3	R_s vs. $R_s(\mu)$ for Gold Films on Mica	58
4.4	ρ_o/ρ_G and ρ_μ/ρ_G vs. λ	59
4.5	R_μ vs. Annealing Temperature of a Film With and Without D.C. Contacts	60
4.6	Deposition of Film on a Cleavage Step	62
4.7(a)	Inductive Iris in a Waveguide	64
4.7(b)	Capacitive Iris in a Waveguide	64
5.1	Resistivity vs. Thickness for Thick Gold Films	71
5.2	Concentration Profile with Time for a Miscible Binary Alloy System	72
5.3	$\rho_o(\text{Au-Pt})$ vs. at.%Pt	74
5.4	R_μ vs. λ for Ultra-Thin Films (Fresh and Aged)	76
5.5	Annealing Effect on R_μ of the Aged Ultra Thin Films	77
5.6	$\rho_\mu/\rho_o(\text{Au-Pt})$ and $\rho_{d.c.}/\rho_o(\text{Au-Pt})$ vs. λ	78
6.1	Film Holder for Mercury Detection	88
6.2	Photograph of the Film Holder with Mercury Detection Film and its Placement in Cell Housing	90

6.3	Schematic Diagram of Mercury Detection Apparatus	91
6.4	Bridge Circuit for Derivation of V_D vs. ΔR	93
6.5	Decay of Mercury Contents of 0.1 g.Hg/5 ml Standard with Time	97
6.6	Air-Flow Rate vs. Sensitivity of Mercury Detection	99
6.7	R and R_s vs. Thickness of Films for Mercury Detection	102
6.8(a)	Normalized Sensitivity of Composite (Au-Ag and Au-Pt) vs. Annealing Temperature	103
6.8(b)	Normalized Resistance vs. Annealing Temperature for the Composite Films	103
6.9	Normalized Sensitivity vs. Annealing Temperature of Pure Gold Films	104
6.10	Normalized Resistance vs. Annealing Temperature of Pure Gold Films	105
6.11	Sensitivity vs. Film Thickness of Gold Films Annealed at 175°C	106

CHAPTER I

INTRODUCTION

The earliest recorded work on thin films of solids dates back to Faraday's time. Chemical reaction and glow-discharge sputtering were first reported by Bunsen [1] and Grove [2], respectively, in 1852. In his 1857 paper, Faraday [3] describes explosive evaporation of wire in an inert hydrogen atmosphere for obtaining thin films of gold, platinum and other metals. Faraday, in particular, was studying the polarization of light by transmission through crystals and attempted to obtain thin, continuous and light transparent films. Nahrwold in 1887 [4] and Pohl and Pringsheim in 1912 [5] are credited, respectively, with devising and further improving vacuum evaporation techniques, which were used in the work reported by Langmuir in 1913 [6] and 1917 [7]. The above seems to be about the only significant reports till about the early thirties; the work accelerated since then and has been reviewed by Holland [8] covering the period upto 1950. An important publication in this period was that of Vand [9] who studied the effect of structure modification on the conductivity of gold films.

The significant work until the early fifties had been theoretical evaluation of size effects on electrical conductivity. Thomson in 1901 [10] predicted a decrease in conductivity in films of thicknesses comparable to the mean free path of conduction electrons. Fuchs [11] derived a more exact theoretical expression,

based on Bloch's quantum mechanical theory of conduction in metals. Further work by Sondheimer [12] led to the currently accepted Fuchs-Sondheimer theory of the size effects on electrical conductivity of thin films. In all the above theoretical work, the films are assumed to be a slice off the bulk metal with perfectly plane, parallel surfaces. In practice this is far from true. Some modifications in the theory have recently been proposed by Halpern [13] and Namba has derived a formula taking into account surface roughness [14].

Edison, at the turn of this century, was the first to predict the importance of vacuum deposition. The current and future uses of this technique have recently been discussed by Holland [15]. In particular, because of the stability and good electrical conductivity of gold, these films are suitable for many applications. Examples are the de-icing of aircraft windows [16], heat reflecting observation windows [17], eye-protection from microwave radiation [18], bolometers for low-level microwave power measurements [19], heat reflecting glass panels for energy conservation in buildings [20,21], thermoelectric power [22], solar energy conversion [23] and ultra-sensitive mercury detectors [24,25], the latter being an application investigated in this thesis.

From the economic point of view, it is important to use as thin a film of gold as is practical in all the above applications. The main problem, however, has been the agglomerate structure of films below 300 \AA . Any improvement in film texture results in a simultaneous increase in electrical conductivity, transmission in

the visible and reflection in the infrared parts of the spectrum, and, for example, microwave shielding. Thinner gold films also display higher sensitivity; that is, a larger proportional increase in resistivity upon surface adsorption of mercury [24]. This results from a larger surface-to-volume ratio of the thinner films. In this work, improved structure and internal stress relief with annealing has been found to increase the mercury detection sensitivity by as much as 300% [25].

Nucleation and growth mechanisms, and the structure of the thin films have long been studied by electron microscopy and x-ray diffraction techniques; the main disadvantages of electron microscopy being poor vacuum conditions ($\sim 10^{-5}$ torr) and the need to strip the film off the substrate [26]. X-ray diffraction methods are difficult to apply because of interference from the substrates. Recent advances in surface science have, to a great extent, obviated some of these difficulties. In situ studies under clean, ultra-high vacuum conditions ($< 10^{-9}$ torr) of the many new and old phenomena are now possible. The techniques comprise electron reflection diffraction [27-30], Auger electron spectroscopy [31-34] and x-ray and nuclear backscattering [35,36]. These features, as well as scanning electron microscope methods, have been incorporated in an integrated system recently reported [37]. Parallel theoretical work has been in progress, particularly to define the initial stages of film growth and the effect of subsequent film structure [38-50].

The understanding of the mechanisms involved in thin film growth is far from complete. Nevertheless, the dominant feature

is believed to be that of island formation during the initial stages of metal films grown on insulating substrates. This determines the subsequent film structure. The film usually grows by the interconnections of the islands as the deposit builds up. The process is called agglomeration, also known as the Volmer-Weber mechanism [44]. Thus, a film in the form of a continuous distribution of atoms is a rarity, if it occurs at all [26]. Indeed it was, at the outset of this work, considered difficult to produce continuous films below a thickness of 300 \AA , and with a mean deviation from surface smoothness of less than 50 \AA . Such films, as in Faraday's work [3], are particularly needed for optical studies [51].

The initiation of agglomeration is best indicated by the onset of electrical conductivity. This occurs at a thickness of about 50 \AA for gold deposited on mica [52]. The resistivity of the film at this thickness, however, is several orders of magnitude higher than the bulk value. Attempts at minimizing the effects of island formation have included deposition of gold on an intermediate layer of bismuth oxide [16,53] or niobium oxide [54], and sandwiching of gold film between layers of bismuth oxide [17]. All these resulted in improved electrical conductivity and light transparency of gold films on glass. The films, however, were still nonconducting below 50 \AA . With r.f. triode sputtering, conducting films of gold at 30 \AA have been recently reported [55]. This represented the state of the art at the commencement of this project.

In an earlier work by the author [56], gold films deposited on 5 to 7 \AA thick nucleating layers of silver on mica were found

highly conducting at a total (gold and silver) thickness of 32 \AA . Evidence of epitaxy was obtained for films prepared in a similar manner on air-cleaved rock-salt crystals by electron microscopy. It was concluded that nucleating layers of suitable materials, of a thickness below which island formation commences, may inhibit, if not altogether prevent, the agglomerate structure of the composite film. The method, it was believed, might enable the production of highly conducting films well below the critical 50 \AA level. This, essentially, was the one objective of the work to be reported in this thesis. The only work reported on thin films of gold of less than 50 \AA thickness has been for studying non-ohmic conduction in discontinuous films [57-61].

Platinum was chosen as a possible nucleating material [62] because of its stability and good adhesion to insulating substrates. Thick platinum and gold couples have been employed for interconnecting circuit components in microelectronics [63-65].

An all metal coating unit was designed and built for these studies. This and the deposition methods are described in the next chapter.

The methods of film thickness measurement and monitoring [66-69] have been reviewed recently [70]. Some of the methods for direct measurement or indirect monitoring of thickness are multiple-beam interferometry due to Tolansky [71-74], x-ray adsorption and interference [75], radio-active tracer technique [76], electrical resistance change [8], direct weighing [77], radio frequency method [78], and quartz crystal microbalance. The last

method is by far the most sensitive and hence applicable to thickness monitoring down to less than one angstrom. Saurbrey [79] was the first to investigate the use of a quartz crystal for microweighing and the method is discussed in detail by subsequent workers [80-82]. The linearity of a quartz crystal microbalance has been shown to be within $\pm 0.3\%$, even under heavy loading [83]. Corrections can also be made for the different densities of quartz and deposit materials, particularly for large frequency deviations of the quartz crystal [84]. The details of this method are discussed in Chapter III of this thesis.

At submicroscopic levels, all substrate surfaces exhibit irregularities compared to, or even greater than the thickness of the film ($< 50 \text{ \AA}$). The d.c. measurements, therefore, become progressively less accurate with decreasing film thickness. Microwave measurements of sheet resistance and hence the resistivity by Slater's method [85] afford the only reasonably accurate alternative [86]. The effects of reflections due to the presence of the substrate were minimized by using less than 0.001 inch thick mica sheets. In Chapters IV and V various aspects of these measurements and the suitability of mica for them are discussed.

McNerney, Buseck and Hansen [24] achieved a maximum sensitivity of 0.05 nanogram in thin gold film mercury detector. This is comparable to the sensitivity limit of any other method [87]. They also found that the sensitivity increases with decreasing film thickness. With a view of achieving a possibly lower detection limit, the ultra-thin, highly conducting gold-platinum films on glass were investigated in a system similar to that of McNerney et al. However,

it was found that alloying of gold with chromium [24], platinum and silver [25], and perhaps other metals, owing to interfusion with aging or annealing, results in a drastic loss of sensitivity. The optimum thickness of e-beam evaporated, pure gold films on glass has been found to be in the region of 100 \AA with an optimum annealing temperature around 175°C [25]. The method of degree of resistance increase on mercury surface adsorption has been discussed as a possible tool for studying annealing kinetics of diffusion in thin-film couples of gold with other metals. It has also been observed to indicate surface sensitization and stress patterns with annealing. These topics form the subject matter of Chapter VI.

In the conclusion, Chapter VII, the results of this research are summarized. The main importance is then given to discussing areas for further research to enable better understanding of the various aspects of the phenomena observed and application of the findings. It was noted, for example, that glass wool coated with gold [88] was far more effective than the lead-chloride on glass wool used by McNerney et al. [24]. It can also be recycled by a simple process of heating in air at about 175°C . This suggests its possible use in safeguarding personnel working in a mercury laden atmosphere and removal and recovery of mercury generated by fossil fuel burning power stations. Thin films of gold on glass have been found to adsorb mercury from weak aqueous solutions of inorganic compounds of mercury. It may be possible to use this effect for speeding up the recovery of the victims of mercury poisoning by removal of mercury from the bloodstream in a manner somewhat similar to that of kidney machines.

CHAPTER II

FILM DEPOSITION METHODS

2.1 Vacuum Deposition System

An all metal (304 series stainless steel) unit was designed and built. The system, shown in Fig. 2.1, employs a 2" (150 l/s) diffusion pump with a liquid nitrogen cold trap and a 140 l/s ion pump. The chamber is rough pumped through the diffusion pump, the latter being switched on when adequate backing pressure ($\sim 50 \times 10^{-3}$ torr) has been reached. This method eliminates the need for a bakeable valve and pirani gauge as in a more conventional roughing line. Valve HV-2 between the cold trap and the main chamber can also be omitted to effect further economy since bakeable valves are the most expensive items in a vacuum system. The disadvantage is that the diffusion pump must be allowed to cool down and emptied of liquid nitrogen before admitting air into the chamber. Another difficulty is in the calibration of the ionization gauge; however, an exact measurement of the chamber pressure is not required. The ion pump also gives a reasonable estimate of the chamber pressure.

With this system, pressures below 10^{-9} torr were achieved after a 72 hour bakeout at 250°C. The excessive outgassing during evaporation, however, caused a rise in pressure up to 5×10^{-6} torr. This indicates the need for higher pumping speeds for work in the ultra-high vacuum range. A pumping speed of 500 l/s at the chamber

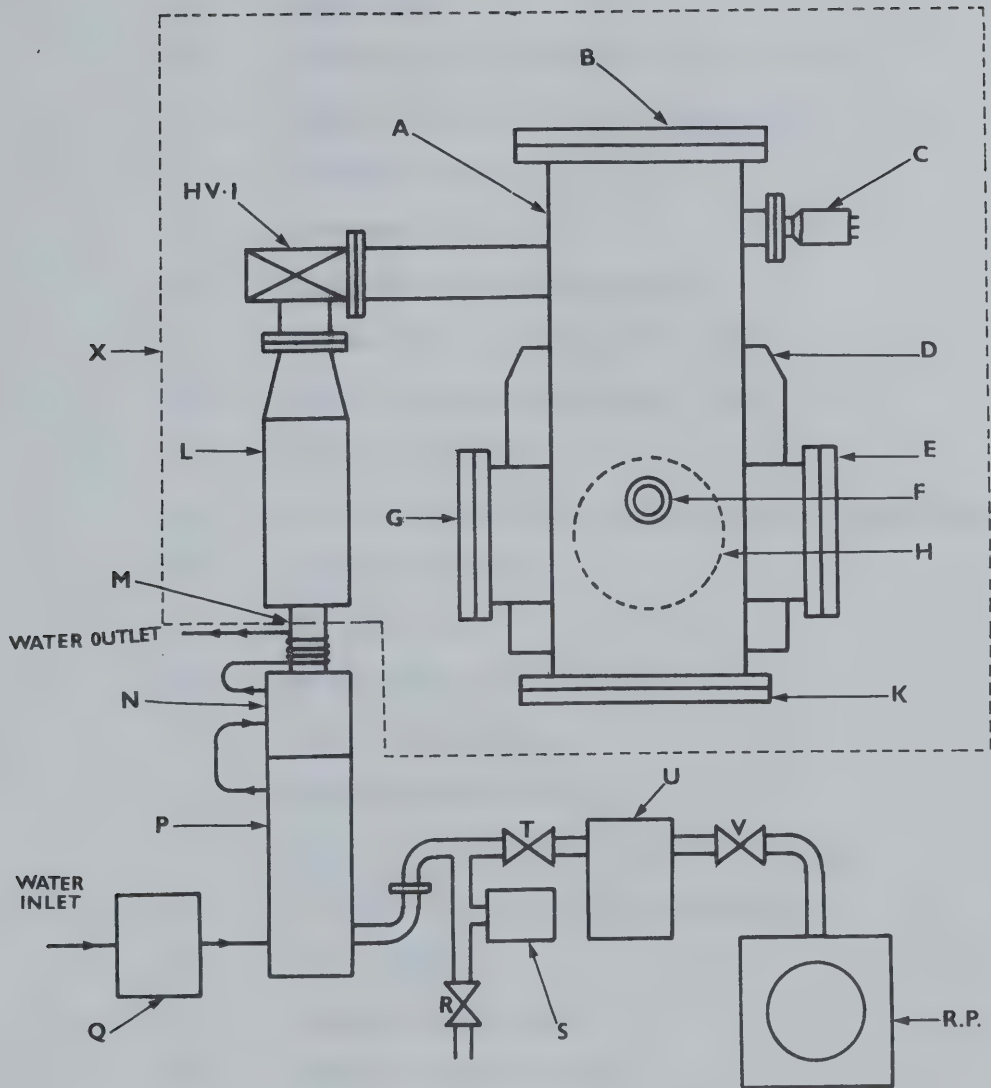


FIGURE 2.1: Vacuum Deposition System.

FIG. 2.1. Description of Notations:

A	Main Chamber
B	Top plate (for substrate holders, Quartz crystal mount, electrical feedthroughs)
C	Ionization gauge
D	Ion pump (140 l./s)
E	Electron-beam evaporator port
F	View-port for crucible positioning
G	Port for shutter and variable leak
H	Port for ion-pump
K	Port for rotary shutter and electrical feedthroughs
HV1	Bakeable UHV valve
L	LN ₂ cold trap
M	Water cooled separator tube
N	Water cooled baffle
P	Diffusion pump (150 l./s)
Q	Water pressure switch for diffusion pump
R	Air inlet valve and leak detection port
S	Pirani gauge
T,V	Roughing line valves
U	Molecular sieve oil trap
W	Rotary pump (150 l./min.)
X	Baking oven; controls and heaters not shown
R.P.	Rotary Vacuum Pump.

input port has been reported for work with an electron beam evaporator [89]. Without baking, the minimum pressure achieved was $\sim 2 \times 10^{-8}$ torr.

It has been found that a gold film coated on stainless steel eliminated adsorption and desorption of CO, CO₂ and sulphur gases from the surface [90]. Therefore a chimney over the evaporation source was not used. It was also noticed that platinum showed gettering action and improved the vacuum.

Another feature of the system is the leak-detector port. This is also connected through the diffusion pump, thus passing the entire amount of tracer gas (helium) to the leak detector. The leak-detection sensitivity is increased substantially by this technique.

2.2 Planetary Target System

The evaporation source employed was a 3 kW, three crucible electron beam evaporator. The beam was bent at an angle of 270° to avoid filament contamination of the substrates. The distribution characteristic of the deposit from such a source approaches cosine law at low evaporation rates [89], and is given by [91]

$$x \propto \frac{\cos \phi \cos \theta}{r^2} \quad 2.1$$

where x is the deposit thickness, ϕ is the angle from the vertical to the source-to-substrate direction, θ is the angle of incidence of

the beam from normal to the substrate, and r is the source to substrate distance. This law was used to design an 8 target planetary system around the axially positioned thickness monitoring quartz crystal. The design procedure is illustrated in Fig. 2.2 where $r = 16"$ and $\phi = 8^\circ$. θ is made equal to zero by tilting the substrate holder by 8° . Equation 2.1 then becomes

$$\lambda \propto \frac{0.99026}{r^2} .$$

The 0.974% decrease in λ was eliminated by making the source to substrate distance 15.85" as compared to the 16" source monitoring crystal distance. The inner and outer edges of the required deposition area are 1" apart, subtending a 3.7° angle at the source. The theoretical decrease in λ from the inner to the outer edges is less than 0.9% (Eq. 2.1). The inclination of the substrate to the horizontal was increased to 9° , making $\theta = 1^\circ$, or $\cos\theta \approx 1$. This brings the outer edge nearer to the source and reduces variation of λ over the substrate. The substrate holder angle from the horizontal can be adjusted between 7.5° and 30° .

The top plate assembly, with the targets and thickness monitoring crystal in position, is shown in Fig. 2.3. Provision was also made for installing a rotary shutter arrangement to permit selection of any one of the eight targets at a time.

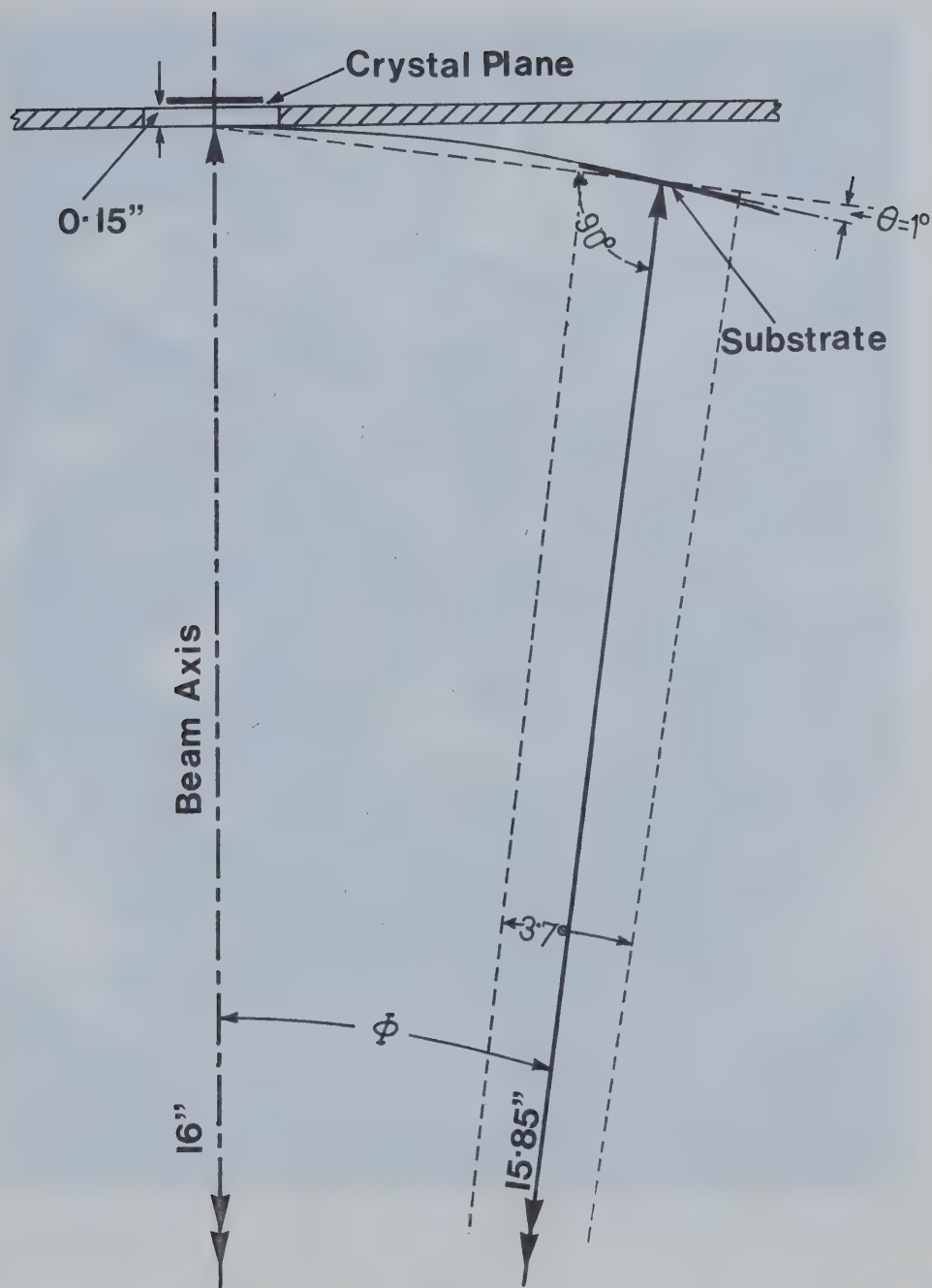


FIGURE 2.2: Design Procedure for the Planetary Target System.

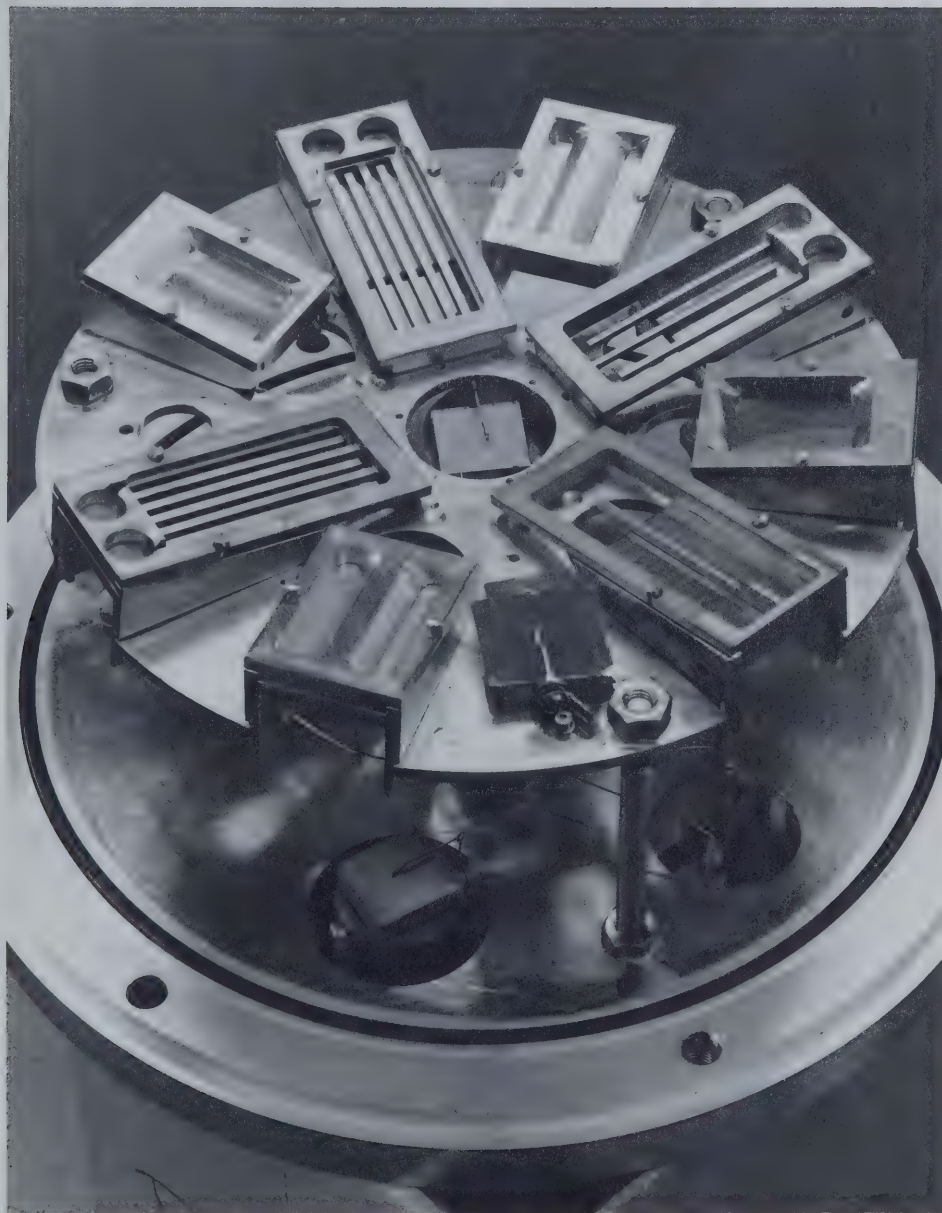


FIGURE 2.3: Planetary Target System Assembly around Thickness Monitoring Crystal. Various Masks are also shown.

2.3 Film Configurations

2.3.1 Films for resistivity measurements

The shape and size of these films (Fig. 2.4) was chosen to permit simultaneous d.c. and microwave measurements of sheet resistance. Standard X-band rectangular waveguide has inside dimensions of 0.4" x 0.9"; the film size was chosen to be 0.5" x 1.0" to cover this area fully between the d.c. contacts B. This geometry gives two squares in parallel such that the film sheet resistance at d.c., R_0 in Ω/\square , is twice the resistance ϕ measured between B. The film, A, is deposited with masks shown in Fig. 2.5(a). The contact masks, Fig. 2.5(b), were placed subsequently for depositing heavier ($\sim 5000 \text{ \AA}$) silver contacts plated with about 500 \AA thick gold layer for protection against tarnishing. Resistance heated sources (tungsten boats) in a separate coating unit were used for contact deposition.

2.3.2 Films for mercury detection

The geometry of these films is shown in Fig. 2.6. The films (gold, gold-on platinum and gold-on silver) were deposited on 1" x 2 3/4" microscope slides. The variation of λ across the length of the film, calculated from Eq. 2.1, is about 1.8%. Four such films can be coated in one cycle; the other four substrates were coated for films on glass in the configuration shown in Fig. 2.4. These were used to obtain the sheet resistance of the films. All four masks were individually machined resulting in a

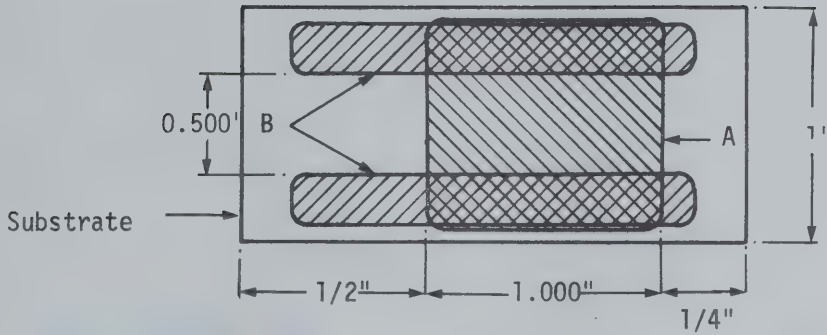


FIGURE 2.4: Configuration of Films for Resistivity Measurements

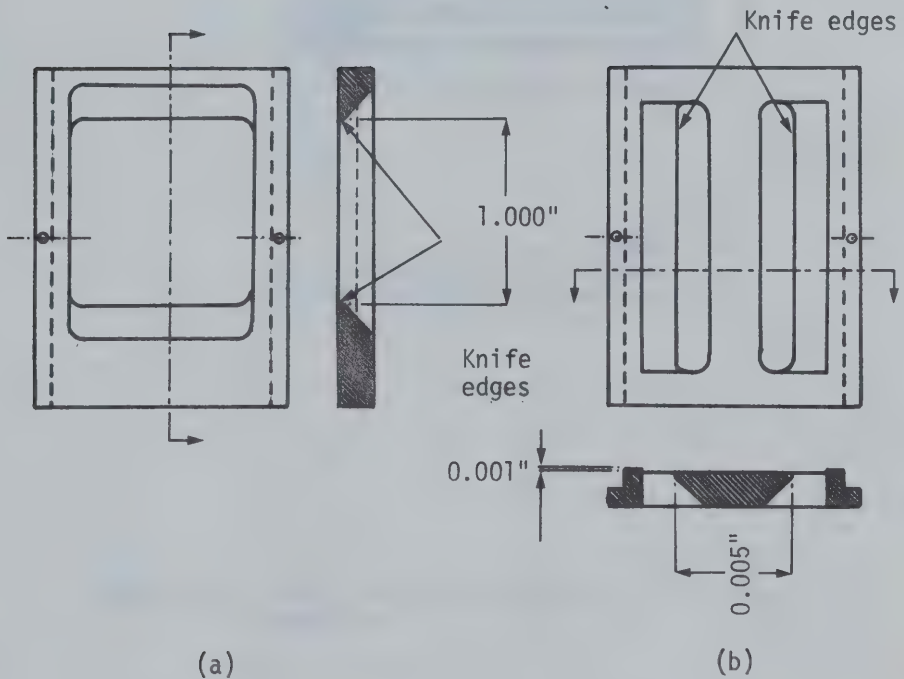


FIGURE 2.5: (a) Mask for Film Deposition, (b) Mask for D.C. Contact Deposition.

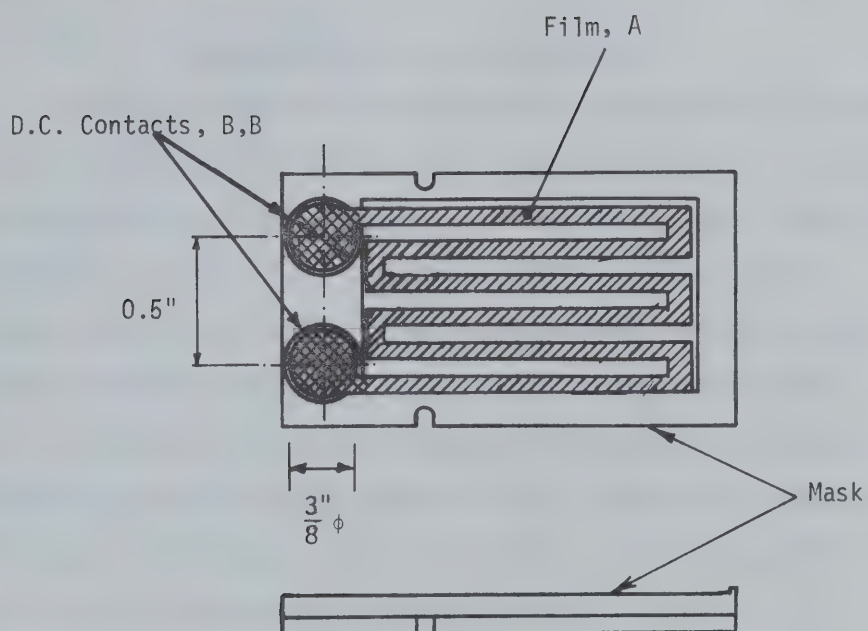


FIGURE 2.6: Configuration of the Films for Mercury Detection.

5% variation in the resistance among the films. The contacts, B, B, were deposited by masking the remainder of the film. As in section 2.3.1, a separate coating unit was used.

2.4 Substrates

2.4.1 Mica substrates for ultra-thin films

Muscovite (ruby) mica was chosen as a substrate for microwave and d.c. measurements of sheet resistance. At microwave frequencies mica is one of the best dielectrics; at 10 GHz it has a dielectric constant of 5.4 and a loss tangent of 0.0003. It can also be cleaved into extremely thin sheets (a few microns thick) and thus creates negligible reflections in a waveguide measuring system.

Chemically, mica is hydrated potassium-aluminum silicate, $\text{H}_2\text{KA}l_3(\text{SiO}_4)$, and by weight contains 45.5% silica, 37.5% alumina, 12% potash, and 5% water of crystallization. The cleavage faces have a {111} crystallographic orientation [92].

Mica was obtained in the form of random sized plates (as supplied by ACIM Industries, Hull, Que., Canada) from which visually flat, defect free pieces were selected. One inch wide and three to four inches long strips were cut from these pieces. Sheets as thin as 0.5 mm were obtained by inserting a fine blade into the edge and then pulling the sheets apart. Further cleaving was done by cutting a line of appropriate depth across the width. On bending along the line, the sheets separated and were then carefully pulled apart. The final required thickness of the substrate was ~ 0.01 mm.

It is important to follow crystal cleaving rules suggested by Gilman [93] in order to obtain a defect free substrate. The rules require the crystal to be cleaved in exact halves with a critical velocity of travel of the cleavage crack. This velocity is a function of the binding energies of the crystal. A deviation from these parameters enhances generation of cleavage steps, dislocations and other surface defects.

Since d.c. measurements of sheet resistance were also planned and the films were too thin to permit this measurement by the four probe method [94], clear and defect free substrates were required. On the other hand, microwave measurements demand the thinnest possible sheets to minimize reflection errors due to the presence of the substrates. These two requirements, for obtaining suitable sheets, were sources of the most difficult and time consuming part of the whole project. The procedure adopted to obtain such a substrate is as follows: the pair of sheets resulting from the final cleavage operation were examined visually by holding them side by side against light. By moving these laterally, gross cleavage steps in the form of hair-line scratches become visible as a result of a diffraction grating effect. If identical defects showed up in the two sheets, particularly over the desired 1" x 1/2" area, the sheets were discarded. Otherwise the two freshly cleaved surfaces were selected for film deposition. On an average it took over 25 attempts to obtain one such pair of substrates.

Although the cleanest substrates are obtained by cleaving inside ultra-high vacuum, the above properties make air cleaving the only alternative. Poppa and Elliot [95] have shown that minute

traces of carbon form the only detectable contaminant of air-cleaved mica surfaces; this is probably due to catalytic reduction of carbonaceous gases and compounds in the presence of humidity. The carbon traces can be removed by heating the mica to 550°C in an oxygen atmosphere of 10^{-5} torr partial pressure for about an hour. This procedure, however, also causes the depletion of potassium atoms on the surface [95] by decomposition. The ionic and structural properties of the surface, therefore, change materially. Cleavage of mica (and NaCl as well) in vacuum is known to leave microscopic dust particles on the surface which cannot be removed. The dust particles may act as preferred nucleating centers [96] or leave pin-holes in the film. Some degree of surface contamination is therefore unavoidable.

2.4.2 Glass substrate for deposition of films for mercury detection

One inch wide microscope glass slides, supplied pre-cleaned (Fisher Scientific Co.), were cut to the required lengths, that is, 1 3/4 inches and 2 3/4 inches respectively for resistivity measurements and mercury detection. These were then further cleaned by the following procedure: Gross contaminants were first removed by washing with domestic liquid soap. The slides were then cleaned in an ultrasonically agitated laboratory detergent solution ("Sparkleen", Fisher Scientific Co.) in lukewarm water for about 15 minutes. These were then thoroughly rinsed in de-ionized distilled water and dried by blowing away the water by air under pressure.

It is important that water droplets should not be permitted to dry on the glass surface [21]. The dried slides were subjected to vapor degreasing in repeatedly distilled acetone and were stored immersed in acetone until required for use. Prior to mounting these slides on the substrate holders, they were dried by evaporating the acetone with nitrogen.

The above cleaning procedure is considered adequate for thin film and micro-electronics applications [96,97].

2.5 Electron Beam (e-beam) Evaporator

Electron beam evaporation is the best known method for obtaining films of the highest purity since source contamination is eliminated. The various aspects of e-beam evaporation have been discussed [89,98-101]. The stray electrons from the cathode charge up the substrates. Evaporated metal atoms, on the other hand, are positively charged and therefore are accelerated towards the substrate. This causes sputtering in some cases [99]. The evaporant atoms may also penetrate the substrate, replacing some surface atoms. These atoms have an anchoring effect on the subsequently deposited film. This phenomenon may account for good adhesion of e-beam deposited gold films [102]. The ion effects are especially pronounced in the evaporation of refractory metals melting above a temperature of 1500°C [100]. The influence of this phenomenon and that of heat radiation from the source on film thickness monitoring are investigated in the next chapter.

The focusing of the electron beam on the crucible needed to be adjusted accurately. As the charge in the crucible melts, it tends to form into a ball. If the beam is focused off-center, the evaporant flux beam is skewed, resulting in deterioration of deposit uniformity. This is illustrated in Fig. 2.7. The e-beam control unit permits 1/8 inch manual scan of the beam. Larger focusing adjustment is made by adjusting the air gap between a permanent magnet and pole-pieces. The procedure adopted in this work was to scan the beam to obtain a maximum deposition rate for some predetermined beam current. During deposition, the beam is continuously moved a small amount above and below this critical point. Compensation for any error in initial beam adjustment is thus obtained. The crucible charge was also kept close to the full capacity of the crucible. It can be seen from Fig. 2.8(a) that a large melt has a relatively flat surface. The smaller charge shown in Fig. 2.8(b) tends to be progressively more spherical in shape. This results in a larger deviation of the evaporant flux beam from the vertical if the e-beam is not focused exactly on the top. In the case of the mechanical crucible adjustment, the beam is centered by visual inspection. This should be done as quickly as possible to avoid x-ray emission hazard, particularly from higher melting point evaporants like platinum [97].

2.6 Film Deposition Procedure

The films, both on mica and glass, were evaporated at a beam

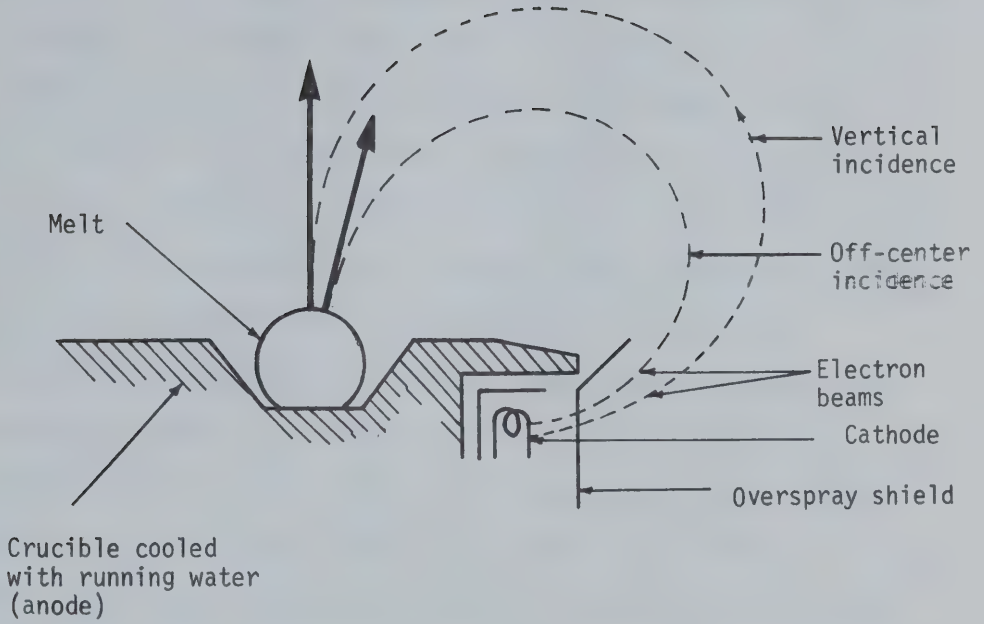


FIGURE 2.7: Effect of e-beam Incidence on the Beam Direction.

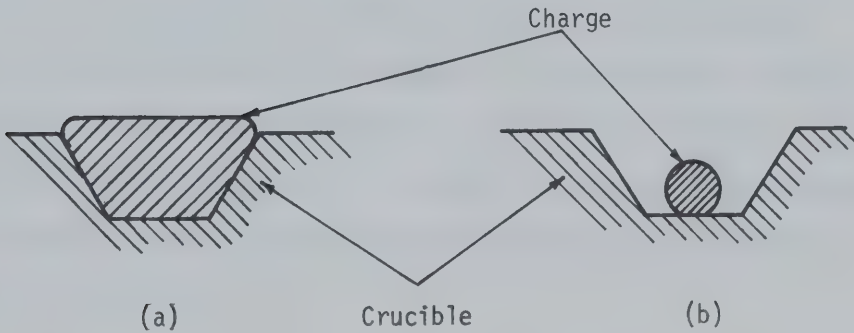


FIGURE 2.8: Melt Shapes of (a) Large and (b) Small Charges.

current of between 130 and 150 mA, corresponding to 0.52 to 0.6 kilowatt. The evaporating spot size appeared to be nearly 1 to 2 mm in diameter. The shutter was kept over the source until evaporation commenced and had continued a few seconds. This eliminated any surface impurities on the melt from reaching the substrates, particularly from metals which have oxide formed on the surface. The evaporation rate rose very rapidly immediately after the evaporation commenced. Exact adjustment of the rate of deposition was, therefore, difficult. The deposition rate on the monitoring crystal at a distance of 40.6 cm from the source was between 0.5 to 1.5 $\text{\AA}/\text{sec}$ within the e-beam current limits stated above for all the metals used (gold, silver, and platinum). Approximate deposit time was estimated from these values and the difference between steady-state pre- and post-deposition frequencies of the monitoring crystal was used to compute film thickness. It is apparent that very precise control of either the film thickness or the rate of deposition is almost impossible as the required deposition is completed within seconds. In the particular case of platinum, the source temperature is in the region of 4000°C. The thermal shock effect, discussed in detail in the next chapter, makes the crystal frequency scintillate erratically during the initial stages of deposition.

2.7 Annealing

The films were studied for the effects of annealing on

resistivity and also the mercury detection. Adjustable stainless steel holders were made with a capacity of 50 samples for both 2 3/4" and 1 3/4" long substrates. After placing the film bearing substrates in the holders, the latter were wrapped in aluminum foil to avoid dust contamination. However, problem was encountered in annealing films for mercury detection as the mercury evolved was unable to escape through the aluminum foil and recondensed on the films, thus affecting their sensitivity. Films for mercury detection were, therefore, annealed without wrapping the holder in aluminum foil.

An air circulating oven (Delta Design Model MK6300), with a rated temperature stability of within $\pm 2^{\circ}\text{C}$ of the final temperature, was used. The average heating rate was nearly $3^{\circ}\text{C}/\text{min}$. In order to affect complete diffusion, as discussed in Chapters V and VI, the films were maintained at the desired temperature for about two hours. The oven was then allowed to cool down to room temperature before removing the films for testing. Each annealing cycle was repeated at a temperature difference of 25°C . This process is generally referred to as "pulse annealing"[103].

CHAPTER III

THICKNESS MONITORING WITH A QUARTZ CRYSTAL MICROBALANCE

3.1 Design Considerations

The quartz crystal plates cut for operating in the thickness shear modes are suitable for thickness monitoring. Of the two such cuts, AT and BT, the AT cut has superior frequency stability with temperature change and mass sensitivity. The nomenclature refers to the orientation of the plates with respect to the crystallographic axes. According to IRE standards [104] an AT cut is $YX\ell + 35^\circ$. This means the plate has one X-axis and an orthogonal Y' axis in its plane; the Y' axis is rotated about the crystallographic Y axis by an angle $\phi = 35^\circ$. The exact choice of the value of ϕ depends on the operating temperature at which a zero-temperature coefficient of frequency is desired. Thus, at a room temperature of 22.5°C and $\phi \sim 35^\circ 8'$ [83], the frequency stability of AT cut crystals is within 1 part in 10^6 between -20 and 60°C .

The frequency thickness constant of an AT cut plate is given by $fxt = 1670 = K$ [105], where f is the crystal frequency in KHz and t is the thickness of the plate. The frequency shift, Δf , as a result of mass Δm deposited over an area A is given by [81] $\Delta f/f = -\Delta m/\rho_q t$, where ρ_q is the density of quartz. In terms of the thickness, ℓ , the uniformly deposited mass Δm of density ρ_f is $\Delta m = \rho_f \ell A$. The frequency shift Δf is then given by

$$\Delta f = -\frac{\Delta m}{A} \times \frac{f^2}{K\rho_q} = -C_f \frac{\Delta m}{A} = -C_f \rho_f \ell \quad 3.1$$

where $C_f = f^2/K\rho_q$ is in $\text{Hz}\cdot\text{cm}^2/\text{unit mass}$. The value of C_f is thus a function of the crystal constants alone. Also, $\Delta f/\ell$ is a constant dependent on the deposit material and is given by

$$\frac{\Delta f}{\ell} = -C_f \rho_f \quad 3.2$$

The equation indicates that the thickness might be determined without knowing the area A . However, it has been shown [81,106] that if the exposed area is much less than the active area of the plate, a second order correction would be required. In the present work, the contact on the top plate shadowed less than 2% area of the crystal and hence Eq. 3.2 was used.

The theoretical value of C_f for a 5 MHz AT-cut plate is $57.6 \text{ Hz}\cdot\text{cm}^2/\mu\text{gm}$ [81]. Eschbach and Kruidhof [107] found an experimental value of $C_f = 57.8 \text{ Hz}\cdot\text{cm}^2/\mu\text{gm}$. Their calibration was carried out by making the quartz-crystal and oscillator circuit part of a vacuum microbalance. Both the mass deposited and the frequency shift were measured simultaneously. In a less rigorous experiment[56] the crystals were weighed in air after noting the frequency shift in vacuum. The value of C_f obtained was $56.2 \text{ Hz}\cdot\text{cm}^2/\mu\text{gm}$. The results demonstrate the validity of the theoretical value of C_f and this was used in this work.

From Eq. 3.2, $\Delta f/\ell$ values for gold, silver, and platinum are, respectively, 11.128, 6.048 and $12.355 \text{ Hz}/\text{\AA}$. These correspond to bulk density values of 19.32, 10.5 and 21.45 for gold, silver and platinum respectively.

The above values of $(\Delta f/l)$ are valid for a maximum frequency shift, Δf , of 2%. In this work, the crystals were changed after a 50 KHz frequency decrease for 5 MHz crystal. The crystals can be used again by dissolving the deposited material in aqua regia and then depositing contacts by vacuum evaporation of gold.

Another factor affecting the accuracy of thickness measurements is the temperature stability of the crystal. A crystal mount cooled by running water was found to give a long term frequency stability within ± 2.5 Hz.

3.2 System Description

Figure 3.2 shows the schematic of the system for thickness monitoring. The crystals used were 5 MHz, 3/4" square and 0.5 mm thick AT-cut plates with $\phi = 35^\circ 13' \pm 2'$ (Sloan Technology Corporation). The oscillator used a tunnel diode circuit [108,109]. This circuit, Fig. 3.1, has the advantage of operating only in the series resonant mode of the crystal. Because of the high Q of the crystal, of the order of 10^6 , the crystal presents a near short circuit at this frequency. The impedance is very high at other frequencies and oscillations cannot occur. The oscillator is direct coupled to the buffer amplifier. The output of this stage was approximately 1.5v peak-to-peak and sufficient to drive a digital frequency counter (Beckman Model 6148 EPUT-TIMER). The three digit, four bit binary-coded decimal output was converted

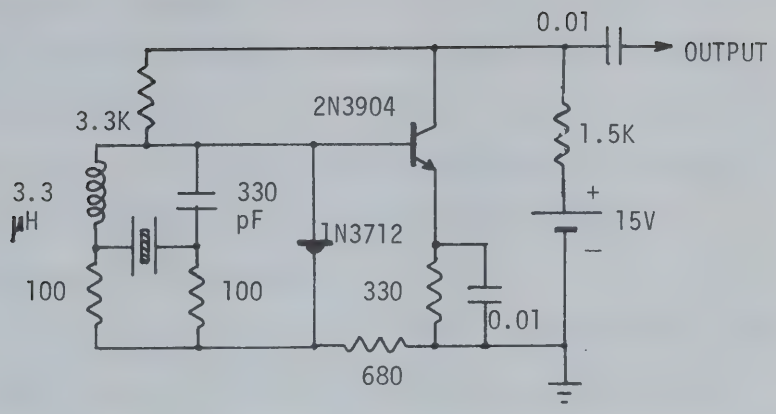


FIGURE 3.1: Tunnel Diode Oscillator Circuit.

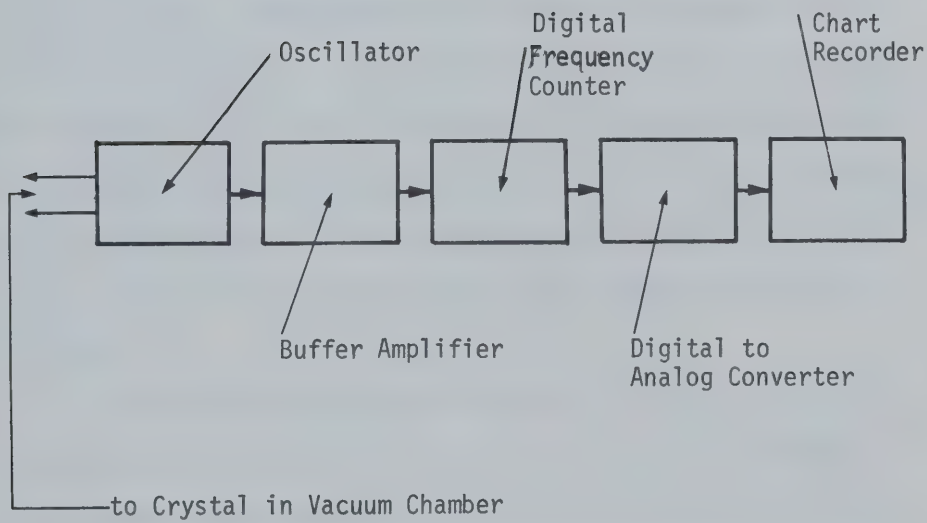
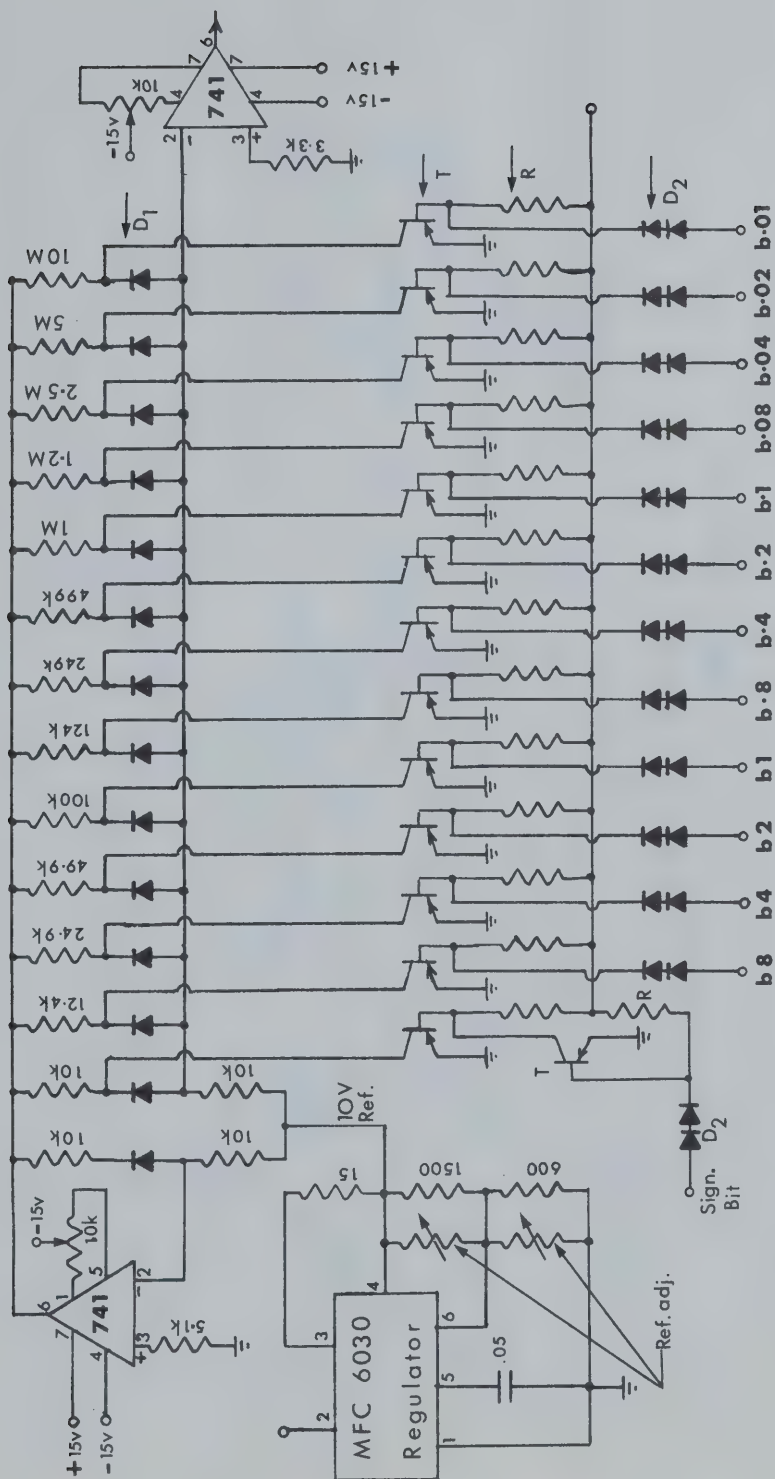


FIGURE 3.2: Schematic Diagram of Thickness Monitoring System.

to analog output by a digital to analog converter shown in Fig. 3.3. This enabled a continuous record of the crystal frequency on a strip-chart recorder to be obtained. The counter gate period used was either 1 or 10 seconds and the markings on the recorder were used for determining accurate time versus frequency characteristics of the oscillator.

The oscillator stability was tested in comparison to the Meacham Bridge circuit [110] shown in Fig. 3.4. The frequency deviation of the two oscillators in response to the air-conditioner cycle in the laboratory are shown in Fig. 3.5. It can be seen that while the tunnel diode oscillator frequency drifted by about 10 Hz, corresponding drift in the Meacham Bridge oscillator case was over 120 Hz. The steady state frequency of the tunnel diode oscillator was within ± 1 Hz whereas that of the other circuit was within about ± 10 Hz. Water cooling of the crystal mount was used during these tests. With improved air conditioning, the frequency of the tunnel diode oscillator was within 5 Hz over a 12 hour test period. This amounts to less than $\pm 0.25 \text{ \AA}$ error for gold or platinum.

The method of mounting the crystal is shown in Fig. 3.6. This incorporated an improved design of a bakeable, ultra-high vacuum, water-cooled crystal mount. As against the conventional system employing a mount located on water carrying copper tubes, the cooling water flows directly on the copper block on the atmosphere side. In the vacuum, a 0.01 mm thick mica sheet insulated the crystal electrically from ground and at the same time



T - 2N5087; R - 15K;
 D₁ - 1N3064; D₂ - 1N4454

FIGURE 3.3: Circuit Diagram of Digital-to-Analog Converter for 3-Digit, 4-bit BCD Output.

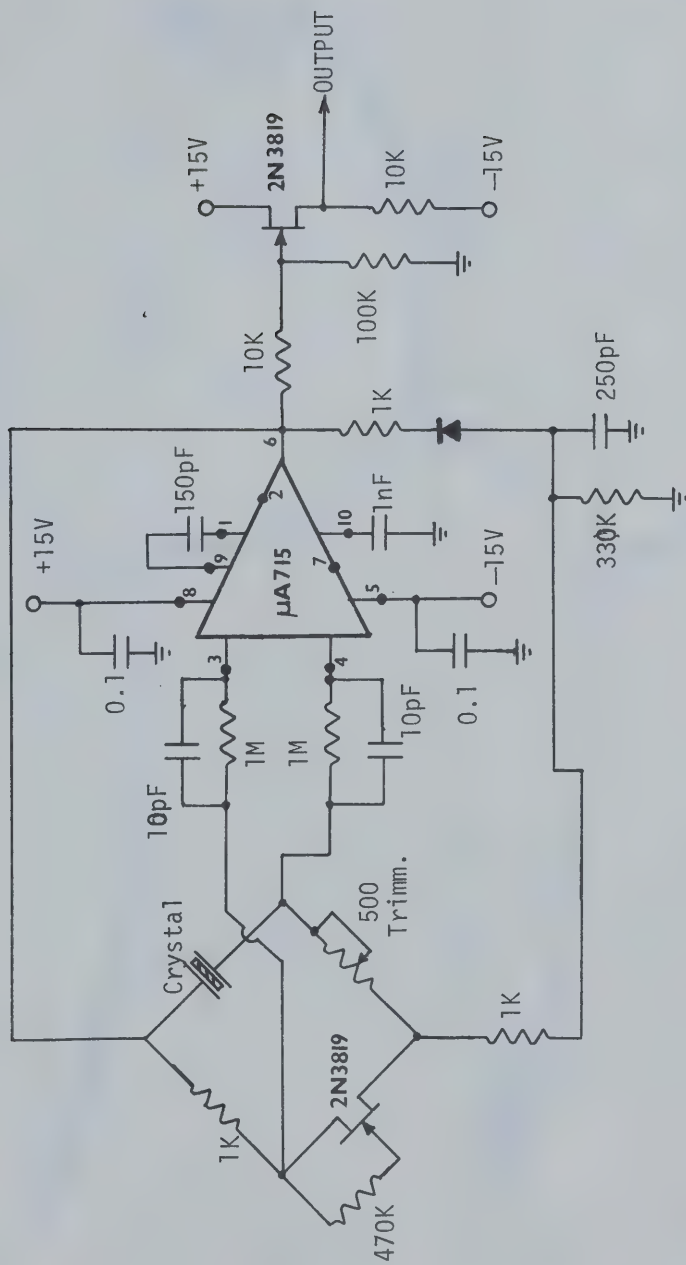


FIGURE 3.4: Meechum Bridge Oscillator

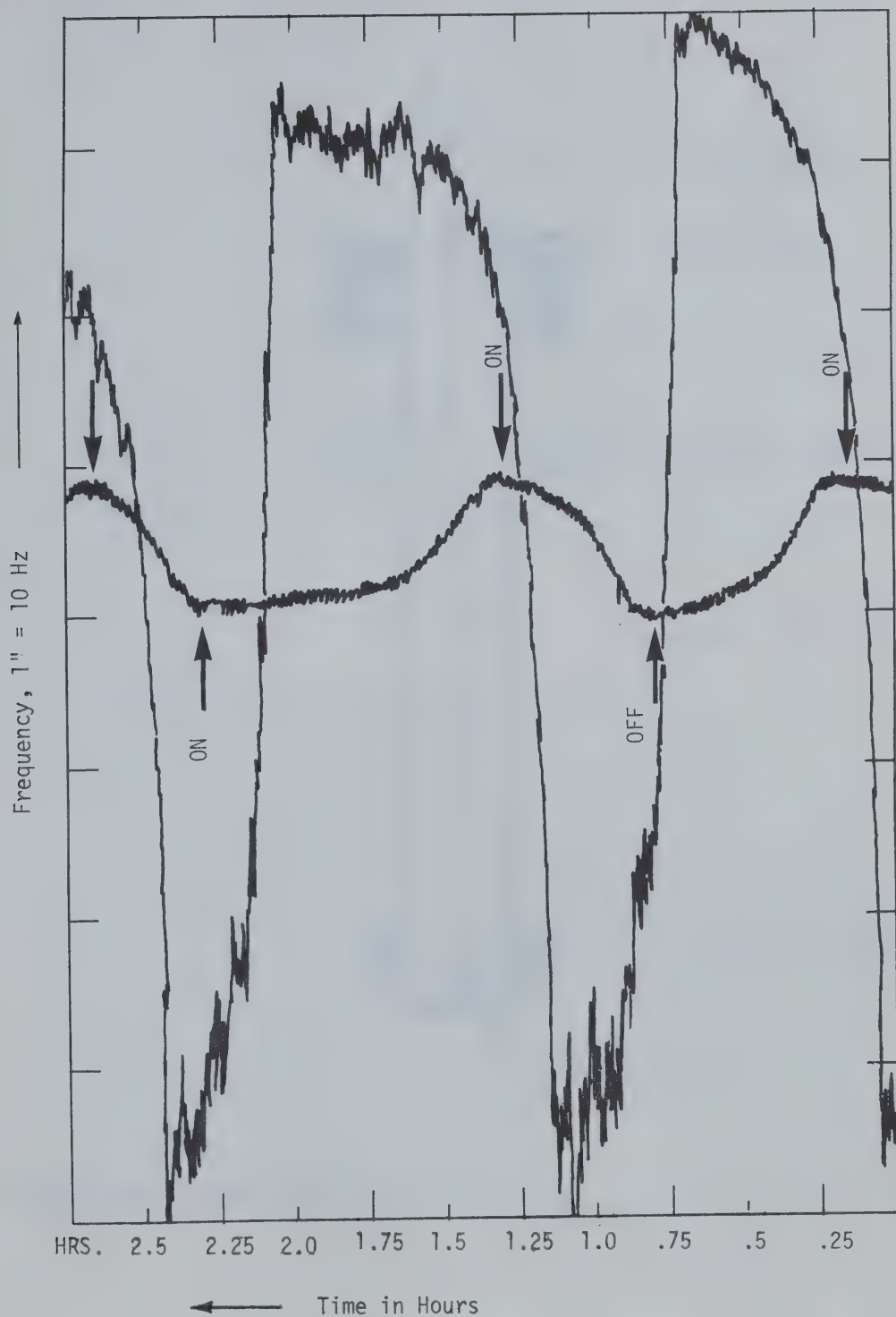


FIGURE 3.5: Comparison of Frequency Stabilities of Tunnel Diode and Meechum Bridge Oscillator Circuits. Thick arrows indicate Booster fan condition.

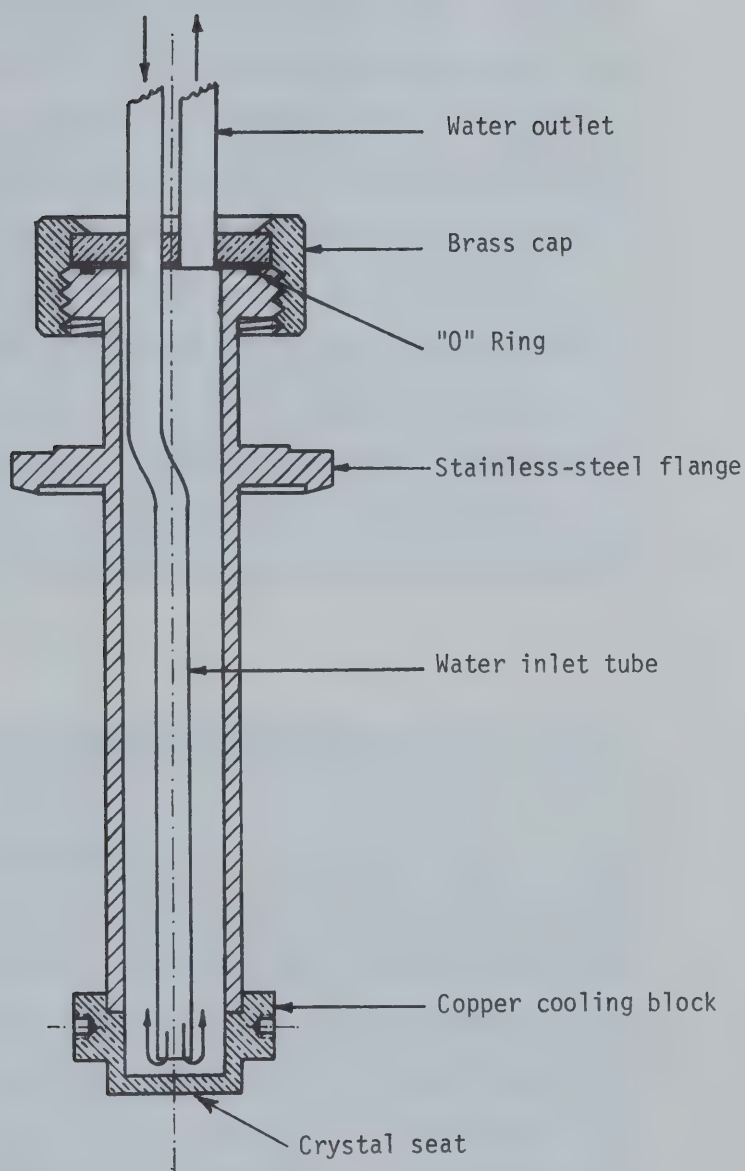


FIGURE 3.6: Water Cooled Crystal Mount.

provided a good thermal contact with the cooling block. A vacuum evaporated $\sim 5000 \text{ \AA}$ thick silver film with $\sim 200 \text{ \AA}$ thick protective gold layer on the above mica sheet provided electrical contact with the cooled side of the crystal. The contact on the exposed side was made by a 0.024 inch diameter spring. The spring shadowed an area of nearly 0.011 sq. inch, or less than 2% of the total area of the crystal. Teflon screws supported the spring and the connection to the gold-plated silver film on mica, to the copper block. Teflon insulated wire was used for bringing the crystal connections out of the vacuum through a dual-coaxial feedthrough. A photograph of the mounting is shown in Fig. 3.7(a) for the vacuum side and Fig. 3.7(b) with the crystal oscillator for the atmosphere side.

3.3 Performance of the Thickness Monitoring System

3.3.1 Charge effects

According to the specifications of the e-beam evaporator (Thermionics Lab., Model No. 100-0031), 98% of the electrons emitted by the cathode are focused on the crucible. Some fraction of the remaining 2% stray electrons accumulate over the crystal and substrates. The frequency of the oscillator was observed to decrease slightly when the e-beam was switched on, with the shutter in place between the source and the crystal.

The evaporant particle flux from the e-beam heated source is known to consist of positive ions [98]. The ions build up a



FIGURE 3.7(a): Crystal Mounting.

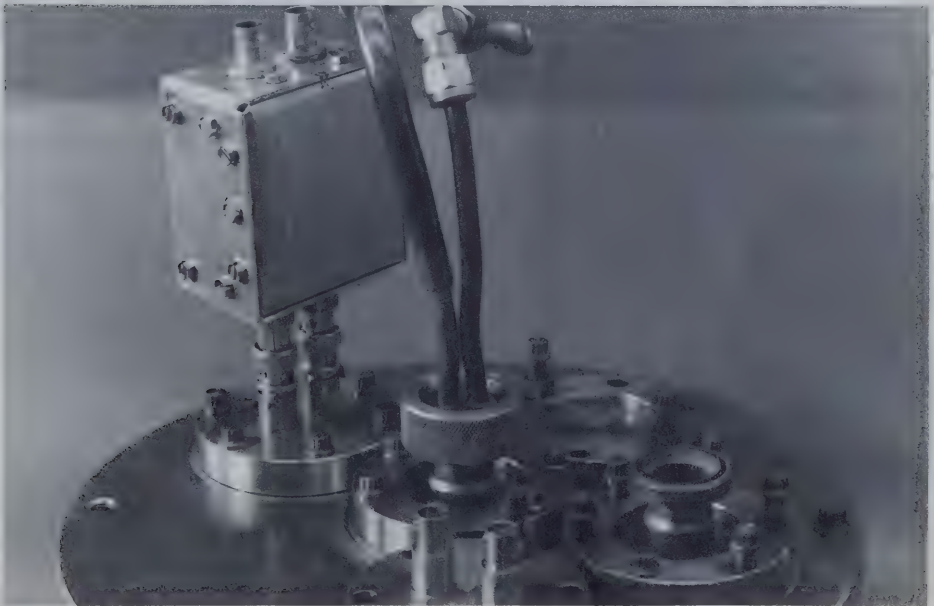


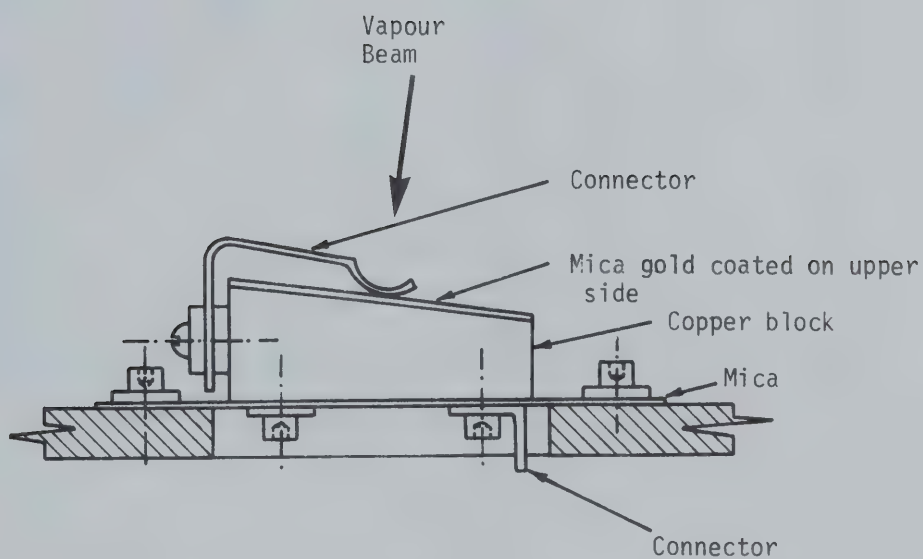
FIGURE 3.7(b): Top Plate Assembly showing Crystal Cooling, Oscillator Connection and other Feedthroughs.

net positive charge on the crystal and tend to change the bias of the tunnel diode. Pronounced oscillator instabilities were noted during deposition, especially in the case of platinum evaporation. The charge effects thus made it mandatory to allow the frequency to stabilize before taking the final frequency value.

A capacitance arrangement, shown in Fig. 3.8, was used to monitor the charge effects. The assembly is placed near the substrates at the same angle of inclination to the horizontal, that is 9° . It consists of a 0.75 inch square copper block forming one plate of the capacitor. A mica sheet coated with gold on one side formed the other plate as well as the insulation. The capacitor output was taken through the top plate by means of dual coaxial feedthroughs. The voltage was measured with a d.c. zero-center vacuum tube voltmeter, and recorded against time on a strip-chart recorder. An empty crucible was used to monitor charge build up due to stray electrons. The charge flux carried by the evaporants (gold, platinum and silver) was also monitored. The beam current in both cases was kept near 130 mA. The results are shown in Figs. 3.9 to 3.12.

3.3.2 Temperature rise due to heat radiation from the source

The crystal temperature rises owing both to the radiation from the source and the heat of condensation of the evaporant. The source temperature reaches a value as high as 4000°C during evaporation of platinum. The sensor face of the crystal thus rises in temperature while the other side is held at the temperature of



Measured probe capacitance = 80 pF.

FIGURE 3.8: Capacitance Probe Arrangement for Monitoring Charge Build-up During e-Beam Evaporation.

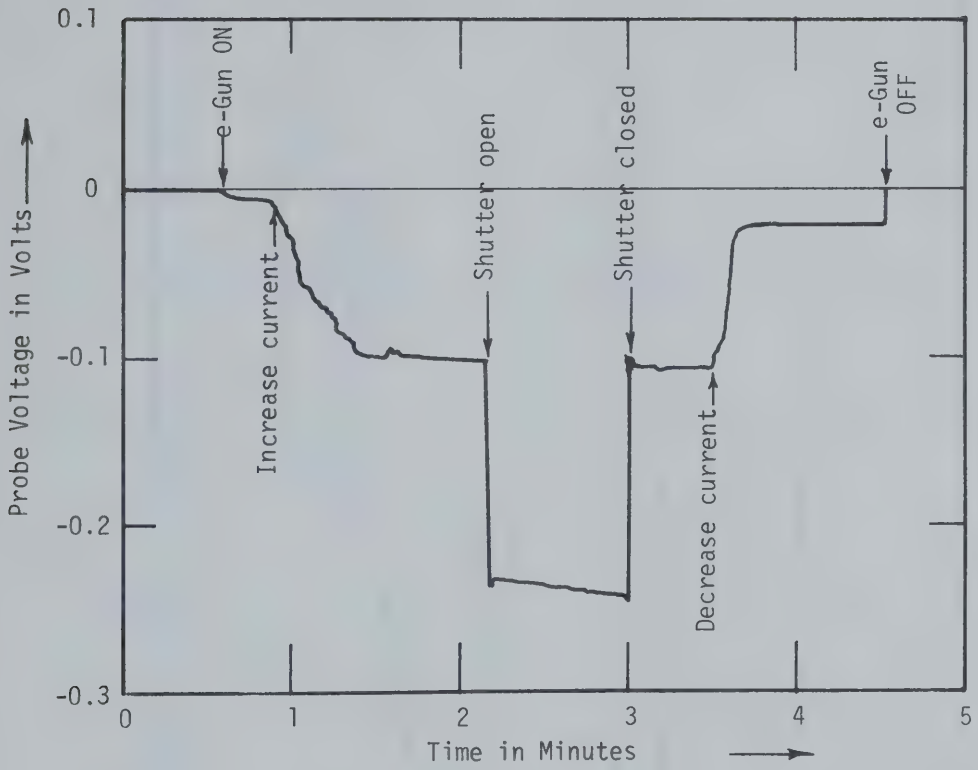


FIGURE 3.9: Charge vs. Time for Stray Electrons from e-Beam Evaporator.

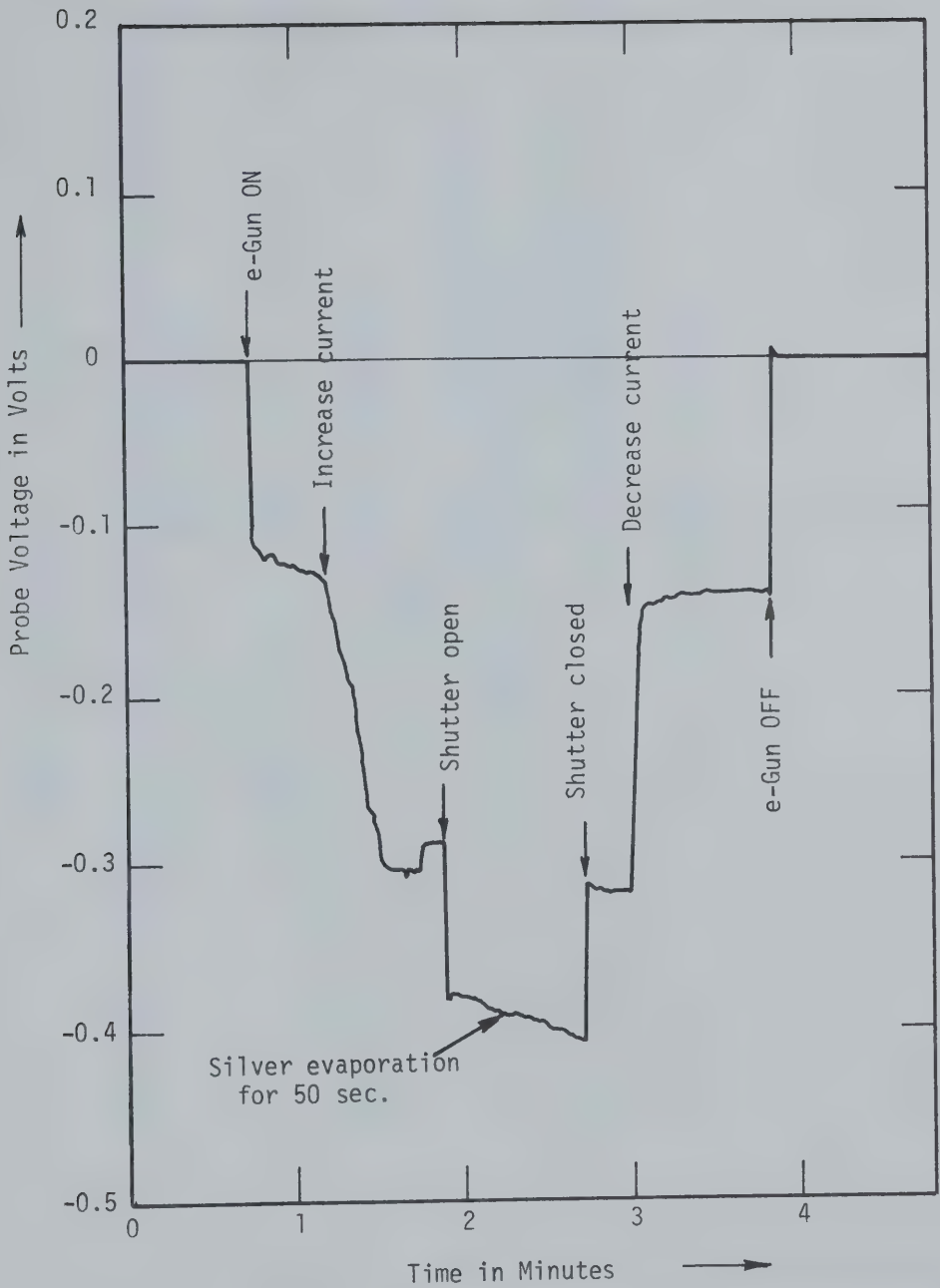


FIGURE 3.10: Charge vs. Time During e-Beam Evaporation of Silver.

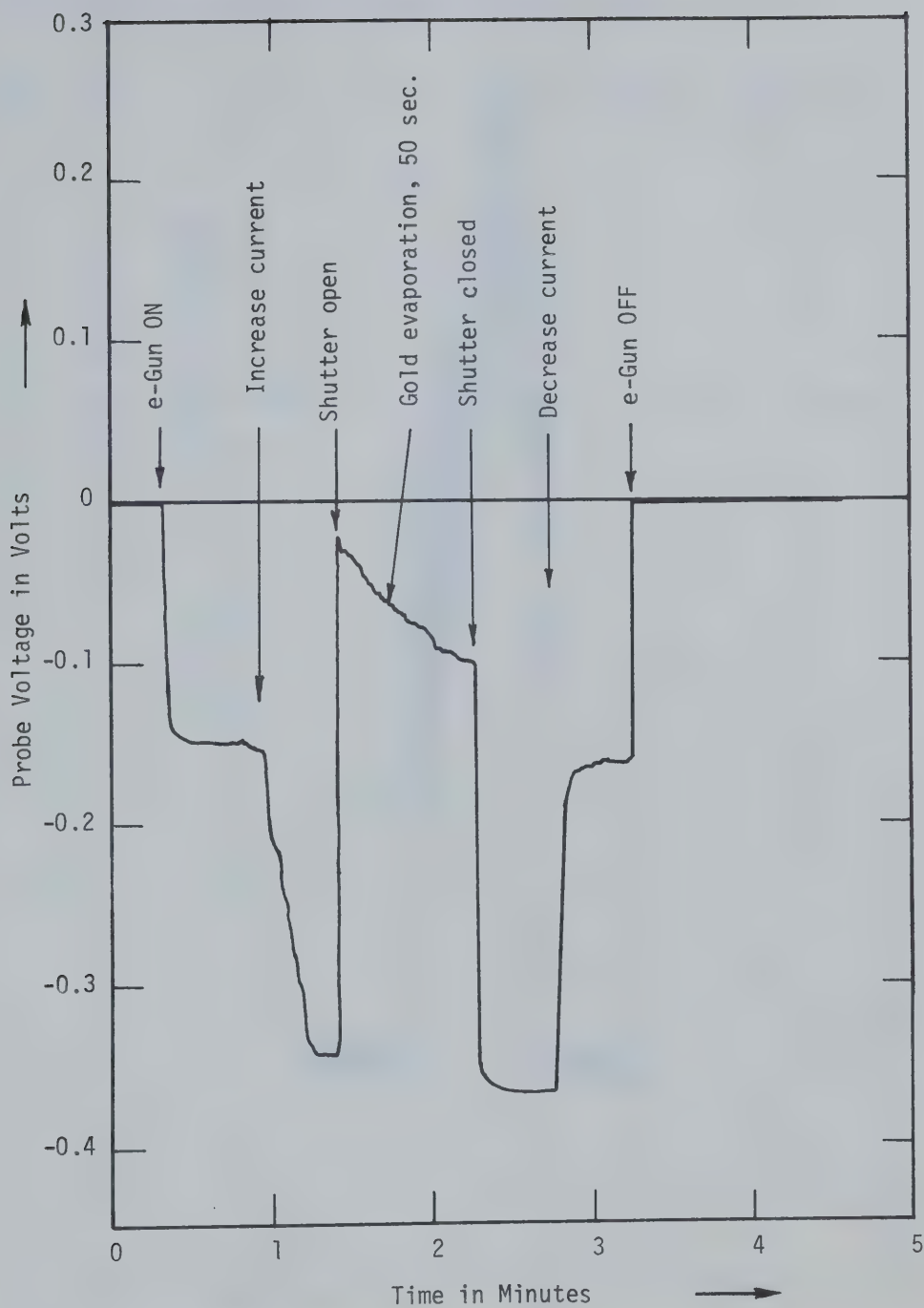


FIGURE 3.11: Charge vs. Time During e-Beam Evaporation of Platinum.

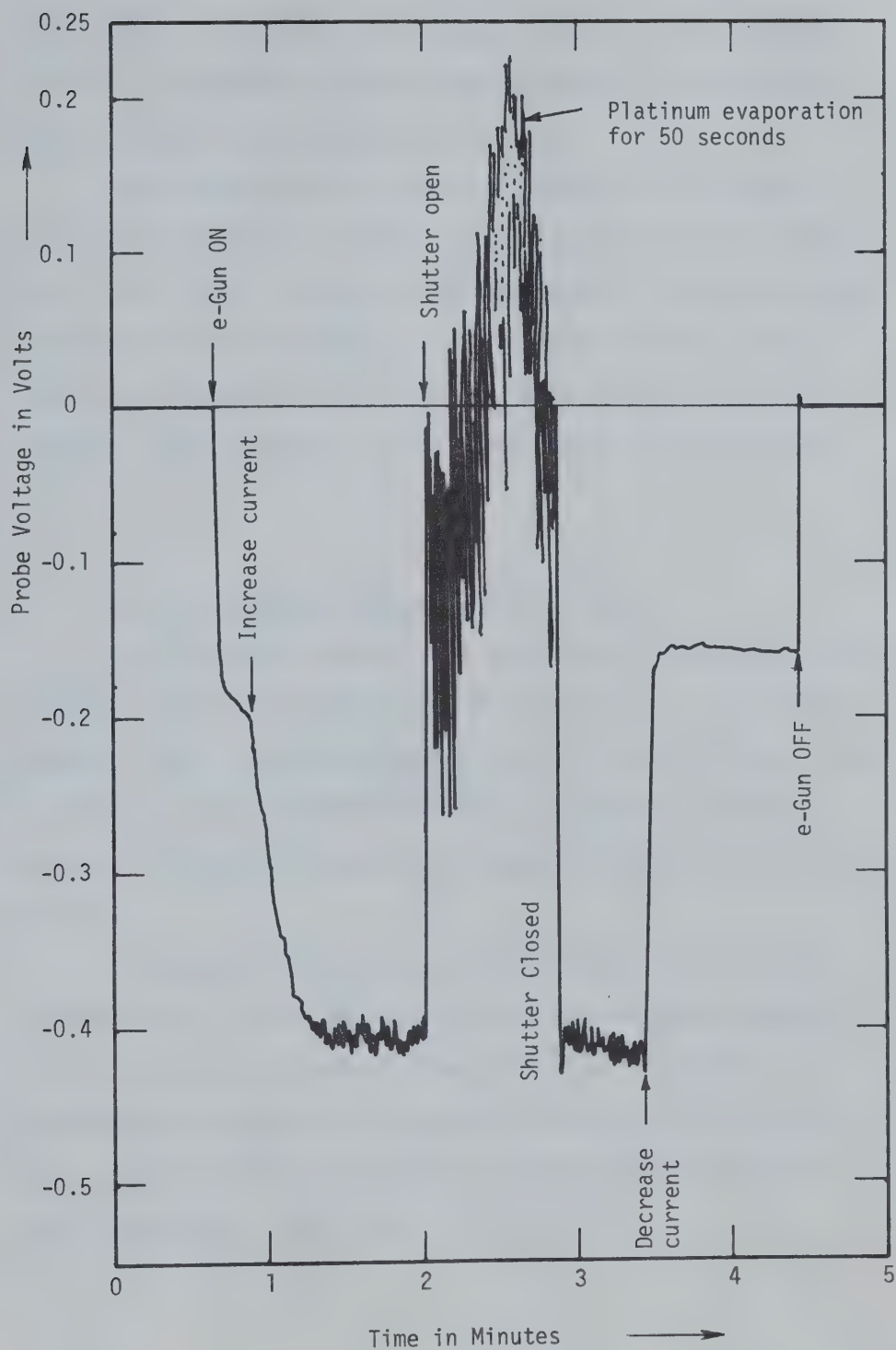


FIGURE 3.12: Charge vs. Time During e-Beam Evaporation of Platinum.

cooling water. This results in a temperature gradient across the crystal. The consequent thermal shock behaviour is discussed by Warner [81] and Stockbridge and Warner [111].

Temperature rise versus time of exposure of the crystal to various evaporants was determined by a thermocouple arrangement shown in Fig. 3.13. The sources were switched off and the shutter closed after exposure of the crystal for known periods of time. Temperature rise and decay, versus time were recorded on a chart recorder. These are shown for the three metals in Figs. 3.14 to 3.16.

3.3.3 Post deposition relaxation effects

The frequency of the crystal increased as the entire crystal reached an equilibrium temperature after deposition. In a typical frequency versus time curve shown in Fig. 3.17, it can be seen that the frequency rise is exponential with superimposed sinusoidal variations. A stable frequency was reached in about 30 minutes to one hour.

An extreme case was the prolonged deposition of platinum, as shown in Fig. 3.18. During deposition, the frequency decrease is seen to become progressively less with time. As soon as the deposition was stopped, the frequency decreased rapidly by about 400 Hz. Subsequently the frequency increased again to a steady value following the pattern shown in Fig. 3.17.

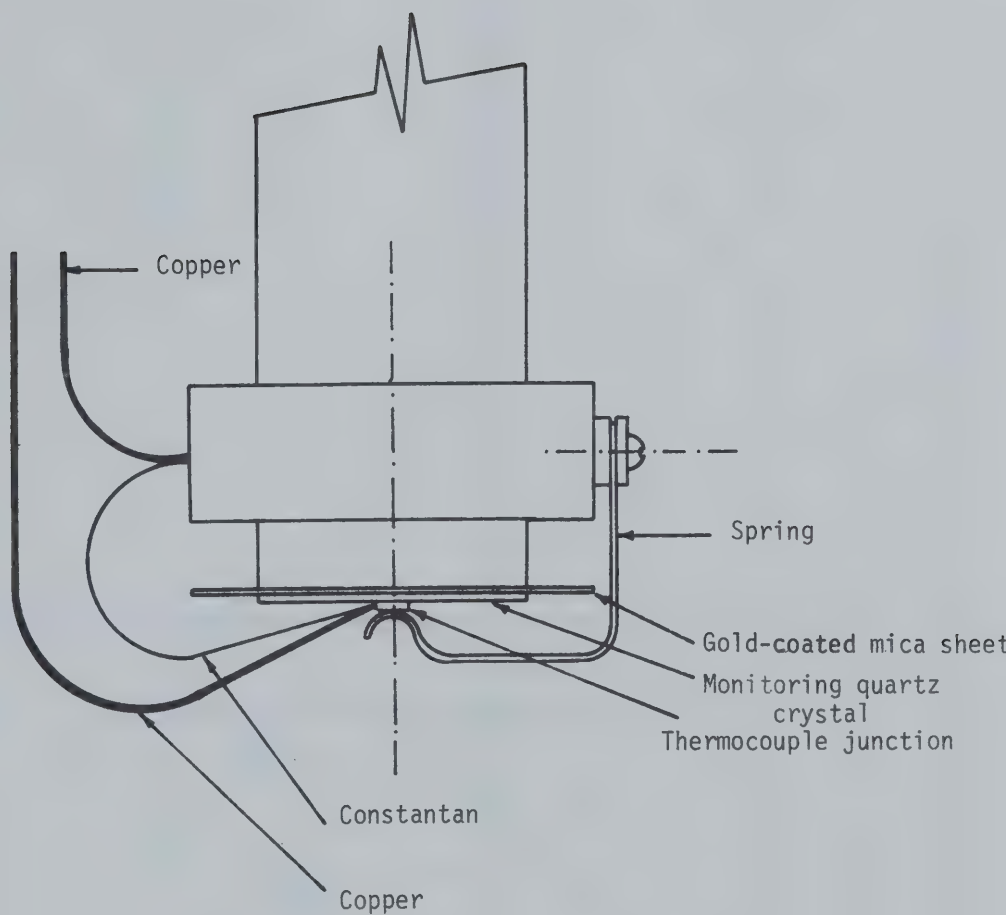


FIGURE 3.13: Thermocouple Placement for Crystal Temperature Measurements.

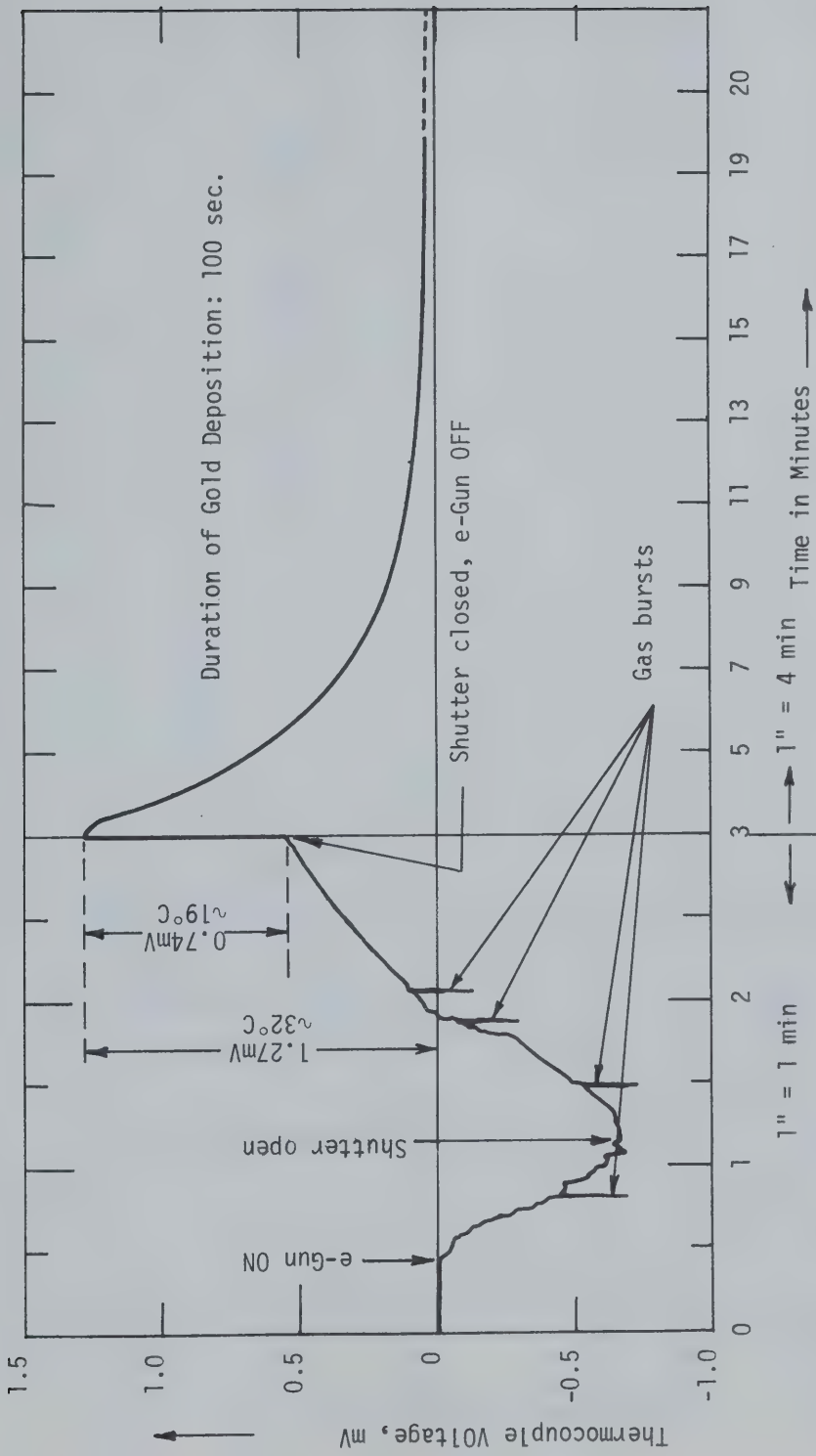


FIGURE 3.15: Thermocouple Voltage vs. Time During Gold Deposition.

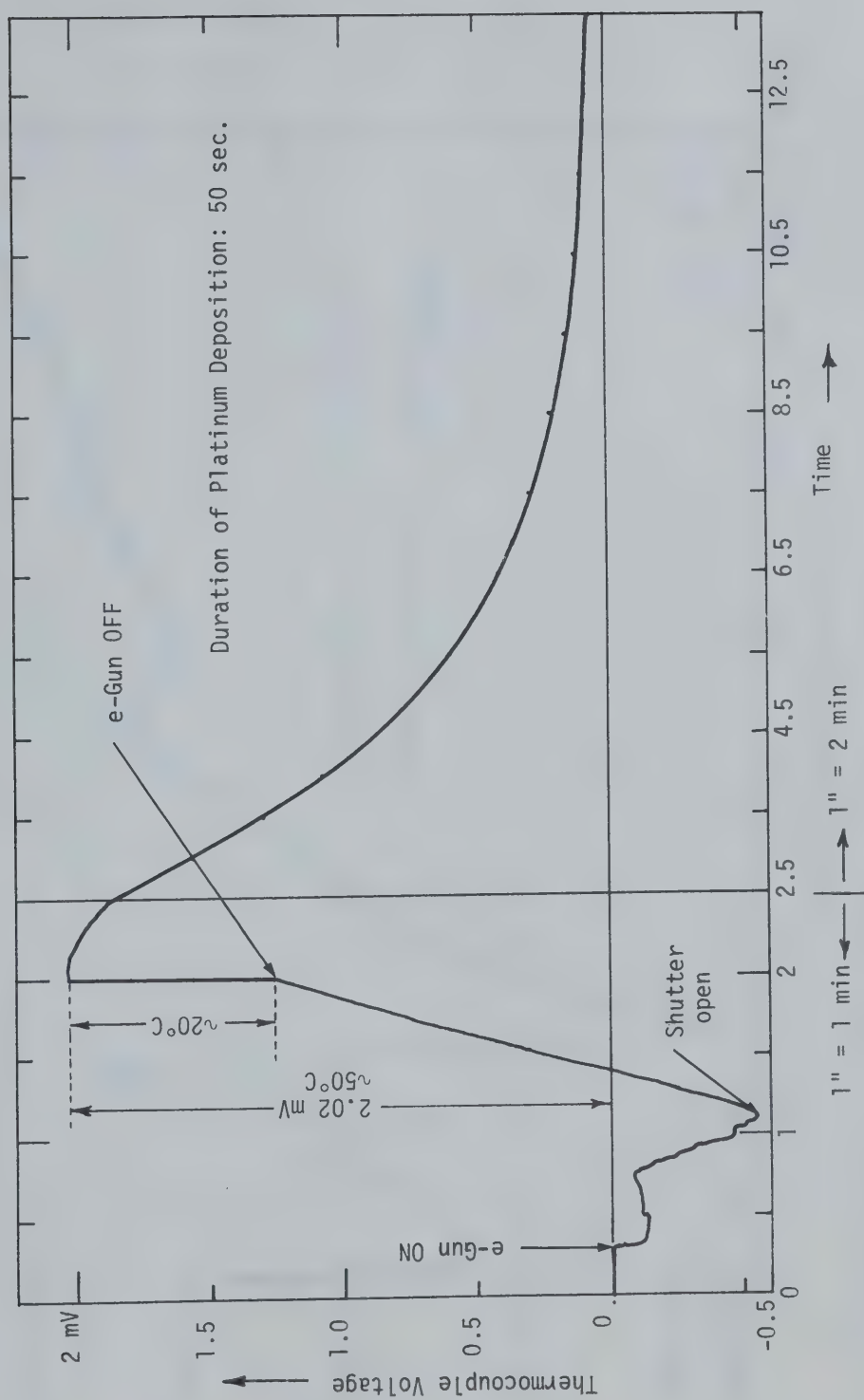


FIGURE 3.16: Thermocouple Voltage During Platinum Deposition.

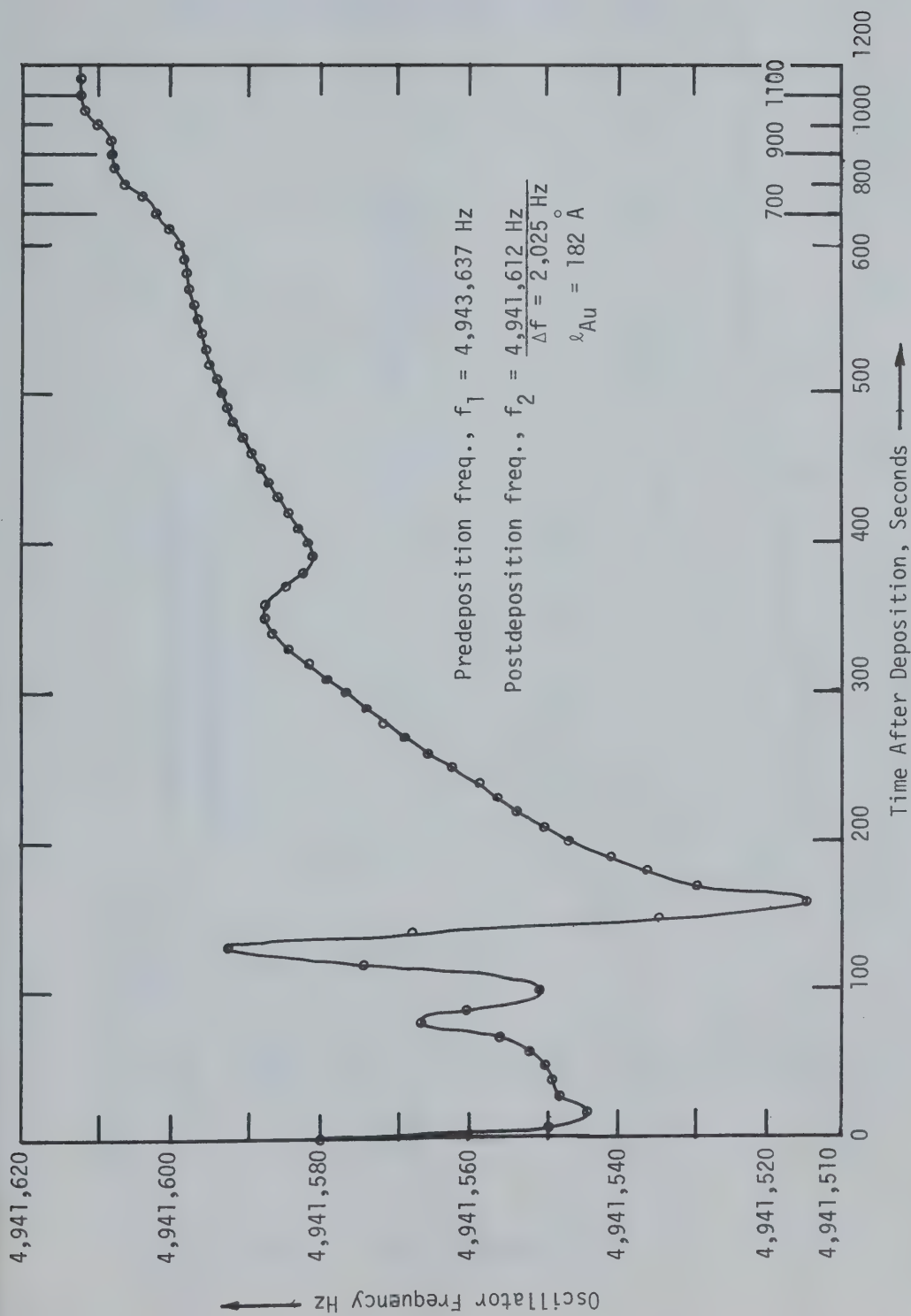


FIGURE 3.17: Post Deposition Crystal Frequency vs. Time

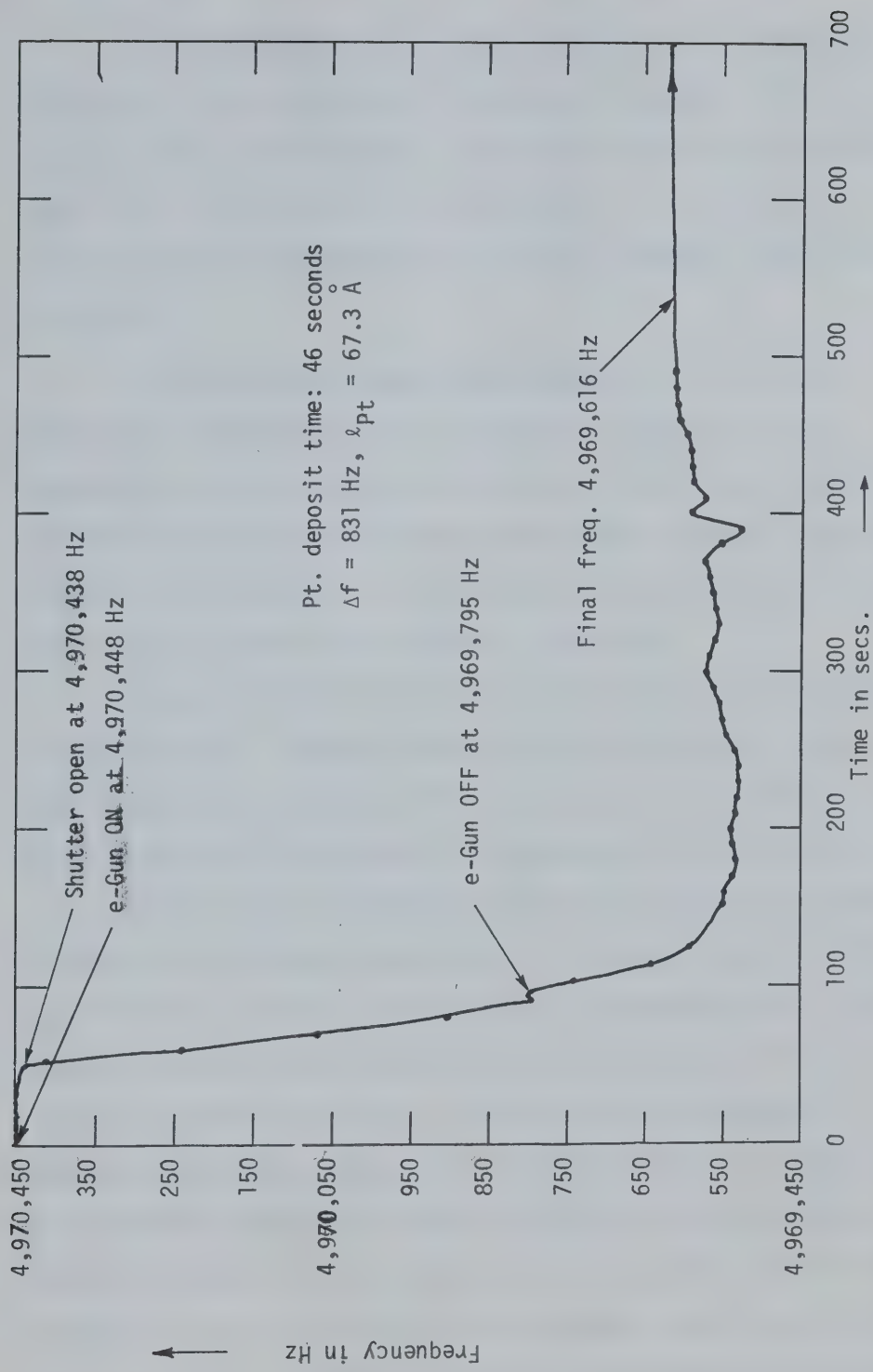


FIGURE 3.18: Crystal Frequency vs. Time for Prolonged Platinum Deposition.

3.4 Discussion

In the QCM method of thickness monitoring, the difference between pre- and post-deposition frequencies is required. Since the oscillator frequency stabilizes in about half an hour after the film deposition is completed, the long term stability and accuracy of absolute frequency measurement by the digital frequency counter are not important

It has also been shown that the mass per unit area of a deposit may be determined without knowing the crystal area [81]. Second order corrections may be required only when the area exposed for deposition and the active area of the crystal plate are materially different. This difference in the present method is less than 2%. Any errors from this source are, therefore, negligible.

The possibility of nonlinearity was eliminated by changing the crystal after a frequency decrease of less than 50 KHz, that is, below 1% of crystal frequency. This also minimized any error due to the different densities of quartz and the deposited materials [84].

A more serious discrepancy between the monitored and actual thickness of the film on a substrate arises from two causes. First, the density of a material in the form of an evaporated film is usually less than the bulk value, particularly below a thickness of 200 \AA [112-115]. The metric thickness, as would have been measured, for example by Tolansky's method [71-74], would therefore be larger than the monitored thickness; the latter is the mass-thickness defined by assuming that the film has the same density as the bulk value and that the deposit is perfectly uniform over the given crystal area. A second, and to some extent a compensating factor, is the decrease in sticking

coefficient, α , with decreasing film thickness [116]. On mica substrates maintained at a temperature of 400°C, Poppa et al. [92] found the value of α to be as low as 0.1 for a zero to 2 Å deposit build up; α approached unity for an average deposit build up reaching 20 Å. They determined the values of α by electron microscope observations and these were not compared with respect to the mass-thickness of the deposit as would be monitored by a QCM. In this work the substrates, mica and glass, were not heated and hence, except for the rise in temperature during deposition, were maintained at room temperature. Detailed experiments are still required for determining the values of α for gold, silver, and platinum on mica and glass under this condition, particularly for film thicknesses below 50 Å. Assuming α having the same values at room temperature as those determined by Poppa et al. at 400°C [92], and that α has a linear dependence on the QCM monitored mass-thickness, a value of 0.5 may be considered appropriate for the thinnest film reported here, which is 10.8 Å. It then implies that the actual deposit on the mica substrate is only about 5 Å in this case; the error between the actual thickness and the mass-thickness as indicated by the QCM is then as large as 100%.

CHAPTER IV

MEASUREMENT OF THE RESISTIVITY OF ULTRA THIN FILMS

4.1 Introduction

In the range below 50 \AA , the film thickness becomes comparable to the substrate surface irregularities. Thus, its macro-conductivity is as much a function of the film structure as the microtopography of the substrates. Cleaved mica faces, the smoothest available, show topographic irregularities of the order of lattice parameters [74]. The d.c. measurements thus become progressively less reliable for decreasing film thicknesses. The substrate surface defects, on the other hand, are at least seven orders of magnitude smaller than a wavelength at 10 GHz, and as such will not affect the wave.

A waveguide impedance method due to Slater [85] for measuring the conductivity of metal films has been used by Clark [117]. This method is simpler than the field approach which has been used for metal and semiconductor films on thick substrates [118-121], and provides a more accurate technique than the d.c. measurements for determining the conductivity of ultra-thin ($< 50 \text{ \AA}$) films [86].

A film of thickness $\ell \ll \delta$, the skin depth, and bulk conductivity σ , placed across a rectangular waveguide operating in the TE_{10} mode, creates an admittance $\sigma\ell + Y_t$, where Y_t is the admittance of the waveguide termination at the film. Y_t is zero

when a perfect short is placed at $z = 0$, that is, $\lambda_g/4$ behind the film in Fig. 4.1, where λ_g is the guide wavelength at the operating frequency. The conductance $\sigma\ell$ then corresponds to the conventional definition of the d.c. sheet resistance, i.e.,

$$R_s = \frac{1}{\sigma\ell} \quad \text{in ohms/square} \quad 4.1$$

The microwave value, $R_s(\mu)$, can be measured as

$$R_s(\mu) = rZ_0, \quad R_s(\mu) \geq Z_0 \quad 4.2(a)$$

or

$$R_s(\mu) = \frac{Z_0}{r}, \quad R_s(\mu) \leq Z_0 \quad 4.2(b)$$

where r is the VSWR and Z_0 is the wave impedance at the operating frequency. Replacing the film by a short circuit at $Z = -\lambda_g/4$, any reactive part resulting from a significant discontinuity due to the substrate and its mounting in the waveguide will be indicated by a minima shift other than zero ($R_s(\mu) = Z_0/r$) or $\lambda_g/4$ ($R_s(\mu) = rZ_0$).

It can be shown that a thin, lossless dielectric sheet of thickness d and relative permittivity ϵ will cause a VSWR given by [122]

$$r_\epsilon = 1 + \frac{2\pi d}{\lambda} \left[\sqrt{\frac{\epsilon - (\lambda/\lambda_c)^2}{1 - (\lambda/\lambda_c)^2}} - 1 \right] \quad 4.3$$

where λ and λ_c are the free-space and cut-off wavelengths, respectively.

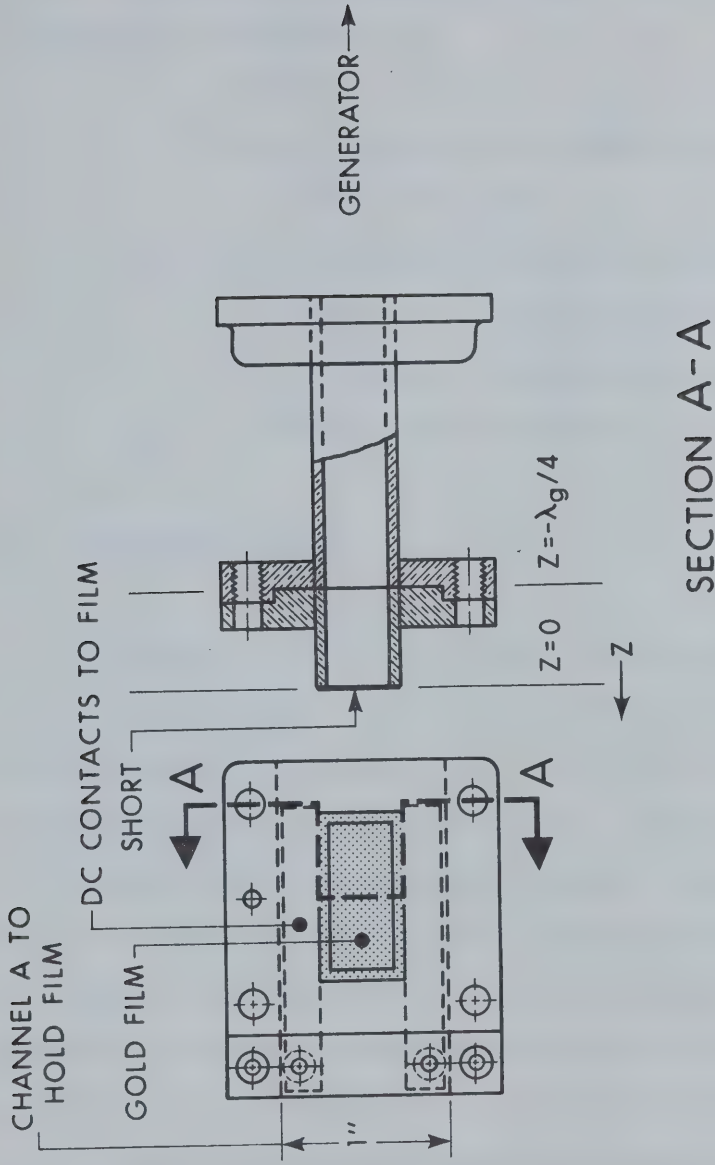


FIGURE 4.1: Thin Film Holder for X-Band Waveguide.

The accuracy with which the resistivity, $\rho_{\mu} = \ell R_s(\mu)$ can be determined thus depends on:

1. making $\ell \ll \delta$;
2. $Y_t = 0$, demanding an ideal short circuit and lossless waveguide;
3. the accuracy of measuring r , particularly when $R_s(\mu)$ is much different from Z_0 ; and
4. the effects of discontinuity caused by the substrate and film holder.

4.2 Experimental Results

Measurements were made at 9700 ± 2 MHz in X-band waveguide for which $Z_0 = 511.8\Omega$. Gold films on mica were deposited by high vacuum evaporation, with $d \leq 0.03$ mm. The method of mounting the film in the waveguide is shown in Fig. 4.1. The film configuration and d.c. sheet resistance measurements were as discussed in section 2.3.1. In practice, even with a mica sheet on both sides of the film, there is sufficient capacitive coupling between the contact strips and the broadside waveguide walls for the film to act essentially as a conductance across the waveguide [19].

The discontinuity was assessed using the sliding load technique [123]. The VSWR of the holder without a mica sheet was 1.035 (corresponding to a reflection coefficient $|\Gamma_1| = 0.017$). With a 0.03 mm thick mica sheet, the VSWR increased to 1.056 ($|\Gamma_2| = 0.027$). Considering Γ_1 and Γ_2 in phase, $\Gamma_e = 0.01$ and

and $r_\epsilon = 1.02$, which agrees closely with the value 1.0124 calculated from Eq. 4.3. The maximum error, at $R_S(\mu) = Z_0$ is then found to be $\pm 2\%$ if r_ϵ is ignored. As the VSWR can be measured to within 2% for $r \leq 10$, after making due corrections for the detector response characteristics, the error is less than $\pm 5\%$ for $50 \leq R_S(\mu) \leq 5000\Omega/\square$.

The short circuit used was a mica sheet coated with silver-gold films as in contacts (section 2.3.1); this sheet was pressed tightly between a metal plate and the waveguide section at a distance $\lambda_g/4$ from the film plane. This arrangement is shown in a photograph, Fig. 4.2. The quality of this short circuit arrangement was far superior to either the commercially available, choke type movable short or a fixed one made by welding a plate at the waveguide end. The mica sheet and the heavy metal deposit being flexible, a good contact is obtained even when minute machining marks are present in the metallic parts.

The measured values of $R_S(\mu)$, R_S , ρ_μ and the d.c. resistivity ρ_0 ($= 2R_S$), the last two normalized to the bulk resistivity of gold ($\rho_{Au} = 2.44 \times 10^{-6} \Omega\text{-cm}$), are shown in Figs. 4.3 and 4.4. Figure 4.5 shows the sheet resistance of a 45 \AA Au/Pt film versus the annealing temperature. Eight of these films were obtained in one deposition cycle (section 2.6). Six of these films were coated with d.c. contacts and one was left without the contacts. This experiment was performed to establish that the d.c. measurements, by the deposition of heavier contacts, render the films useless for subsequent annealing studies.



FIGURE 4.2: Waveguide Film Holder and Short Circuit Arrangement.

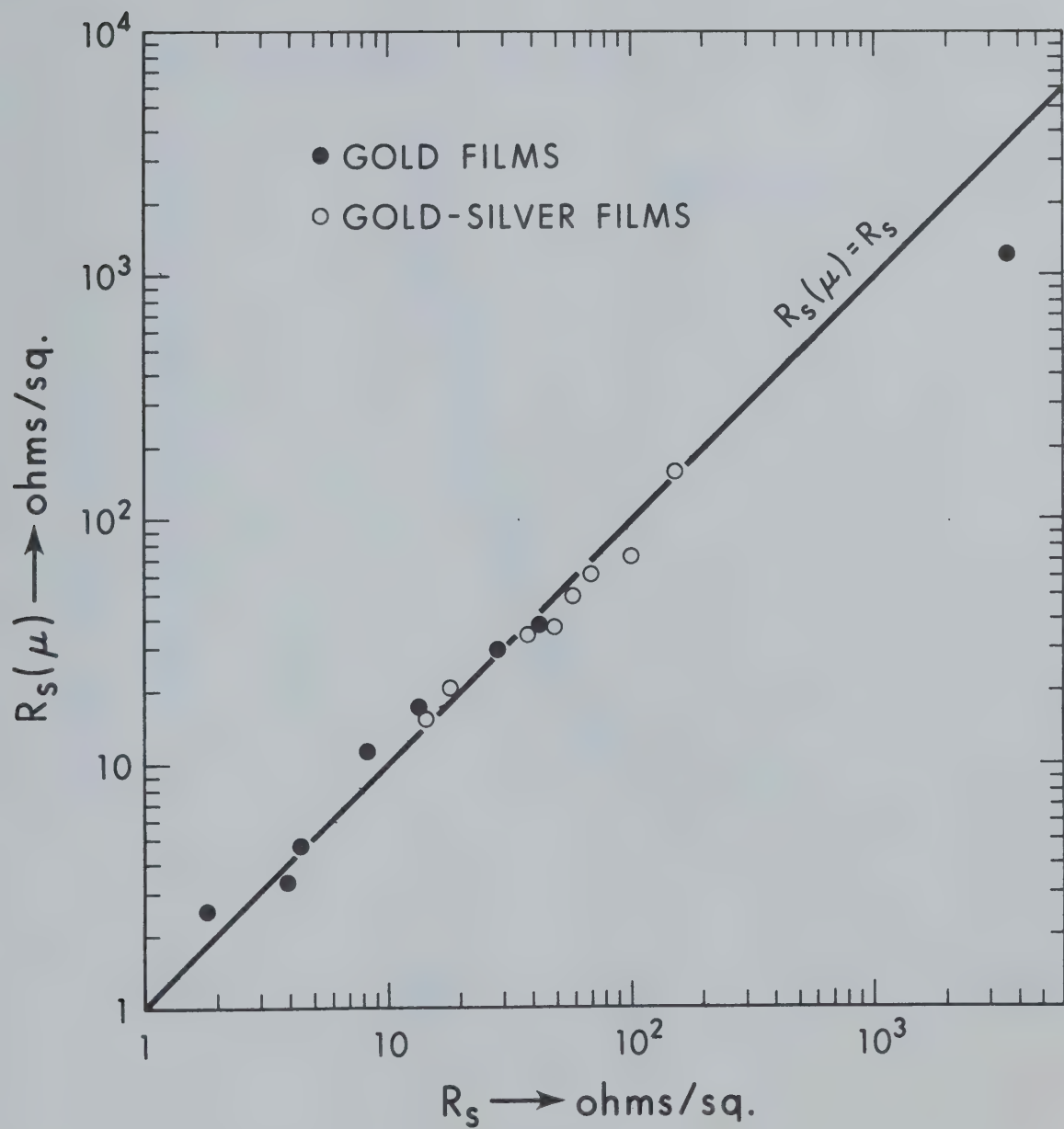


FIGURE 4.3: R_s vs. $R_s(\mu)$ for Gold Films on Mica.

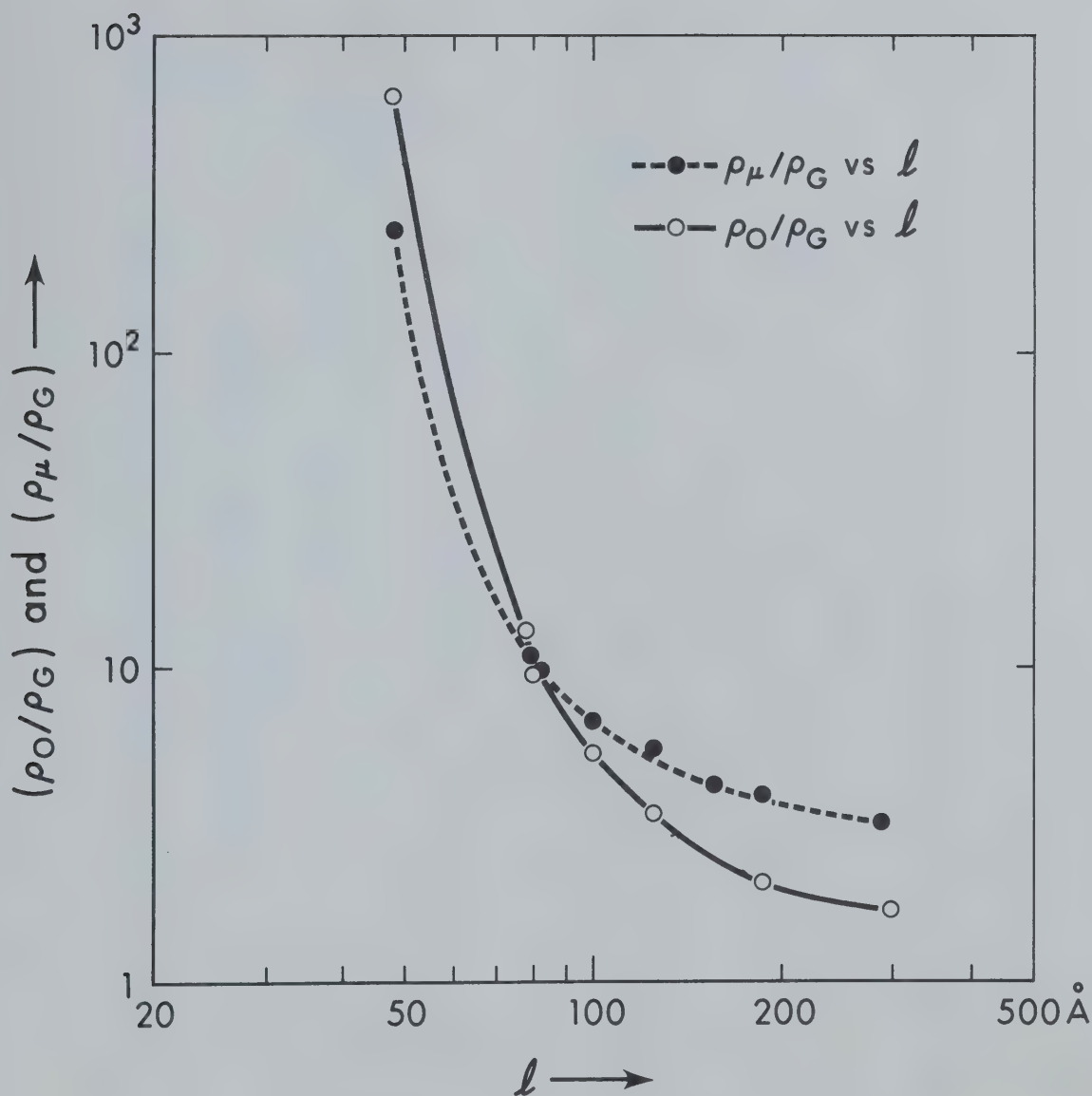


FIGURE 4.4: ρ_O/ρ_G and ρ_μ/ρ_G vs. l .

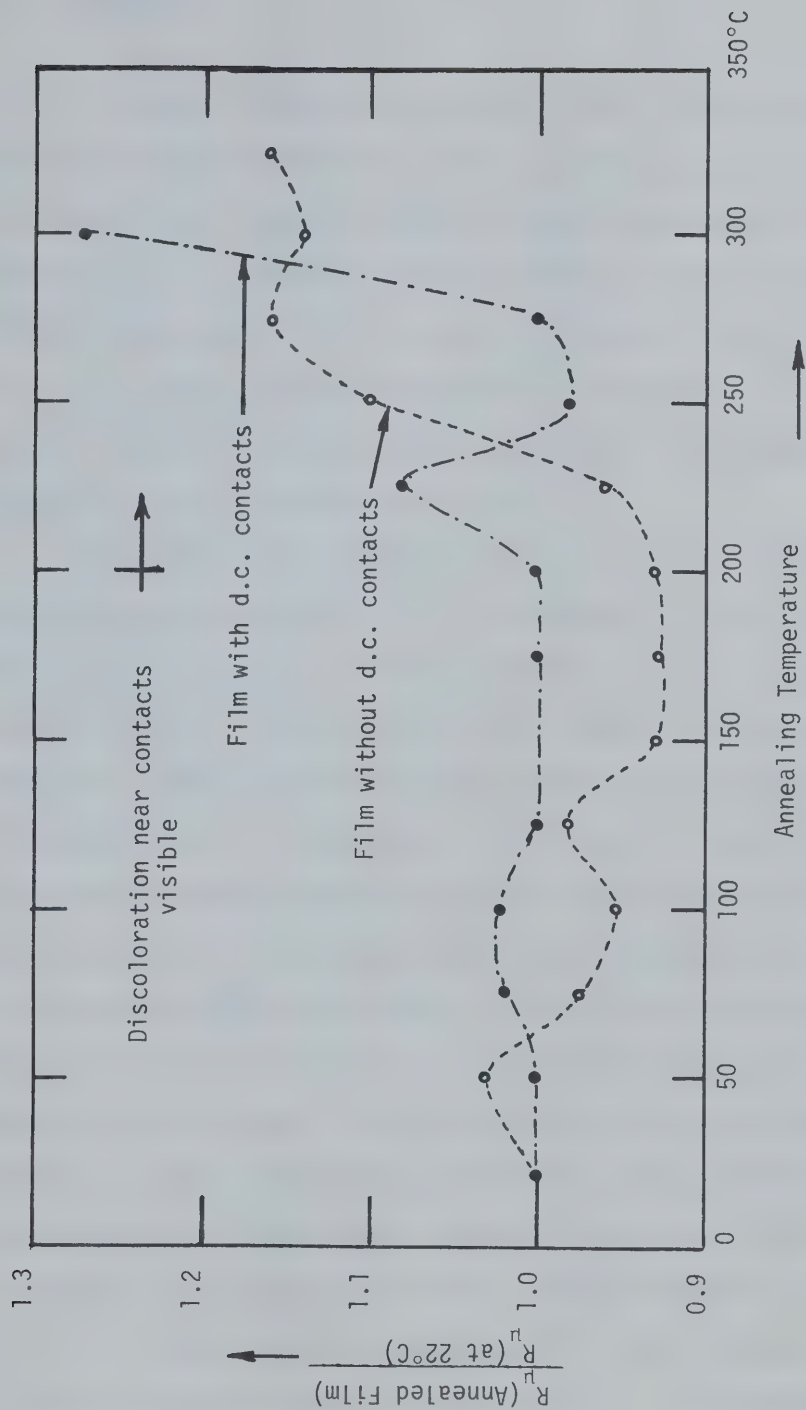


FIGURE 4.5: R_u vs. Annealing Temperature of a Film With and Without D.C. Contacts.

4.3 Discussion

No direct correlation between R_S and $R_S(\mu)$ has been found. Figure 4.3 suggests that for R_S below about $40\Omega/\square$, $R_S(\mu)$ is generally greater than R_S ; there are some points where $R_S(\mu) \approx R_S$; otherwise $R_S(\mu)$ is generally smaller than R_S . These factors are further emphasized in Fig. 4.4 where a transition from $\rho_o/\rho_{Au} < \rho_\mu/\rho_{Au}$ to $\rho_o/\rho_{Au} > \rho_\mu/\rho_{Au}$ is seen to occur for ℓ around 80 \AA . At 50 \AA , ρ_o/ρ_{Au} is about three times larger than ρ_μ/ρ_{Au} , a difference far beyond the limits of experimental error.

Waveguide losses and an imperfect short circuit are likely to reduce the measured value of r . Thus when $R_S(\mu) = rZ_o$, $R_S(\mu)$ will be smaller than R_S ; for the case when $R_S(\mu) = Z_o/r$, $R_S(\mu)$ will be larger than R_S . For the former case, however, ℓ is less than about 80 \AA and a much more important factor is the surface microtopography of the substrates. As discussed in section 2.4, the mica sheets, although carefully cleaved, still exhibit hill-and-valley topography and cleavage step heights are known to be $\sim 20 \text{ \AA}$ or integer multiples thereof [74]. Figure 4.6 shows an idealized cross-section of a film with ℓ slightly larger than h and no deposition on the step. The resulting constricted area through A'D forms a higher resistivity path for d.c. and a multiplicity of such defects would considerably increase the measured R_S value. E_y , however, is essentially the same at faces AB and A'B; since $h \sim 10^{-7} \lambda_g$. Also, $E_y(\text{film})$ and the resulting film current density $\sigma E_y(\text{film})$ are uniform over ℓ , since $\ell \leq 10^{-3} \delta$. Surface undulations

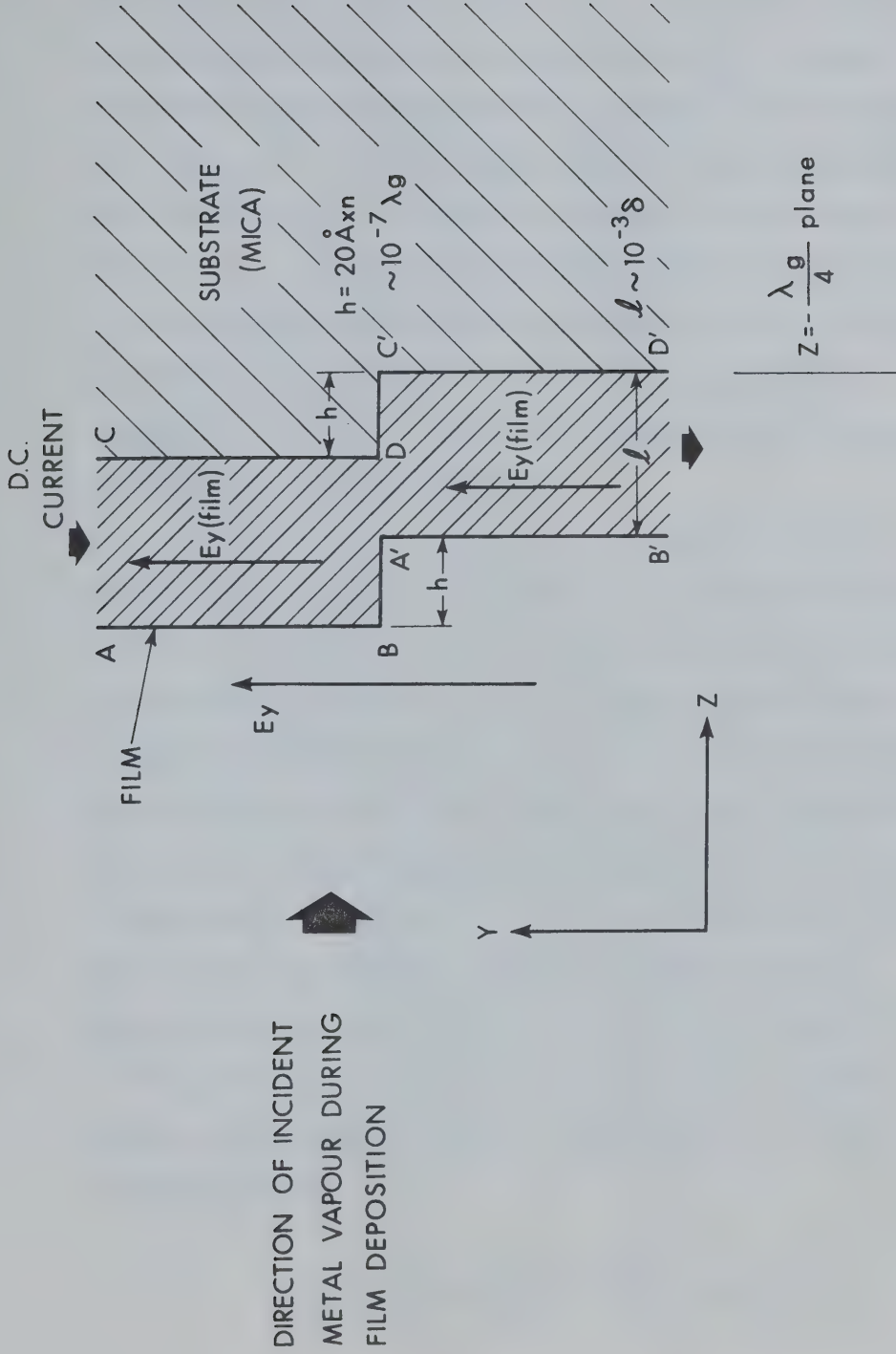


FIGURE 4.6: Deposition of a Film over a Cleavage Step.

further lengthen the d.c. path. At microwave frequencies on the other hand, Ament [124] has shown that an approximate value for the reflection coefficient of a perfect conductor with randomly distributed surface irregularities is $\exp(-2k^2 \overline{h^2} \sin^2 \theta)$, where $k^2 = \omega^2 \mu_0 \epsilon_0$, $\overline{h^2}$ is the mean-square height of the irregularities, and θ is the angle of incidence of the wave. This is almost unity for $\overline{h^2} \ll \lambda^2$. The result of microscopic surface irregularities on $R_s(\mu)$ measurements must therefore be minimal. The d.c. resistivity calculated using macroscopic film geometry is meaningless as λ approaches h or $(\overline{h^2})^{1/2}$, particularly because no two cleavage faces will have the same microtopography.

An extreme case is when $h > \lambda$, so that the film will show an open circuit at d.c. At microwaves, such a film may be considered an iris in a waveguide, with infinitely small openings as compared to the waveguide dimensions. Ramey, Landes and Manus [125] have treated the microwave properties of lossy thin films with apertures. For rectangular apertures these authors have shown that the reactance approaches zero as the aperture opening becomes vanishingly small. A simpler approach would be to consider the discontinuity as two distinct cases of either an inductive or a capacitive iris. These are shown in Fig. 2.6(a) and 2.6(b) respectively. Since h is still $\sim 10^{-7} \lambda_g$, the fields at AB and A'B' are unchanged. Assuming symmetry, the normalized inductive susceptance, \bar{B} , for Fig. 4.6(a) is given by [126]

$$\bar{B} = \frac{2\pi}{\beta a} \cot \frac{2\pi d}{2a} \left[1 + \frac{av_3^{-3\pi}}{4\pi} \sin^2 \frac{\pi d}{a} \right] \quad 4.4$$

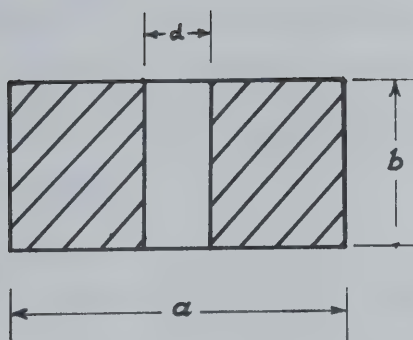


FIGURE 4.7(a): Inductive Iris in a Waveguide.

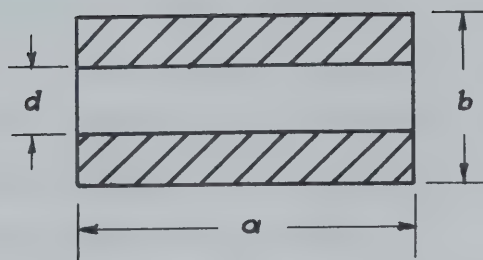


FIGURE 4.7(b): Capacitive Iris in a Waveguide.

where d is the width of the discontinuity seen by the wave as a fraction of the waveguide width, a ; $\beta = \{\omega^2 \mu_0 \epsilon_0 - (\pi/a)^2\}^{1/2}$ and $\nu_3 = [(3\pi/2)^2 - \omega^2 \mu_0 \epsilon_0]^{1/2}$. It can be seen from Eq. 4.4 that as $d/a \rightarrow 0$, $\cot(d/a) \rightarrow \infty$ and the aperture has virtually no effect. Similarly, for the capacitive case in Fig. 4.6(b), the normalized susceptance is given by [126]

$$\bar{B} = \frac{2\beta b}{\pi} \left[\ln \operatorname{cosec} \frac{\pi d}{2b} + \left(\frac{2\pi}{b\nu_2} - 1 \right) \cos^2 \frac{\pi d}{2b} \right] \quad 4.5$$

where $\nu_2 = [(2\pi/b)^2 - \beta^2]^{1/2}$ and b is the waveguide height in the y -direction. Again, as $d/b \rightarrow 0$, $\operatorname{cosec}(d/b) \rightarrow \infty$, so that $\bar{B} \rightarrow \infty$; or the aperture is a virtual short circuit for the wave.

The microscopic defects, therefore, have a minimal effect on the resistivity measurement by the present method. This removes the difficulty of examining films deposited on vacuum cleaved mica sheets for resistivity measurement; it may not be possible with d.c. measurements if $h > \ell$. It is well known [37] that the nucleation and growth characteristics of materials deposited on a clean, vacuum cleaved surface is likely to be quite different from those on air-cleaved, contaminated surfaces.

From Fig. 2.5 it can be seen that annealing the films with d.c. contacts reduces the conductivity of a 45 \AA Au/Pt film on mica by a far larger proportion than that of the films without contacts. The deposition of heavier contacts also causes diffusion

of the contact material, silver in this case, into the film [127]. Annealing studies on the same films are, therefore, not possible with d.c. measurements. There is no such restriction with the microwave method.

CHAPTER V

RESISTIVITY OF GOLD FILMS ON PLATINUM NUCLEATING LAYERS

5.1 Problems in the Analysis of Composite Films

The dependence of the electrical resistivity on film thickness is generally compared with the size effect theory by Fuchs [11] and Sondheimer [12]. It relates the resistivity of the film, ρ_f , normalized with respect to the bulk resistivity, ρ_b , to the film thickness, ℓ , by [12]

$$\frac{\rho_f}{\rho_b} = \frac{\Phi(\ell/\lambda_0)}{\ell/\lambda_0} = \frac{\Phi(\kappa)}{\kappa} \quad 5.1.1$$

where λ_0 is the mean free path of the conduction electrons in thin films. $\Phi(\kappa)$ is given by

$$\frac{1}{\Phi(\kappa)} = \frac{1}{\kappa} - \frac{3}{2\kappa^2} (1-p) \int_1^\infty \left(\frac{1}{t^3} - \frac{1}{t^5} \right) \frac{1-e^{-kT}}{1-pe^{-kT}} dt \quad 5.1.2$$

in which p is the fraction of electrons scattered specularly at the boundary surfaces, t is the integration variable, k is Boltzmann's constant and T is the film temperature ($^{\circ}\text{K}$).

This theory is based upon the use of relaxation time to represent the effect of scattering of electrons inside the film. The theory is rigorous for spherical Fermi surfaces [128] and hence can only be applied to alkali metal films [129,130].

The electron mean free path, λ_0 , is given by [128]

$$\sigma_0 = \frac{e^2}{12\pi\hbar} S_F \lambda_0 \quad 5.1.3$$

where σ_0 , e , \hbar , and S_F are, respectively, the bulk conductivity, electron charge, modified Planck's constant ($\hbar = h/2\pi$) and the area of the Fermi surface. It is considered very difficult to deduce the values of either λ_0 or S_F theoretically. The Fermi surface is complicated enough for pure noble metals [129]: it is impossible to determine S_F for crystal structures complicated further by alloying and/or epitaxial growth. These difficulties are generally circumvented by assuming the value of λ_0 identical for metal in bulk or in film form. Thus, for example, Namba [14] assumes $\lambda_0 = 340 \text{ \AA}$ for gold at room temperature. His experimental results are in reasonable agreement with the theoretical model.

The resistivity of a metal in the form of a film varies considerably from the bulk value for two main reasons. First, the structure is altered, especially in the case of epitaxial, single crystal films. Secondly, the high concentration of structural defects (dislocations, stacking faults, vacancies, interstitials, grain boundaries) and the presence of foreign atoms including occluded gas particles [131] cause diffuse scattering of conduction electrons. Experimentally, the value of "bulk resistivity", ρ_0 , is determined from ρ_f versus thickness curves in the region where ρ_f appears independent of ℓ . Chopra and Bobb [54] found that, for epitaxial gold films grown on mica, ρ_f was constant for $\ell > 300 \text{ \AA}$. As ρ_0 is invariably higher than ρ_b [131], λ_0 is also decreased. As a convenient approximation, λ_0 may be assumed inversely

proportional to ρ_0 ($= 1/\sigma_0$) (Eq. 5.1.3). It may be emphasized that this approach is not strictly valid; however, there is no other alternative. Also, size effects [12] in this region are ignored.

In the case of composite films, ρ_0 is further affected by alloying. For the present work, 5 to 40 Å thick gold films were deposited on 3 to 10 Å thick platinum nucleating layers.

Penetration of gold atoms and consequent alloying at the Au-Pt interface occurs instantaneously owing to the kinetic energy of the impinging atoms in the metal vapor. Further alloying continues by the process of interdiffusion even at room temperature [132]. The composite film presents, in practice, a combination of alloyed films. The Au-Pt proportions vary continuously across the film thickness. There are three layers, with indeterminate boundaries: (a) a platinum layer with increasing concentration of gold atoms towards the interface, (b) highly alloyed regions on both sides of the interface, and (c) a gold layer with progressively decreasing concentration of platinum atoms towards the outer surface. The composition changes continuously with both time and annealing. A unique determination of ρ_0 is, therefore, not possible.

5.2 Results and Discussion

In view of the difficulties described above, an attempt has been made to approximate the actual physical conditions as closely as possible. The analysis is made based on the following methods:

(i) In order to determine the thickness at which ρ_0 is not dependent on ℓ , gold films between 70 to 1000 Å thick were deposited

on $\sim 10 - 15 \text{ \AA}$ thick platinum nucleating layers with mica as a substrate. Before d.c. contact deposition, the films were annealed at 175°C for about 2 hours. The d.c. resistivity $\rho (= R_s \ell)$ versus ℓ is shown in Fig. 5.1. Eight films of the same thickness were deposited simultaneously in one coating operation and the average, with standard deviations, is shown. The results are similar to those of Chopra and Bobb [54] and ρ has been found nearly constant for $\ell \gtrsim 300 \text{ \AA}$. ρ is seen to increase slightly for film thicknesses above 600 \AA .

(ii) Based on the results above, $\ell \sim 400 \text{ \AA}$ was chosen to determine the "bulk resistivity", $\rho_0(\text{Au-Pt})$, for Au-Pt alloy films with various atomic percentage concentrations of platinum (at.%Pt). Platinum and gold were deposited in a total of seven alternating layers. First, $\sim 10 \text{ \AA}$ thick platinum nucleating layer was deposited; this range has been found to be suitable for inducing epitaxy [56]. Next, three layers each of gold and platinum were deposited alternately such that (a) the total thickness was about 400 \AA and (b) the maximum diffusion distance was never greater than $\sim 50 \text{ \AA}$ in each direction from the interfaces. The reason behind assuming that this procedure would help simulate the actual physical composition of the Au-Pt film is discussed below.

Figure 5.2 shows concentration profiles for a miscible system, for example Au-Ag [132]. At time $t = 0$, the profile has a square-wave shape; as t increases to t' this profile changes to an approximately sinusoidal form due to interdiffusion. Finally, at $t = \infty$, the concentration, C equals 50%, denoting a uniform alloy.

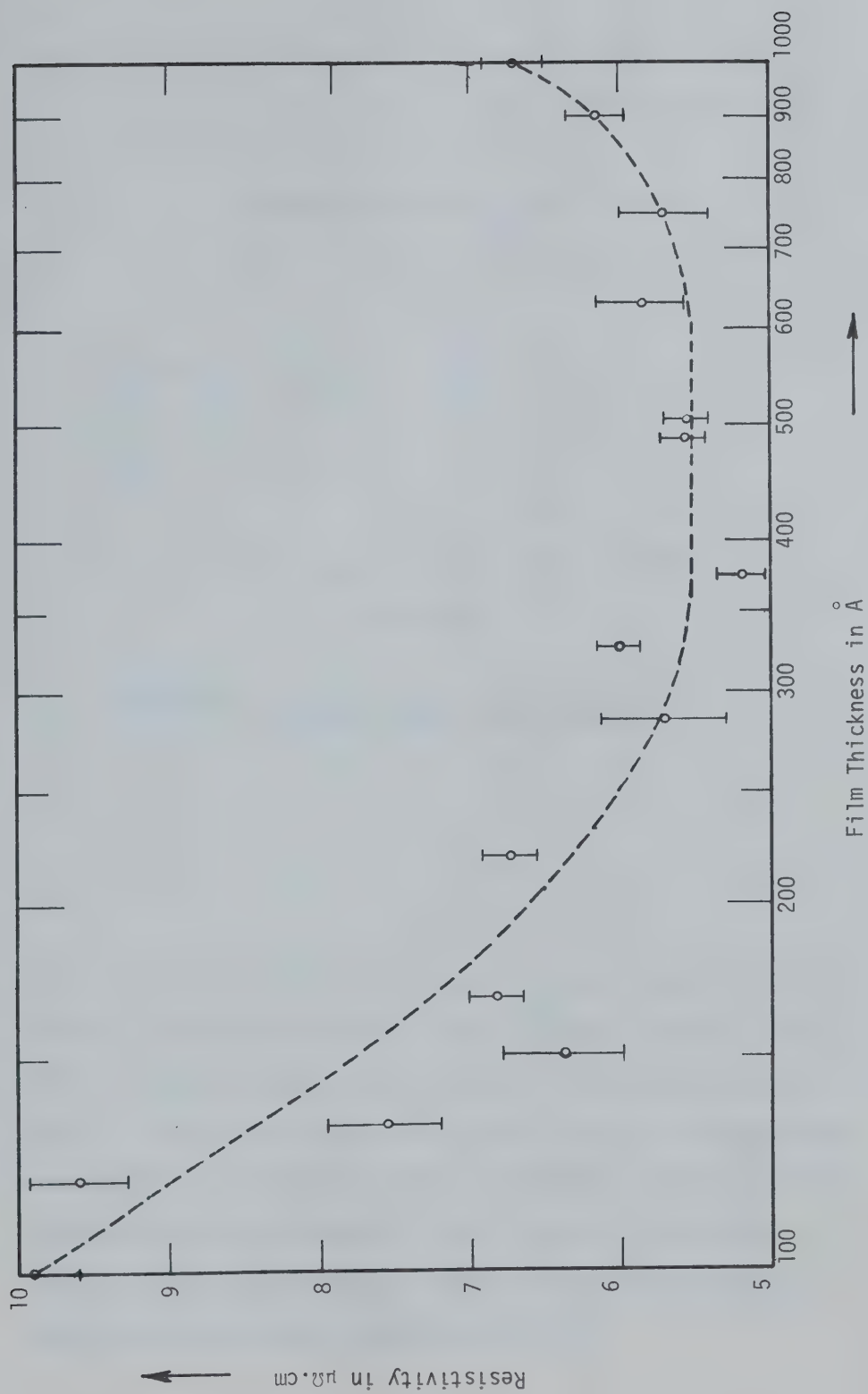


FIGURE 5.1: Resistivity vs. Thickness for Thick Gold Films.

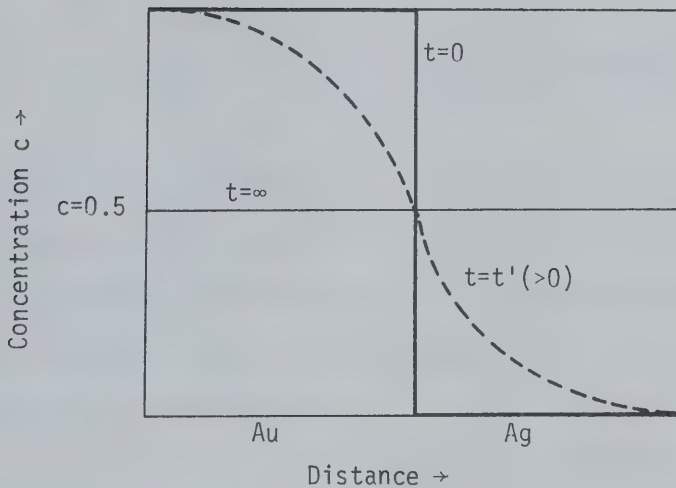


FIGURE 5.2: Concentration Profile with Time for a Miscible Binary Alloy System

The Au-Pt system, however, has miscibility gaps between 15 to 98 at.%Pt. For bulk Au-Pt alloy, it has been shown [64,134] that at 500°C the platinum concentration drops discontinuously from 0.98 to 0.15. It is not possible to heat Au-Pt films to a temperature above 200°C without damaging them. On the other hand, due to the very small diffusion distances ($\leq 50 \text{ \AA}$) and also because the diffusion law is approximately (x^2_{act}) , alloying in thin films occurs at relatively lower temperatures [132].

According to Sinha et al. [133], the diffusion coefficient, D , is $\sim 4 \times 10^{-8} \text{ cm}^2/\text{sec.}$ at 175°C and the concentration of platinum into gold for a film thickness ℓ is given by

$$\frac{C}{C_0} = 1 - \frac{4}{\pi} \sum_{n=0}^{\infty} \frac{(-1)^n}{2n+1} \exp\left\{-\frac{D(2n+1)^2 \pi^2 t}{4\ell^2}\right\}$$

where C_0 is the concentration of platinum at the interface. For $C/C_0 \sim 0.5$, a D_t/ℓ^2 is nearly 0.4. Thus, for $\ell \sim 50 \text{ \AA}$, alloying may be complete in about six hours. The seven layer Au-Pt films were maintained at 175°C for about four hours; the total time in the oven was nearly 10 hours.

The resistivity of an alloyed film, $\rho_0(\text{Au-Pt})$ for various at.%Pt is shown in Fig. 5.3. As in (i) above, eight films were measured to obtain average and standard deviations. $\rho_0(\text{Au-Pt})$ is seen to increase linearly up to about 20 at.%Pt, then is seen to drop to a lower value. This could possibly be caused by the miscibility gaps [134] where a temporary PtAu_3 phase is indicated at about 25 at.%Pt [135]; an anomalous alloying behavior is reported at 5 at.%Pt also [136]. Ignoring the three points between 5 and 20 at.%Pt, a least square fit was obtained for the remaining points corresponding to the equation

$$\rho_0(\text{Au-Pt}) = 14.86 \sin \frac{0.6416\pi}{200} X + 5.0239$$

5.2.1

with a correlation coefficient of 0.99732; where X is at.%Pt. A

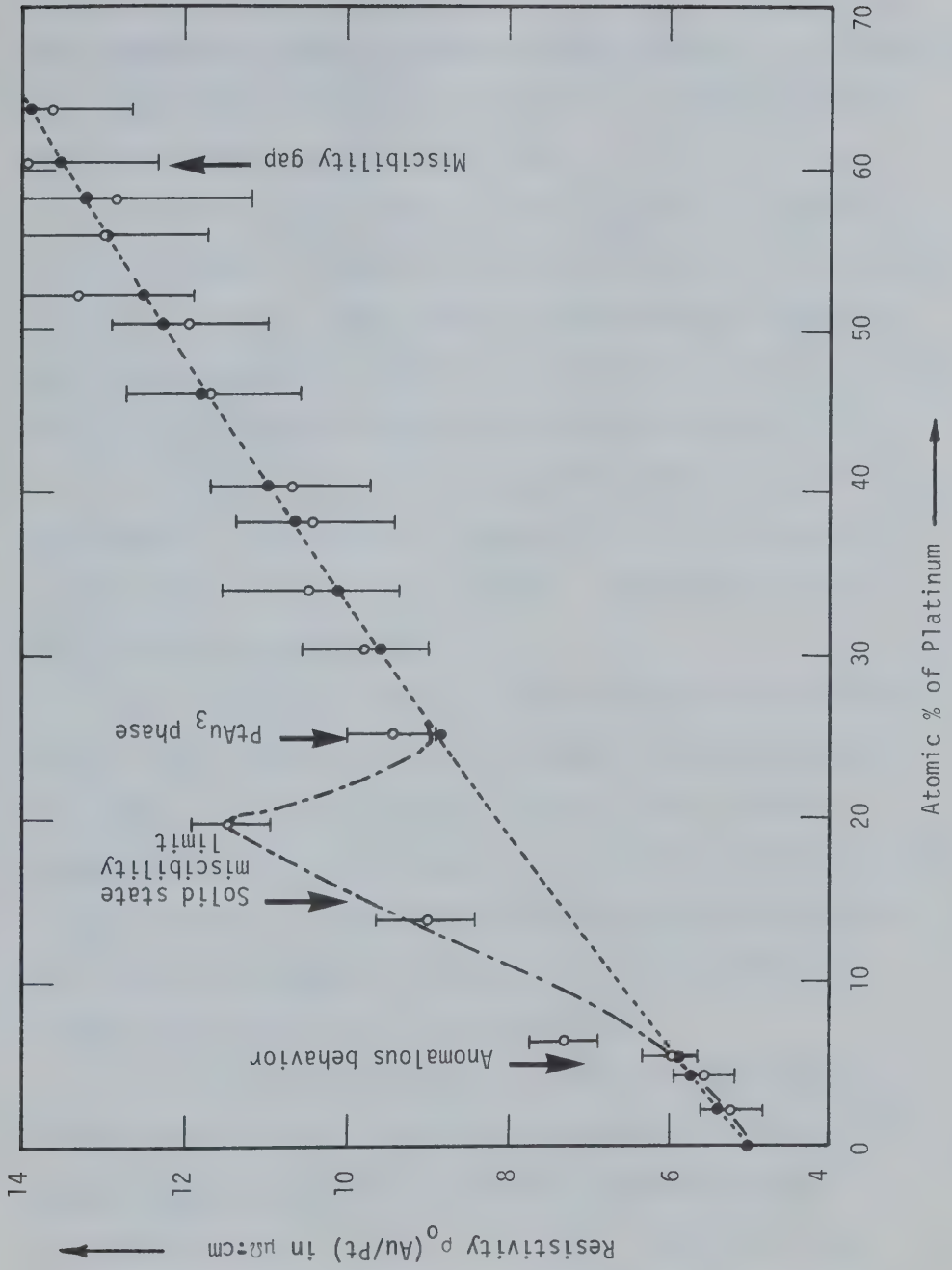


FIGURE 5.3: ρ_0 (Au/Pt) vs. at.%Pt.

value of $\rho_0(\text{Au})$ for 0 at.%Pt is seen to be $5.0239 (\sim 5) \mu\Omega\text{-cm}$ and this compares well with ρ_0 for Au-Pt films in Fig. 5.1 λ_0 corresponding to $5 \mu\Omega\text{-cm}$ "Bulk resistivity" is computed to be nearly 150 \AA from the value of 340 \AA taken by Namba [14].

(iii) Microwave sheet resistance, R_μ versus ℓ , the total (Au-Pt) thickness is shown in Fig. 5.4 for ultra-thin (~ 10 to 15 \AA thick) Au-Pt films. These values of R_μ were measured immediately after the preparation of each set of eight films. Adjusted standard error markings [86] are omitted here for the sake of clarity.

(iv) These films (iii) were aged for about one year at room temperature; R_μ was found to increase for all the films and this is also shown in Fig. 5.4 (R'_μ versus ℓ). These results confirm that alloying is taking place.

(v) The effect of annealing was studied on one of the eight films in (iv); the film showing R_μ closest to the average value was chosen. The films were pulse annealed at 25°C intervals between 50 and 350°C . $R_\mu(\text{A})$ versus the annealing temperature $T_A(^{\circ}\text{C})$ is shown in Fig. 5.5; the actual points are omitted for clarity. The films show a gradual decrease in $R_\mu(\text{A})$ with annealing upto $\sim 175^\circ\text{C}$, above 200°C $R_\mu(\text{A})$ increased rapidly.

(vi) From the above data, $\rho_\mu (= \ell R_\mu)$ was calculated for minimum values of $R_\mu(\text{A})$. $\rho_0(\text{Au-Pt})$ is computed from Eq. 5.2.1 for at.%Pt composition that corresponded to individual films.

$\rho_\mu/\rho_0(\text{Au-Pt})$ versus ℓ is shown in Fig. 5.6. The ratios ρ_f/ρ_0 indicated by the Fuchs-Sondheimer theory (Eq. 5.1.2) is reproduced for $\lambda_0 = 150 \text{ \AA}$ from values tabulated by Chopra [137]; p is taken

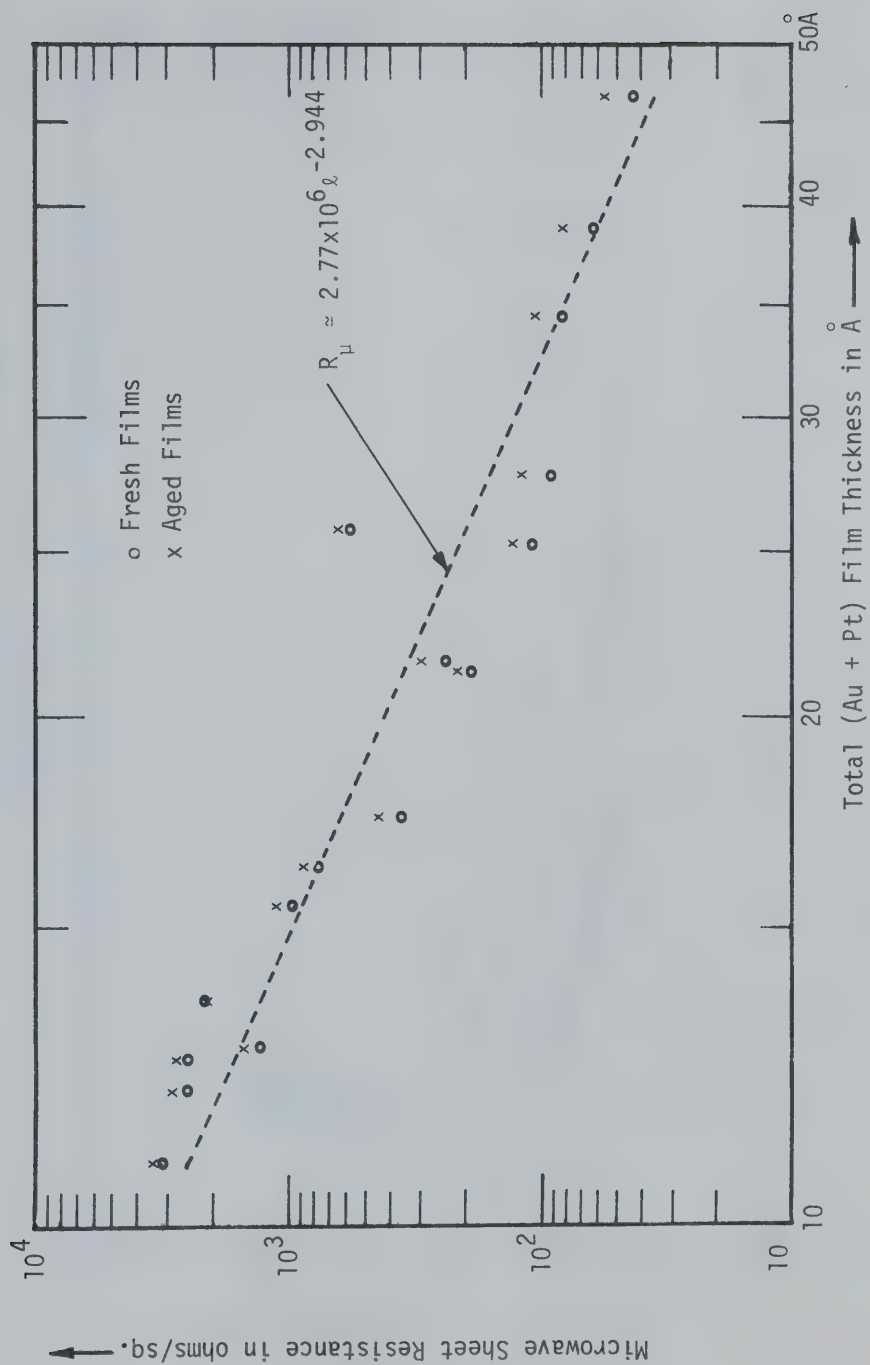


FIGURE 5.4: R_{μ} vs. d for Ultra Thin Films (Fresh and Aged)

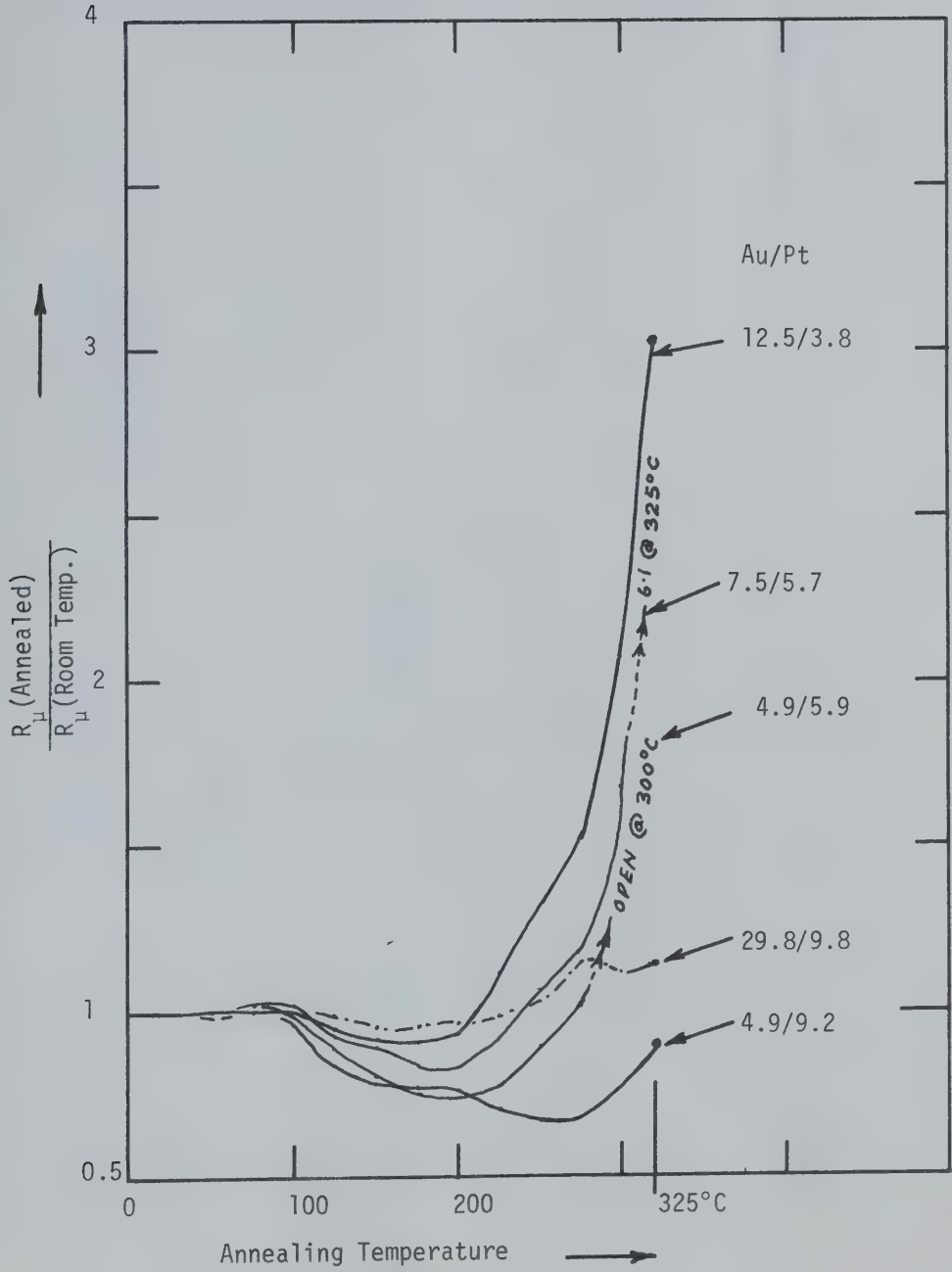


FIGURE 5.5: Annealing Effect on R_{μ} of the Aged Ultra-Thin Films

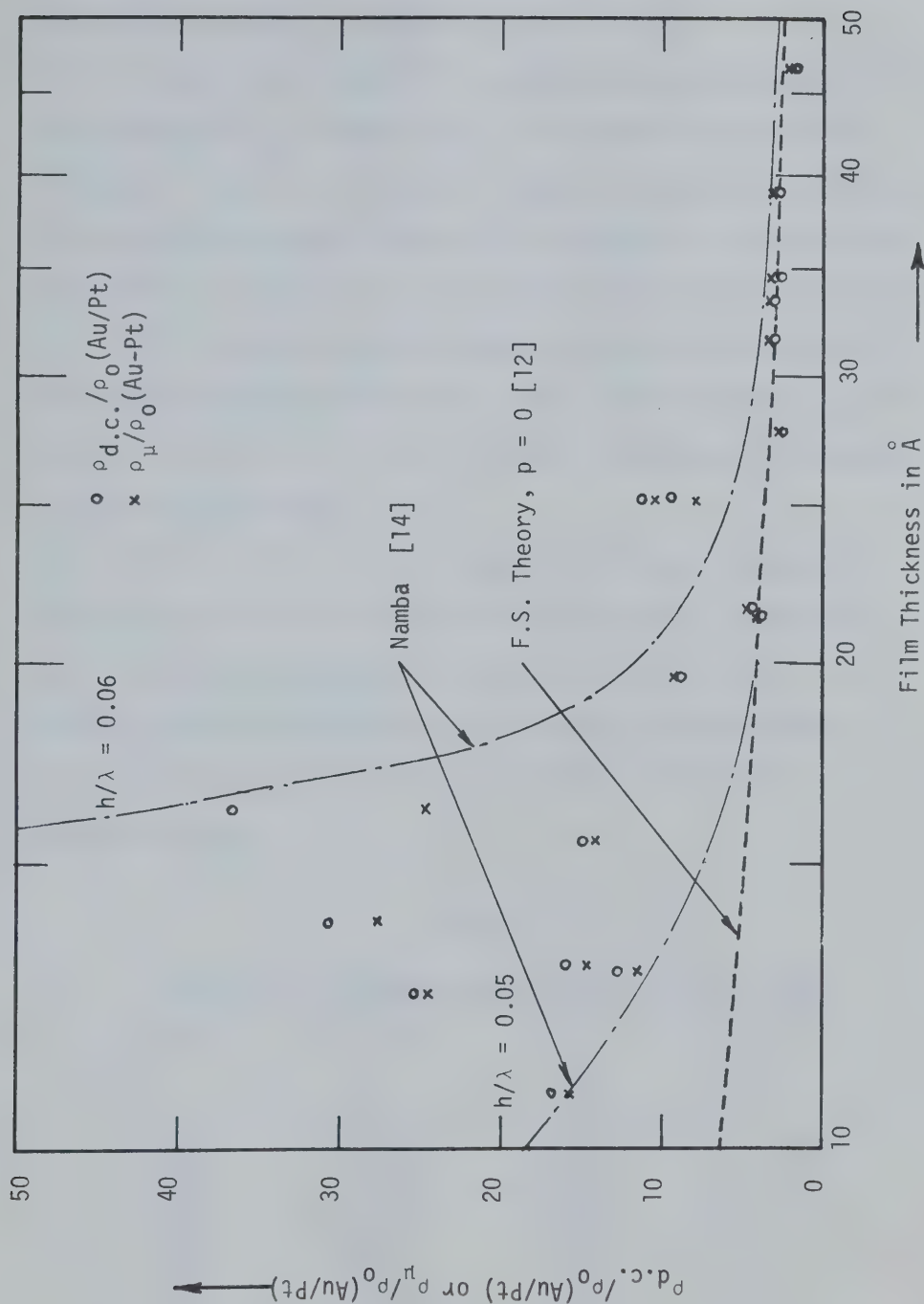


FIGURE 5.6: $\rho_u/\rho_0(\text{Au/Pt})$ and $\rho_{d.c.}/\rho_0(\text{Au/Pt})$ vs. λ .

as zero. The effects of surface roughness, h , [14] are also shown in Fig. 5.6 for $\bar{h}/\lambda_0 = 0.05$ and 0.06 .

It can be seen that all the values for $\rho_\mu/\rho_0(\text{Au-Pt})$ correspond to $h/\lambda_0 \sim 0.06$ or less. The at.%Pt composition was in general higher for the thinner films and therefore $\rho_0(\text{Au-Pt})$ was also correspondingly more, with a maximum of $\sim 14 \mu\Omega\text{-cm}$ for a 12.5 \AA film. The value of λ_0 , assumed proportional to $1/\rho_0(\text{Au-Pt})$, is $\sim 50 \text{ \AA}$. On comparison with Namba's theoretical results [14], the surface roughness amplitude, h , has a corresponding value of $\sim 3 \text{ \AA}$ for $h/\lambda_0 \approx 0.06$. This indicates a high degree of continuity of the films described.

(vii) One of the eight films in (iv) was retained as a control and the remaining six were tested for d.c. resistivity, $\rho_{\text{d.c.}}$, by depositing contacts (Chapter II, section 2.3.1). The values of sheet resistances at d.c., $R_S(\text{d.c.})$, and microwave frequency, $R_S(\mu)$, for the thinnest (10.8 \AA) Au-Pt films are tabulated below.

TABLE I

Comparison of $R_S(\text{d.c.})$ and $R_S(\mu)$ of 10.8 \AA Films

FILM No:	$R_S(\text{d.c.})$ Ω/\square	$R_S(\mu)$ Ω/\square	$\frac{R_S(\text{d.c.})}{R_S(\mu)}$
125	2.67 K	2.43 K	1.10
126	2.57 K	2.27 K	1.13
127	2.15 K	1.94 K	1.11
128	2.03 K	1.89 K	1.07
129	2.93 K	2.53 K	1.16
130	4.09 K	3.63 K	1.13

It is seen that although $R_S(\text{d.c.})$ is always larger than $R_S(\mu)$, as predicted in Ch. IV, $R_S(\text{d.c.})/R_S(\mu)$ ratios do not change materially. Since the films were only about half as thick as the minimum height of a cleavage step ($\sim 20 \text{ \AA}$) on a cleaved mica surface [74], the d.c. continuity indicates a complete absence of such a defect. It, therefore, confirms Tolansky's observations that mica cleavage faces are atomically smooth over large areas except for the hill-and-valley type surface undulations. The latter increase the path of d.c. current and hence the value of $R_S(\text{d.c.})$ as compared with $R_S(\mu)$. The results shown in Table I are also a further proof of the basic validity of Slater's theory [85] showing that the d.c. and microwave sheet resistances are identical.

Table II shows d.c. and microwave sheet resistivity of a batch of films, 21.7 \AA thick, on imperfectly cleaved mica sheets.

TABLE II
Comparison of $R_S(\text{d.c.})$ and $R_S(\mu)$ of 21.7 \AA Film;
Results for Imperfect Mica Cleavages

FILM No:	$R_S(\text{d.c.})$ Ω/\square	$R_S(\mu)$ Ω/\square	$\frac{R_S(\text{d.c.})}{R_S(\mu)}$
141	309.24	259.49	1.19
142	339.36	243.43	1.39
143	∞	229.20	∞
144	258.84	231.31	1.12
145	240.02	206.13	1.16
146	822.64	293.79	2.80

Average value of $R_S(\mu) = 243.89 \Omega/\square$.

It is seen, especially in the case of Film No. 143, that whereas the film is an open circuit at d.c., $R_s(\mu)$ is even smaller than the average value. The conclusion of Chapter IV, that surface defects do not affect microwave measurements is, therefore, supported further.

$\rho_{d.c.}/\rho_0(\text{Au-Pt})$ is also plotted on Fig. 5.6. Since $\rho_{d.c.}$ differs widely in many cases, as for example in Table III, only the minimum of the six values is chosen for each value of λ . Comparison with Namba's theoretical results [14] shows that these films also have a surface roughness amplitude of the order of 3 \AA or less. Assuming totally diffuse scattering at the film surfaces, it can be said that the films are continuous.

CHAPTER VI

EXPERIMENTS ON MERCURY DETECTION

6.1 Introduction

McNerney et al. [24] showed that the mercury detection sensitivity of gold films increased with decreasing film thickness. Since it was possible to obtain composite gold-platinum films which were highly conducting down to a thickness of 10 \AA , it was decided to test these for this practical application. The results did not meet the expectation; however, some new, hitherto unreported affects were observed [25] which justified further investigations.

6.1.1 Environmental mercury and its effects

Mercury has been used in various crafts and medicine for over a thousand years; in modern industries it has more than 3000 applications [138]. Accompanied by the resulting benefits, the toxic effects of elemental mercury and its compounds had also been recognised for some time. An example is the two hundred year old health regulation in Spain restricting workers in mercury mines to eight days per month [138]. It may be pointed out that Spain has half the world's known remaining reserves of mercury, the latter estimated at 200,000 tons [139].

Left open to the atmosphere, mercury evaporates and an

equilibrium concentration level of 20 mg Hg/m^3 of air is reached at 72°F ; this level is doubled at 93°F [140]. The effects of mercury vapor inhalation were studied as early as 1934 by Fraser, Melville and Stehle [141] who exposed dogs to 6 mg Hg/m^3 air for 8 hours a day. Death resulted from about 40 days of exposure. The exposure level of 6 mg Hg/m^3 air is only just above the recorded concentration of 1.2 to 5.9 mg Hg/m^3 of air in mercury mines [142].

The potential dangers of mercury pollution caused by industries were exposed by the Minamata tragedies in 1953. In a fishing village of this name in Japan, deaths and irreversible physical disabilities, including those in unborn children, resulted from eating fish caught in polluted waters [139,143,144]. Swedish studies on mercury pollution [145] were prompted by a noticable decrease in the population of seed eating birds and symptoms of mercury poisoning in them. These studies eventually led to banning of seed treatment by panogen and other organo-mercurial fungicides. Accidental cases of human poisoning were also noted in Iraq and a family in the USA [139] caused by eating the panogen treated wheat or the flesh of fowl and hogs fed on such seeds.

In their study of the effect of water pollution by industrial waste containing mercury and its compounds, Jensen and Jernelöv [145,146] duplicated stream bottom conditions in their laboratory. The results led to an understanding of the mechanism involved in the conversion of elemental mercury and its compounds into methyl mercury. Methyl mercury is the most toxic of mercury compounds and one of the few poisons capable of penetrating the

membrane forming the blood-brain barrier. It was found that in the oxygen free atmosphere of the sediments, certain bacteria perform the transformation process; methyl mercury then enters the aquatic food chain via the phytoplanktons and reaches ever increasing concentrations in larger fish.

In spite of the earlier knowledge of mercury hazards, it was only after the publication of Fimreite's reports on mercury contamination of fish in the great lakes [147] that the rather disproportionate "mercury scare" of the 1970-1972 period commenced. An all out effort seems to have been initiated to reduce, and eliminate if possible, all traces of mercury, particularly from the food sources. Although the urgency of the need for mercury pollution control cannot be over-emphasized, too little mercury could be as dangerous as too much [148,149].

The relative increase in atmospheric mercury during the industrial era was demonstrated by the doubling of the amounts of mercury in the ice sheets of Greenland after 1950 [150]. The industries using mercury and its compounds directly are not the only source of increase in the environmental mercury content. A comparable amount of mercury, presently about 3000 tons per year in the USA alone, is discharged into the atmosphere as elemental mercury vapor by coal burning power stations[151,152]. Coal and peat are now considered as possibly the most important sources of energy to fill the gap between increasing energy demand and energy supplied from oil, natural gas, and hydroelectric and nuclear power [153,154]. Since transportation of coal over long distances,

as for example in Canada, is not economical at present [154], it has been suggested that coal be converted into electricity and gas at the production sites and then fed into national grids. The major coal resource area, western Canada, might then become more susceptible to mercury pollution from this source. The coal reserves of this area have been estimated to be about 200 billion tons; by a conservative estimate of 1 part per million (ppm) of mercury in coal [152], there is a 200,000 ton total mercury discharge potential from this region alone - a quantity of mercury equal to the known world reserves. It is estimated that the world supply of mercury may be totally depleted during the next sixteen years at the present rate of consumption [155]. It is a possibility, howsoever remote, that fossil fuels could provide an alternative source of mercury.

6.1.2 Mercury detection

Different methods for the analysis of the mercury content of materials have been reviewed recently by Lindstedt and Skerfving [150] and include colorimetric method, atomic absorption spectroscopy, neutron activation analysis, and a micrometric method. Of these, atomic absorption spectroscopy, based upon the absorption of the ultraviolet radiation at 2537 \AA , is the most sensitive; the minimum detectable quantity of mercury is a few tenths of one nanogram. Except for the colorimetric method, which is also the least sensitive, all other methods require instrumentation that is either costly, or non-portable, or both.

McNerney et al. proposed a relatively inexpensive and portable instrument for mercury detection employing thin films of gold [24]. They used 75 to 400 Å thick gold films with chromium underlayers on glass and ceramic substrates. The sheet resistivity, R_s , of the films was between 2 to $10\Omega/\square$, with a film design to give resistance, R , between 300 to 1500Ω , giving an R/R_s ratio of 150 with a film area of 2.5 cm^2 . The films were deposited with no substrate heating and were annealed at 150°C in atmosphere. The film design produced a linear increase in resistance for amounts of mercury ranging from 5×10^{-11} to 1×10^{-7} gm; the thinner films displaying higher sensitivity. It was suggested that the saturated films be heated at 150°C for 10 minutes to release mercury so that the same films might be used repeatedly.

The present work was undertaken with a view to lowering the detection limit of mercury below 5×10^{-11} gm. This was considered desirable because only minute quantities of samples might be available for analysis in certain cases, for example organs of very small fish or human hair. Since gold on platinum films were found conducting to a thickness as low as 10 Å [62], these were tested because McNerney et al. predicted higher sensitivity for thinner films [24]. In a preliminary investigation [25] it was found that alloying due to interdiffusion of either platinum or silver into gold, particularly on annealing but also just by aging, drastically reduced the sensitivity. McNerney et al. encountered similar problems on heating gold films on chromium underlayers above 150°C [24,157]. Joyner and Roberts [158], on the other hand,

have shown that total desorption of mercury from gold surfaces occurs at about 177°C. This is, then, the annealing temperature range required if the films can be used repeatedly.

6.2 Experimental Methods

6.2.1 Films for mercury detections and the film holder

Following the results of preliminary investigations [25], the films selected for mercury detection were of two types. One was the composite film of gold on either platinum or silver nucleating layers; the film thicknesses being about 110 Å with about 10 Å thick nucleating layers. The other type comprised 55 to 420 Å thick, pure gold films. The film deposition procedure is outlined in Section 2.6. During deposition the substrates were not heated.

The film geometry was designed to keep an R/R_s ratio of 150; this is the ratio used by McNerney et al. [24]. The film area was about 6 cm² as compared to 2.5 cm² selected by these authors. Larger film area permits increased saturation limit [24]. Other film geometries tested gave R/R_s ratios of 0.5, 10, and 47 with film surface areas of 3.23, 10.04 and 9.13 cm² respectively. The sensitivity was found to decrease for smaller R/R_s ratios even for larger film areas in films corresponding to R/R_s equalling 10 and 47. It was not possible to obtain R/R_s value larger than 150 because of machining difficulties in preparing masks.

The film holder, shown in Fig. 6.1, was designed so as to

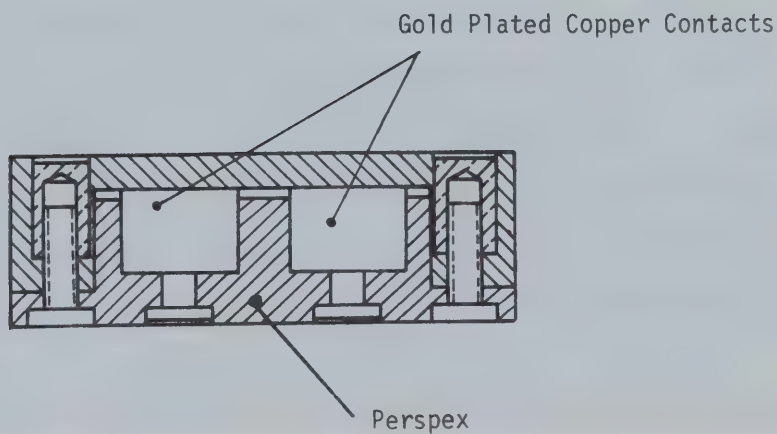
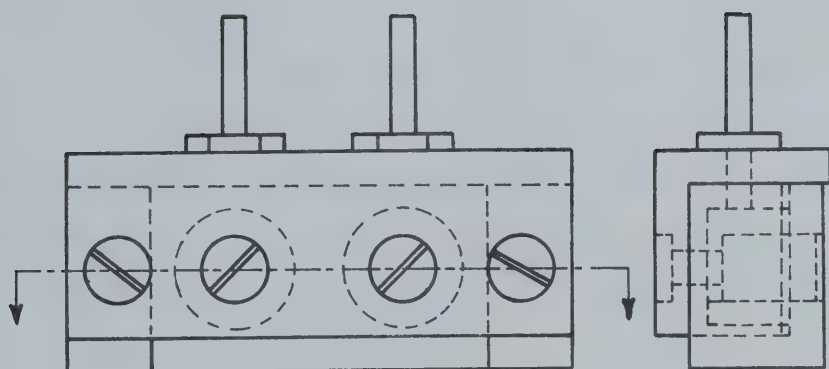


FIGURE 6.1: Film Holder for Mercury Detection.

avoid exposure of metallic parts other than the sensor area of the film to the carrier gas. Since mercury amalgamates with all metals except platinum and iron, this design prevented any loss of sensitivity due to mercury adsorption on unwanted surfaces. The photograph of the film holder and its method of placement in the cell housing is shown in Fig. 6.2.

The inlet of the carrier gas, N_2 , to the glass cell was arranged in the form of a right-angle nozzle to cause turbulent flow of N_2 in order to increase its contact with the film. Although no experiments to determine the efficiency were performed, a flow rate of 200 ml/min was used. McNerney et al. reported about 85% adsorption at this flow rate.

6.2.2 System description

The mercury detection apparatus employing the principle proposed by McNerney et al. [24] is shown in Fig. 6.3. Mercury is released with dry nitrogen from standard samples [159] containing 0.1 μg of mercury in the aerator tube. The drying agents, magnesium perchlorate (MgClO_4) and ascarite (A.H. Thomas Co., Philadelphia), remove moisture and acid vapors from the carrier gas. The acid removal is necessary because gold films have been found sensitive to H_2S [24].

Mercury is removed from the N_2 -stream entering the reference arm of the bridge by gold coated glass wool. This was found more satisfactory and convenient than PbCl_2 on glass wool used by McNerney et al., particularly since mercury can be desorbed from

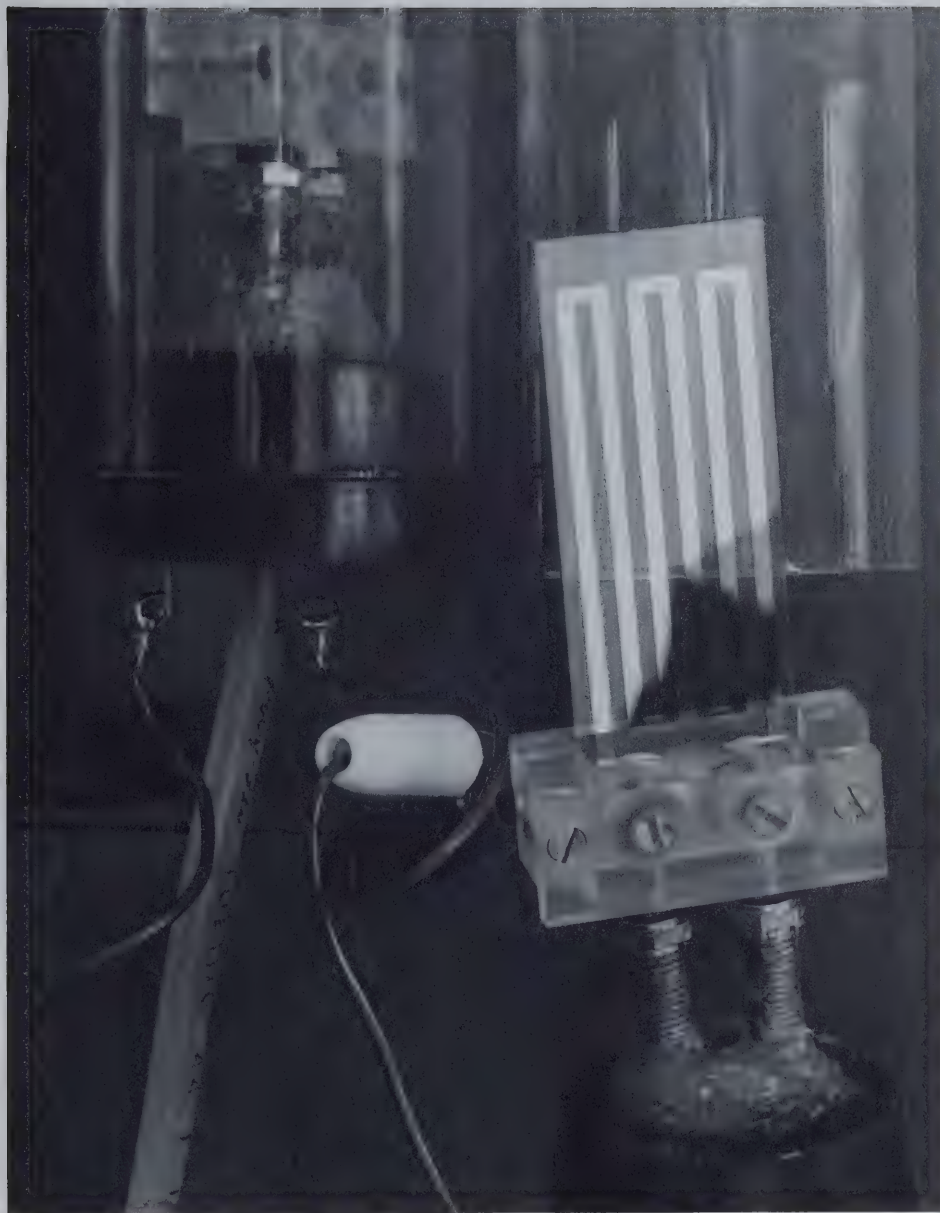


FIGURE 6.2: Film Holder with Mercury Detection Film and its Placement in Cell Housings.

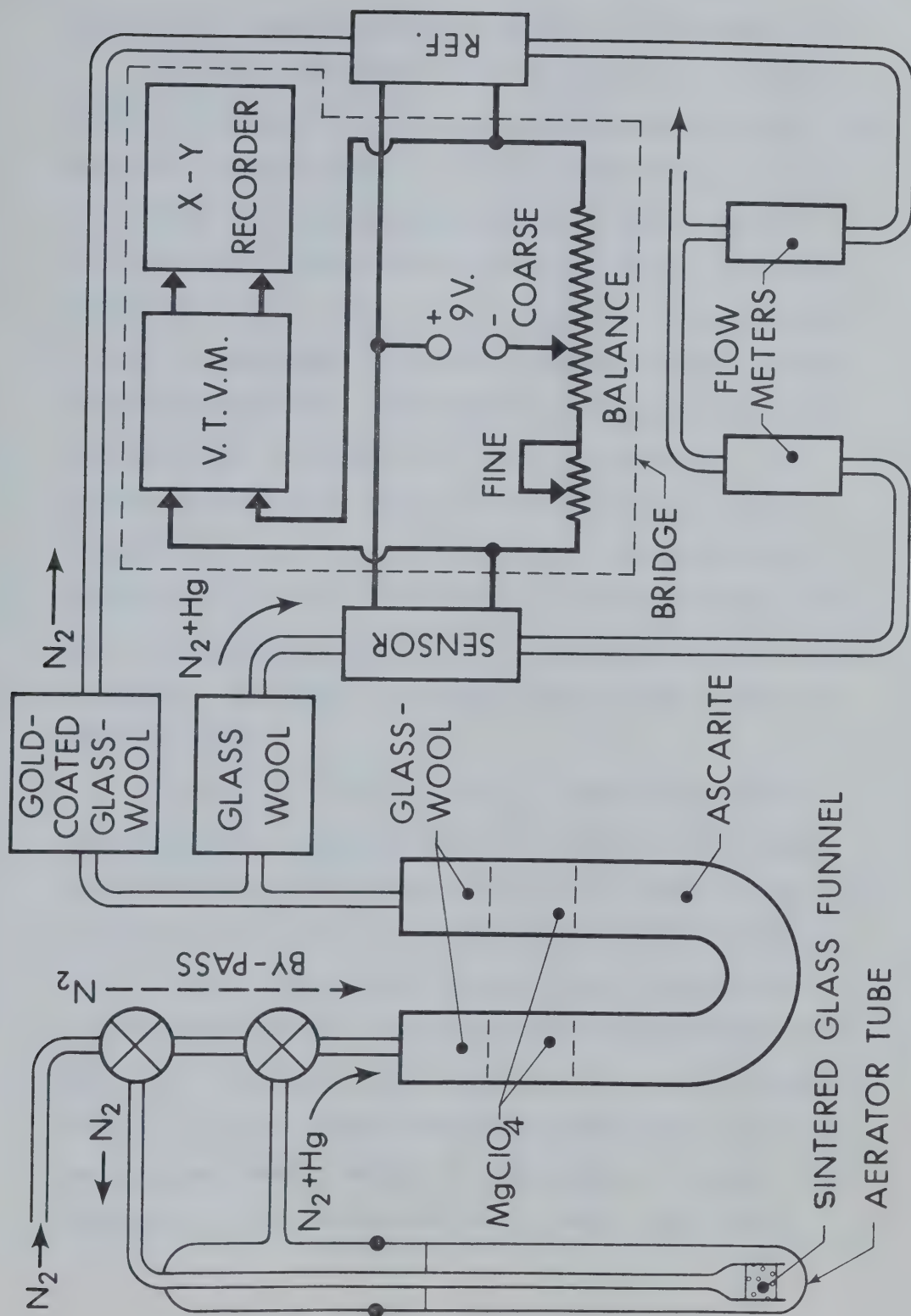


FIGURE 6.3: Schematic Diagram of Mercury Detection Apparatus.

saturated gold coated glass wool by heating in air at about 175°C.

The sensor and reference films form two arms, R_1 and R_2 , of a Wheatstone bridge. The other two, balancing arms, R_3 and R_4 , are made up of a center-tapped 2 K Ω , 10 turn potentiometer in series with a 100 Ω , 10 turn potentiometer used as a variable resistor; the latter permits fine control of the bridge balance. A multi-range (10 μ v to 1v) vacuum tube voltmeter (Hewlett Packard Model 423A d.c. microvoltmeter) was used as a detector. After placing the films in their cells, the bridge was initially balanced with the VTVM in the 1 volt range using the 2K potentiometer. Fine control was subsequently used to balance the bridge in the final working range of 0.3 to 3 mv. This range was found suitable for calibration of 55 to 419 \AA films with 0.1 μ g standard samples. The lower ranges were necessary for films of the extreme lower and upper thicknesses. The bridge was balanced after each test by means of the fine control.

The choice of 9 volts for the d.c. supply was prompted by the availability of dry batteries in this range. Higher voltages can be used for increasing the sensitivity. The upper voltage limit is governed by the maximum permissible current density through the films to prevent failure either by joule (ohmic) heating or by electromigration [160]. It can be seen that for a 2 mm wide, 100 \AA thick film, a current of 2 mA is equivalent to a current density of 10^4 A/cm²: this is normally the maximum current density level that can be achieved without melting the bulk samples. In case of films, substrates are very effective heat sinks so that joule heating

causes about 10 to 20°C temperature rise for a current density of 10^6 A/cm^2 [160]. With large surface area to volume ratio for decreasing film thickness, the film cooling on the surface exposed to the airstream is also more effective. Thus current densities of 10^4 A/cm^2 are permissible, for example, thin film interconnections in integrated circuits operate at current densities of about 10^6 A/cm^2 .

It can be shown by a simple analysis that for a small change ΔR in the resistance R_1 of the sensor film ($\Delta R \ll R_1$), the detector voltage is directly proportional to ΔR .

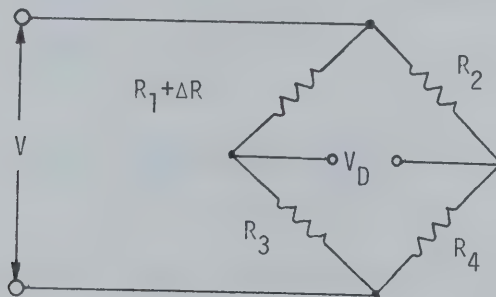


FIGURE 6.4: Bridge Circuit for Derivation of V_D versus ΔR .

In Fig. 6.2, initially, without ΔR , the bridge is balanced, hence

$$R_1/R_3 = R_2/R_4 \quad \text{or} \quad \frac{R_3}{R_1} = \frac{R_4}{R_2}$$

and let

$$A = 1 + \frac{R_3}{R_1} = 1 + \frac{R_4}{R_2} \quad . \quad 6.1$$

With an increase $\Delta R \ll R_1$, the detector voltage V_D is given by

$$\begin{aligned} V_D &= V \left\{ \frac{R_1 + \Delta R}{R_1 + R_3 + \Delta R} - \frac{R_2}{R_2 + R_4} \right\} \\ &= V \left\{ \frac{1 + (\Delta R/R_1)}{A + (\Delta R/R_1)} - \frac{1}{A} \right\} \\ &= \frac{V(A-1)}{A^2 R_1} \Delta R \left\{ 1 + \frac{\Delta R}{AR_1} \right\}^{-1} \end{aligned}$$

Expanding $(1 + \Delta R/AR_1)^{-1}$ binomially and ignoring second and higher order terms in $\Delta R/AR_1$, we get

$$V_D \approx \frac{V(A-1)}{A^2 R_1} \Delta R \left\{ 1 - \frac{\Delta R}{AR_1} \right\} \quad 6.2$$

McNerney et al. (1972) give a value of 4×10^{-5} for fractional resistance change for 1 ng. of Hg. Saturation occurs at 100 ng. If $R_1 = 1 \text{ K}\Omega$, this gives a resistance change of 4Ω on saturation; or in Eq. 6.1, with $A = 2$, $[(A-1)/A^2]$ is maximum for $A=2$, $\Delta R/AR_1 = 0.002$. Ignoring this term in Eq. 6.2, maximum error is 0.2%. Hence we may again write, after substituting for A,

$$V_D \approx \frac{VR_3}{(R_3 + R_1)^2} \Delta R$$

V_D is recorded on the X-Y recorder as deflection D or D_A for unannealed and annealed films, respectively. The measurement of the

absolute value of ΔR , a more complicated process, is therefore not necessary for calibrating the instrument. The ratio D_A/D was used to indicate relative performance of the films with annealing. D_A/D can equally well be replaced by $\Delta R_A/\Delta R$, where ΔR_A is the resistance change of the annealed sensor film.

The aerator tube was bypassed when not in use to keep N_2 flowing through the system. This stabilized the temperature of the reference and sensor films and hence minimized the instrument drift. Any residual mercury was also flushed through the system.

6.2.3 Standard samples

The calibration was performed using 0.1 μg of mercury per 5 ml of sample, a pH balancing solution, and a reducing agent. De-ionized distilled water and reagent grade chemicals were used to prepare these solutions as described below:

(a) A 500 μg Hg/ml standard stock solution was prepared by dissolving 0.6767 g of mercuric chloride (HgCl_2) in 2 ml concentrated HCl and diluting this to make 1 litre.

(b) The acidity of the standard was balanced by a 20% weight/volume (w/v) solution of hydroxylammonium chloride ($\text{NH}_2\text{OH} \cdot \text{HCl}$) solution obtained by dissolving 20 g of this chemical in 100 ml water.

(c) The reducing agent was 10% (w/v) stannous chloride solution. 25 g $\text{SnCl}_2 \cdot \text{H}_2\text{O}$ was dissolved in 50 ml concentrated HCl and diluted with water to make 250 ml. (This solution should be stored over metallic tin to be kept for a long time. It is otherwise

dissociated and this is indicated by the pale yellow coloring of the solution typical of chlorine).

Immediately before use, the working solution containing $0.1 \mu\text{g Hg}/5\text{ml}$ was prepared by adding 0.1 ml of the standard stock (a) to 500 ml water. 5 ml of this solution was pipetted into a test tube, with 0.3 ml of solution (b) and 0.1 ml of solution (c) added. The test tube was then put promptly in the aerator system.

6.2.4 Decay of $0.1 \mu\text{g Hg}/5 \text{ ml}$ solution with time

Weak solutions of inorganic compounds are generally in a dissociated, ionized state. The mercury content of the standard solution decayed rapidly by surface evaporation of mercury. This decay phenomenon was observed for solutions stored in the following forms:

- (a) Stored in 500 ml volume and occasionally stirred,
- (b) Stored in 500 ml volume and stirring only due to pipetting, and
- (c) Stored in 5 ml quantities in test tubes.

The mercury content of these samples with time is shown in Fig. 6.5. Sample (b) was found more stable than sample (a), whereas (c) decayed the most rapidly. The analysis of one sample takes about 3.5 minutes and significant decrease of mercury content in either (a) or (b) was observed after 5 or 6 tests. This was generally the number of test results used for calculating averages and adjusted standard errors.

The errors due to the decay phenomenon can be minimized by

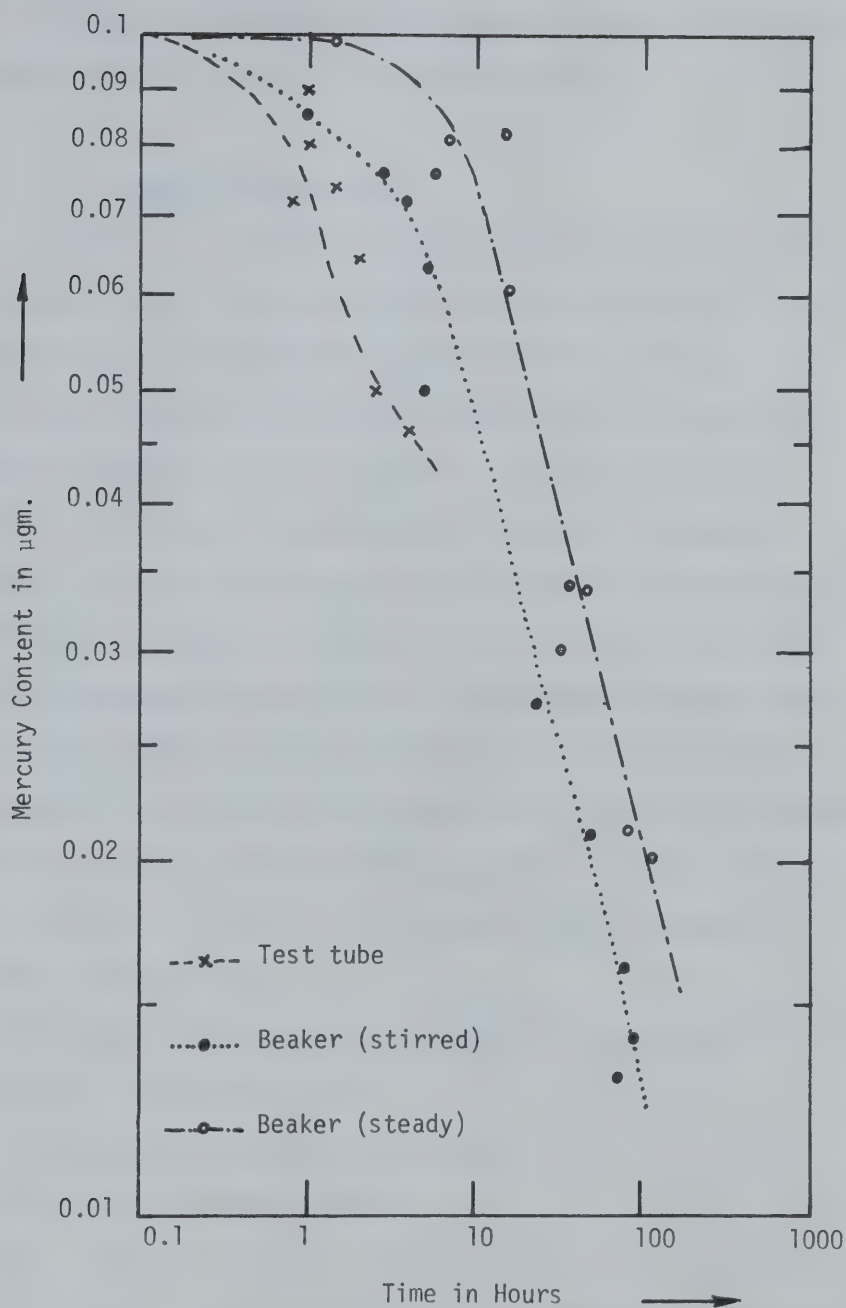


FIGURE 6.5: Decay of Mercury Content of $0.1 \mu\text{g.Hg}/5\text{ml}$ Standard with Time.

- (1) commencing the tests immediately after preparing the solution,
- (2) stirring the solution as little as possible, and (3) pipetting the sample from near the bottom of the container.

6.2.5 Summary of precautions

Stability of the rate of airflow through the film housing is the most critical factor in obtaining consistent results. Also, identical rate of flow through the sensor and the reference film cells is required to maintain equal temperature of the two films. Hence the flowmeters must be accurately calibrated and stable; these would constitute the most expensive items in a commercial instrument. The airflow rate may also vary due to crystallization of MgClO_4 upon absorption of moisture, causing greater resistance to airflow through the drying tube. This was seen by the necessity to adjust the airflow rate after about 20 tests. As about 200 tests were required for each annealing temperature, it was found convenient to place an auxiliary tube with MgClO_4 between the valves and the U-tube in Fig. 6.1. This tube could be easily replaced upon saturation with moisture.

The effect of carrier gas flow rate over the films on sensitivity is shown in Fig. 6.6.

Other possible sources of error are

- (1) Supply voltage stability,
- (2) Subjective error in preparing and pipetting samples,
- (3) Delay in aerating the sample after adding the reducing agent, and

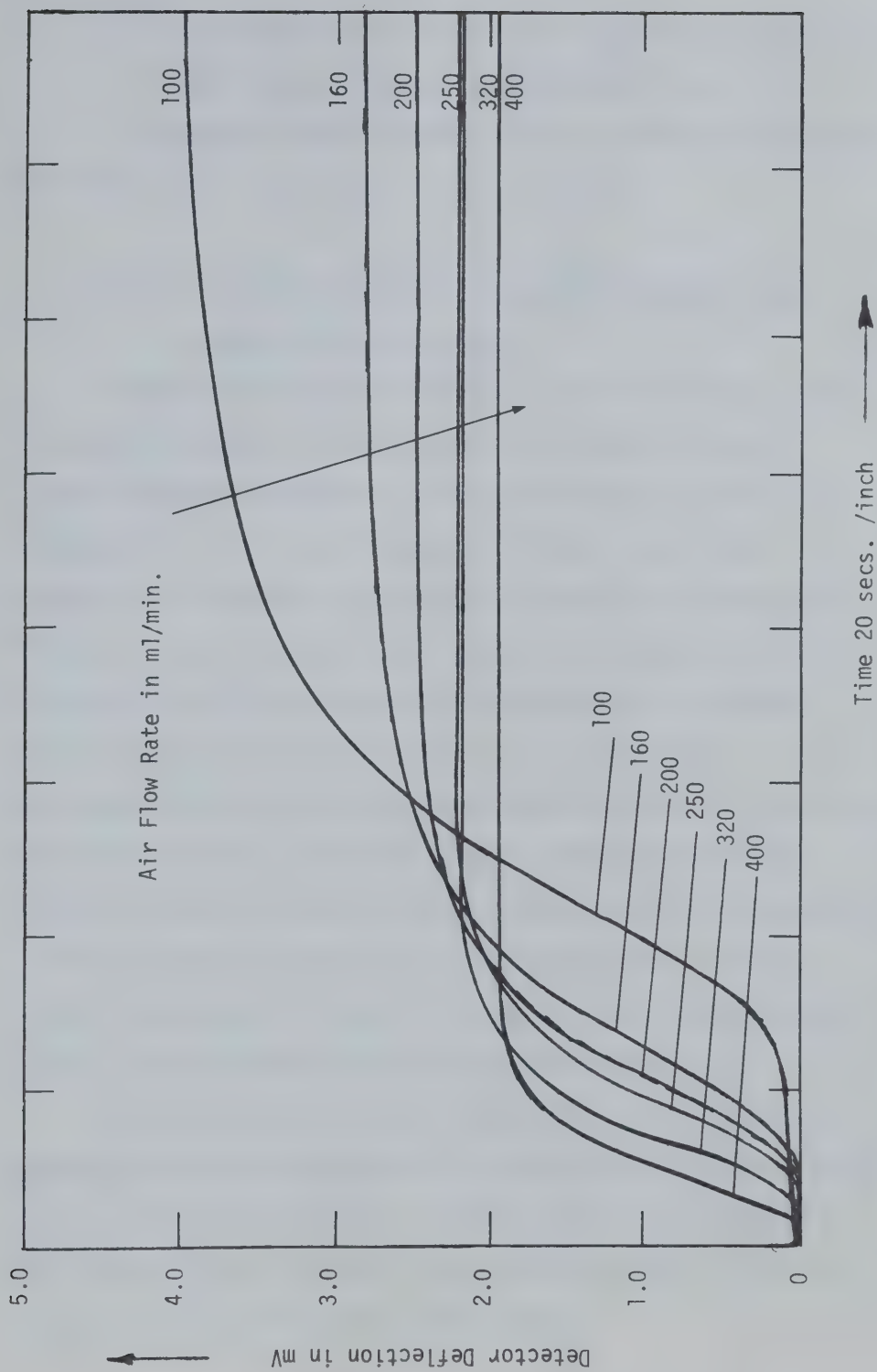


FIGURE 6.6: Air-Flow Rate vs. Sensitivity of Mercury Detection.

- (4) Instrument drift if there is a large difference in the resistances of sensor and reference films.

The maximum adjusted standard error by averaging six results was within $\pm 5\%$ in most cases for 0.1 μg samples.

6.2.6 Extraction of mercury with gold films from weak aqueous solution of HgCl_2

These experiments were performed to ascertain whether gold films might be used to extract mercury from weak solutions of inorganic mercury compounds. It has been pointed out [161] that irrespective of the form of mercury poisoning, that is, by inhalation of elemental mercury vapor or ingestion of organic and inorganic mercury compounds - the excretion of mercury via blood circulation in the form of sweat or urine occurs as inorganic mercury compounds. The human kidney is very inefficient in filtering out mercury, resulting in the accumulation of mercury in the kidney as well as the liver. These two organs, along with the brain, lymph nodes and peripheral nervous system are the most affected by mercury poisoning. A possibility, therefore, exists to enable removal of mercury from the bloodstream with the use of otherwise neutral gold in a form similar to dialysis machines.

The films similar to those used in the mercury detection apparatus were first immersed in distilled water, then taken out and dried. No resistance change was indicated due to this procedure. The films were next immersed in HgCl_2 solution, rinsed in water, dried and checked for any resistance change.

6.3 Results

The average resistance, sheet resistance and resistivity at d.c. of 55 to 419 \AA thick gold films versus the film thickness are shown in Fig. 6.7.

The affect of annealing gold-on silver and gold-on-platinum films was studied. Fig. 6.8(a) shows the relative sensitivity, D_A/D , of these films for various annealing temperatures, T_A . The relative resistance, R_A/R vs. T_A is shown in Fig. 6.8(b) where R_A and R are, respectively, the film resistances of annealed and unannealed films.

The results as above, for 55 to 419 \AA gold films are shown in Fig. 6.9 (D_A/D vs. T_A) and Fig. 6.10 (R_A/R vs. T_A). Adjusted standard error markings are omitted for the sake of clarity, these being within 5% for D_A or D . The variation of sensitivity with film thickness for 0.1 ug mercury after the 175°C anneal are shown in Fig. 6.11.

The change in resistance of one gold film, 199 \AA thick, upon three successive immersions in HgCl_2 solution containing 500 micro-gram Hg in 500 ml is shown below in Table III; resistances are in ohms.

TABLE III

Initial Film Resistance.	Res. after immersion in distilled water	Res. after immersion in HgCl_2 solution		
		First 30 seconds	Second 30 seconds	Third 30 seconds
474.34	473.13	475.85	476.60	477.88
Total Resistance Increase		1.51	2.26	3.54

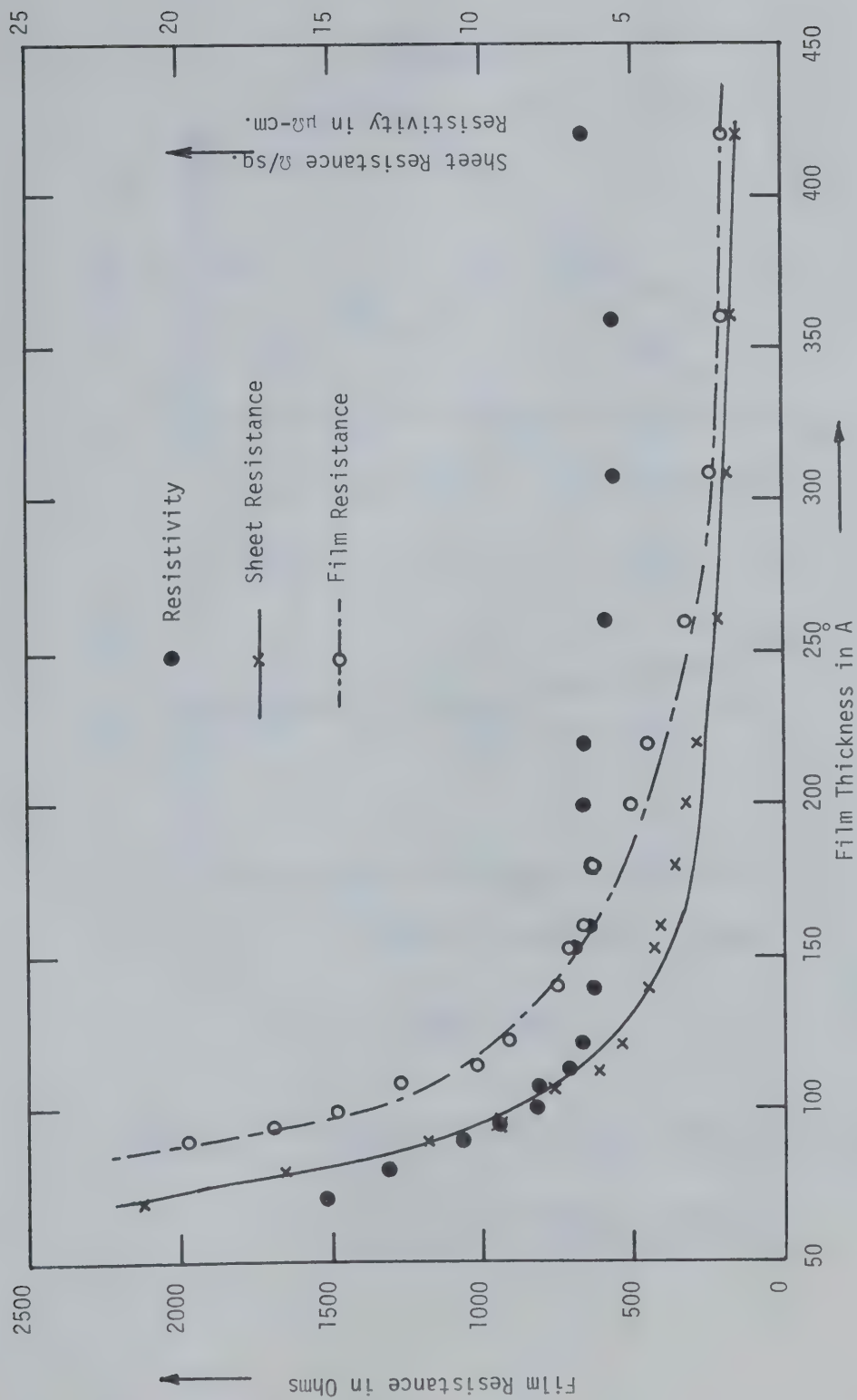


FIGURE 6.7: R and R_s vs. Thickness of Films for Mercury Detection.

FIGURE 6.8(a)

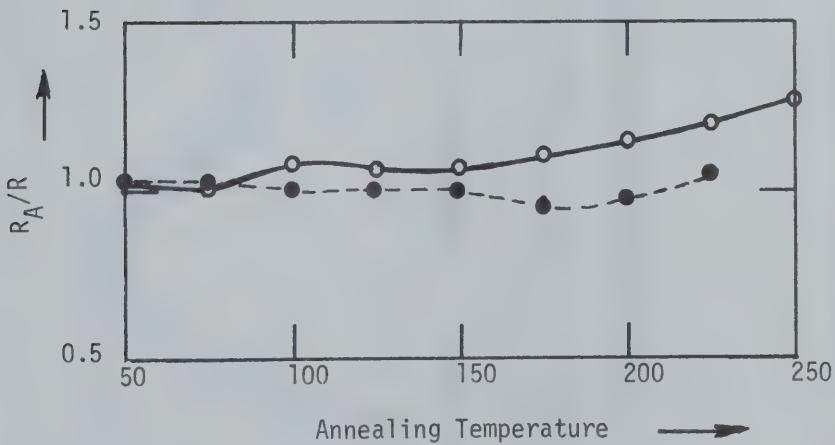
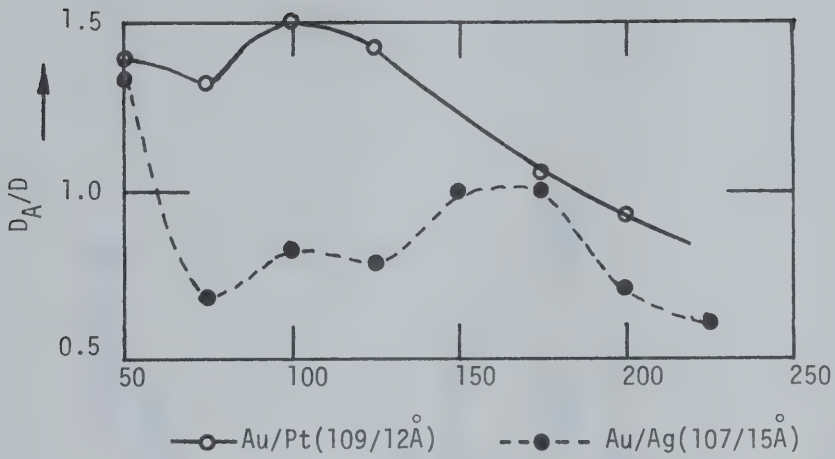


FIGURE 6.8(b)

- FIGURE 6.8: (a) Normalized Sensitivity of Composite (Au-Ag and Au-Pt) Films vs. Annealing Temperature.
 (b) Normalized Resistance vs. Annealing Temperature for the Composite Films.

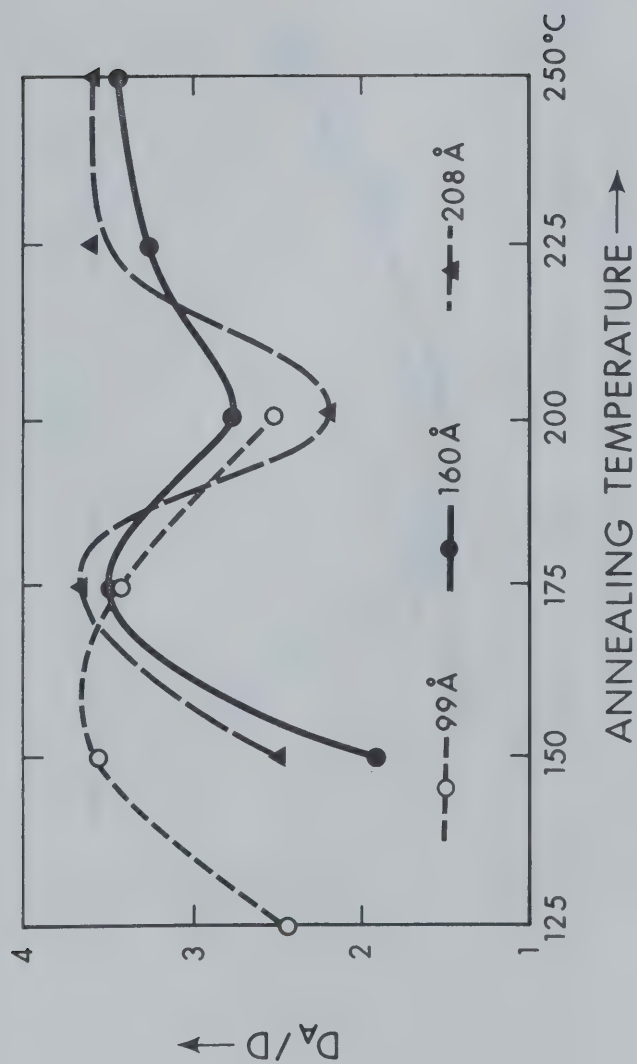


FIGURE 6.9: Normalized Sensitivity vs. Annealing Temperature of Pure Gold Films.

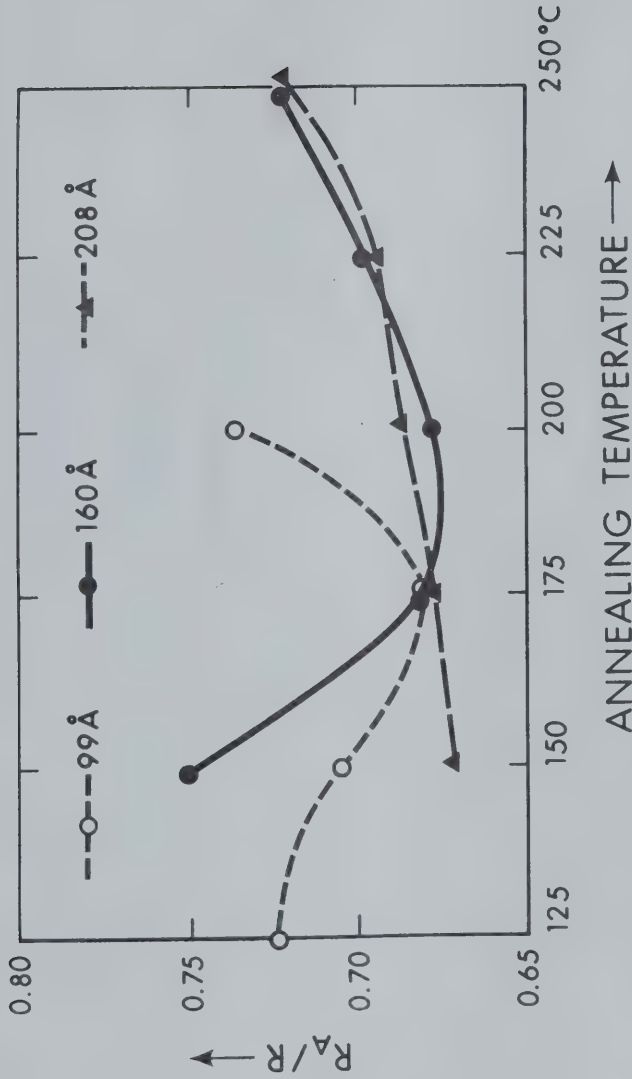


FIGURE 6.10: Normalized Resistance vs. Annealing Temperature of Pure Gold Films.

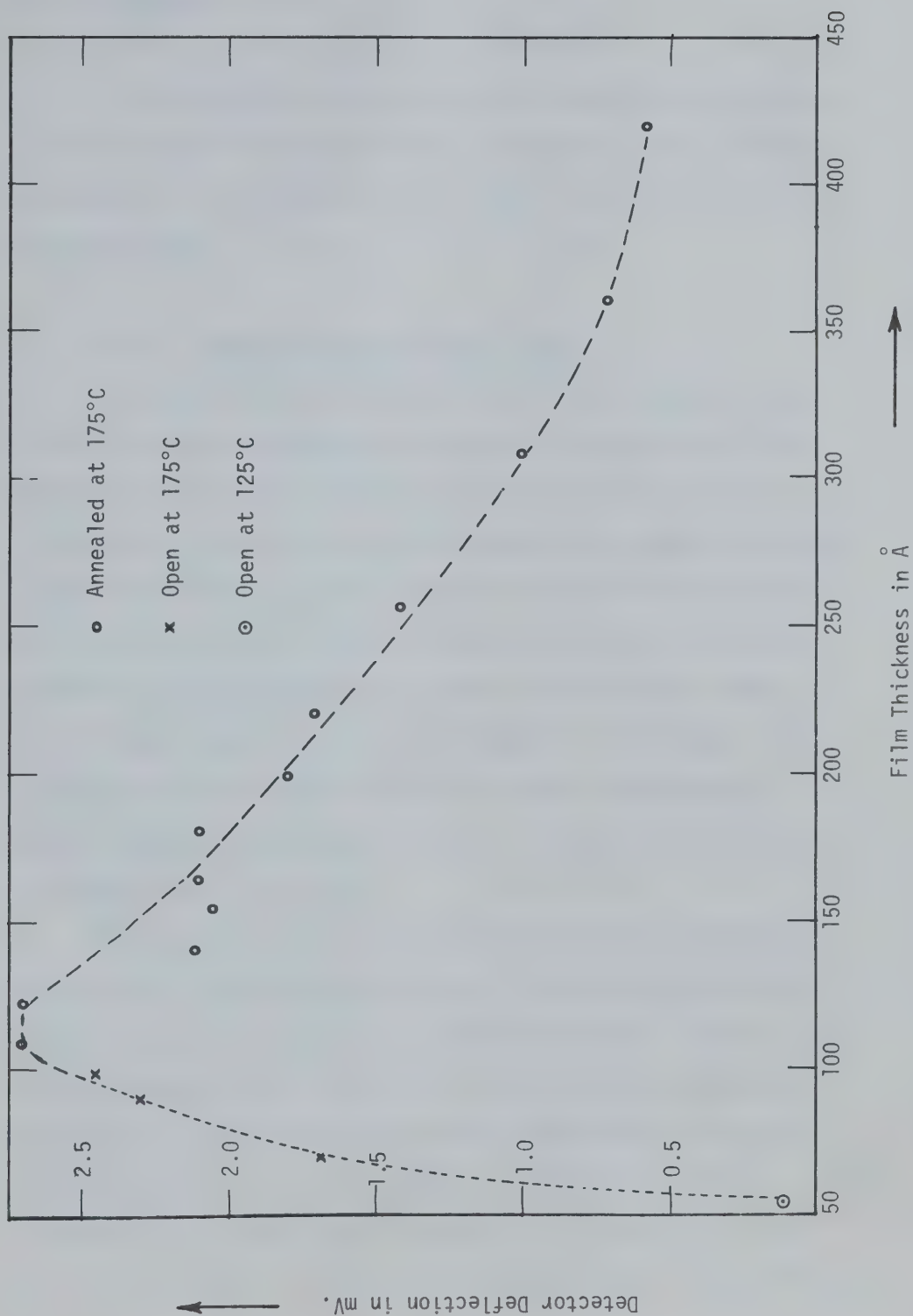


FIGURE 6.11: Sensitivity vs. Film Thickness of Gold Films Annealed at 175°C.

6.4 Discussion

In the following discussion, the term sensitivity is used to denote the relative magnitude of ΔR as indicated by the recorded deflection of the detector, D or D_A , from the null position of the balanced bridge.

6.4.1 Composite Au-Pt and Au-Ag films

The composite gold-on-platinum or silver nucleating layers (Au-Pt or Au-Ag) display higher conductivity even below 50 \AA , the thickness at which pure gold films become non-conducting [52,56]. The mercury detection sensitivity of these films, however, decreases progressively with aging and annealing. The 60 \AA Au- 10 \AA Pt and 50 \AA Au- 10 \AA Ag films showed decreasing sensitivity with aging, the sensitivity became negligible on annealing these films at 100°C [25]. These results indicated that alloying of the surface layer with the nucleating layer material (Pt or Ag) is the cause of desensitization to mercury adsorption. This effect was also noted by McNerney et al. [24,158].

Observations on 107 \AA Au- 15 \AA Ag and 109 \AA - 12 \AA Pt (Figs. 6.8(a) and (b)) confirm these results. The loss of sensitivity on annealing these films even above 150°C is not total. The films have 8 atomic percentage (at.%) of Ag and 11 at.% of Pt in the total material, the diffusion distance is also larger than the thinner composite films. The results appear to indicate that loss of sensitivity is dependent upon the amount of alloying material as well as the degree of alloying of the surface layer by interdiffusion

at various temperatures.

In this case, the mercury detection sensitivity is thus a function of two distinct processes: (1) diffusion in thin film couples, and (2) annealing characteristics of the films. The annealing of films controls stress patterns, re-crystallization and consequently the structure of the films [9,103].

6.4.1.1 Diffusion processes

The study of diffusion in thin films [132,154] and particularly on gold films deposited on platinum [64,133] has been a subject of recent publications because these films are used as reliable interconnections in integrated circuits [63,64]. Diffusion in pure metals and alloys has been reviewed by Peterson and Chen [162] and it is noted that self-diffusion leading to recrystallization and smoothing out of structural defects occurs even at low temperature in thin films [163]. The aging can thus have a significant effect on the properties of either pure or composite films stored even at room temperature.

The diffusion process is accelerated at higher temperatures, its rate at any particular temperature depending upon the metals-pair. This need not necessarily lead to the formation of a uniform alloy because of (i) the miscibility gaps at different at.% compositions, especially for platinum and gold [164] resulting in discontinuous concentration drops, and (ii) surface enrichment tendency even in dilute alloys, more so at elevated temperatures [165]. The latter phenomenon has been utilized to obtain perfectly pure

surfaces for analysis by electron diffraction and Auger electron spectroscopy [166].

The process of diffusion in alloys of different at.% compositions is thus complex. It can, however, be concluded that the surfaces of composite films become alloyed even to a degree inconsistently higher than the overall composition. The consequence is decreased mercury adsorption efficiency on the film surface and hence loss of sensitivity. The rate of diffusion can be seen to be higher in the Au-Ag films as compared to that in Au-Pt films. This is indicated by the more pronounced loss of sensitivity in the Au-Ag film at lower annealing temperatures. Au-Ag alloys have no miscibility gaps and uniform solid solutions of the two metals can be obtained at any at.% composition [164,167,168].

6.4.1.2 Effect of annealing on the mechanical properties of thin films

A well recognised feature of annealing is the improvement of the film texture by smoothing out of the structural defects like stacking faults, vacancies, dislocations; this results in reduced resistivity [9]. X-ray analysis shows that annealing increases crystalline parts and relaxes the crystal stress [169], an effect also predicted theoretically [170]. Annealing behavior of thin gold films has also been reported recently by White [171]. These and other studies [169-172] indicate the following mechanical properties of thin films:

Metal films, in general, are under tensile stress of the order of 10^9 to 10^{10} dynes/cm²; this magnitude of stress is comparable to the yield strength of most bulk metals [172]. The stress reaches a minimum on annealing up to a certain temperature and then increases again as the films are cooled down from a higher temperature [173]. Small cracks eventually appear at the dislocation sites, resulting in stress relief. The shear stress at the film-substrate interface due to different thermal expansions increases for thicker films. If the film does not peel off (as happens for films a few thousand angstroms thick) stress relief may also occur, besides fracture, by plastic flow. This happens when stresses are greater than the yield strength of the films.

6.4.1.3 Effect of annealing on the sensitivity of composite films

The stress pattern dependence on annealing temperature is reflected in the mercury detection sensitivity of Au-Ag and Au-Pt films as seen in Fig. 6.8(a). These, as also the pure gold films, show that (i) the sensitivity increases up to an optimum annealing temperature in the 175°C range, (ii) decreases to a low value around 200°C, and (iii) recovers subsequently at about 250°C as stress relief occurs.

6.4.1.4 Effect of annealing on the resistance of composite films

The resistances of the composite films [Fig. 6.8(b)] are

relatively less effected by annealing than the mercury detection sensitivity. The improvement in conductivity by annealing [9] appears to be offset by the increased resistivity on alloying [164] as diffusion produces an alloy of higher composition at increasing temperatures [64,133,162].

6.4.2 Effect of annealing on pure gold films

6.4.2.1 Resistance of pure gold films

The resistance of 55 to 419 Å films decreases on annealing [Fig. 6.10] as postulated by Vand [9]. It also proves that the adhesion of electron beam evaporated films and their texture is superior to the films deposited by resistance heated sources [101].

6.4.2.2. Relative sensitivity of pure gold films

Except for the 55 Å film, D_A/D improves with annealing upto a critical temperature range around 175°C. This is both as a result of (1) recrystallization and smoothing out of structural defects [9,169] and (2) stress relief [170,174]. It may be concluded that surface sensitization to mercury adsorption occurs for films under the two optimum conditions. D_A/D decreases to a low value at about 200°C. Compared to about 5% change in film resistance, the decrease in sensitivity is nearly 200% or more for thicker ($\lambda > 200$ Å) films. Since the stress increases with film thickness [169], D_A/D appears proportionately reduced. Subsequent annealing at higher temperatures causes fracture or plastic flow and hence stress relief [172] resulting in the recovery of sensitivity above 250°C.

The film eventually fails due to fracture; d.c. open circuit results above 300°C.

To summarize, it is reasonable to assume that the increase in resistance of gold films depends essentially on the amount of mercury adsorbed. It may then be concluded that the adsorption efficiency of the films for free mercury contained in the N_2 -stream is adversely affected by alloying and stress, whereas improved film structure increases this efficiency.

Fig. 6.11, showing sensitivity versus film thickness, indicates that films in the thickness range of 100 \AA are the most sensitive. The optimum annealing temperature of 175°C is also one at which total desorption of mercury occurs [158]. Hence the most suitable films for mercury detection appear to be of pure gold, having a thickness of about 100 \AA and annealed at 175°C.

6.4.3 Adsorption of mercury from aqueous solutions

The continuous increase in film resistance upon successive immersions in $HgCl_2$ solutions, Table III, indicates adsorption of mercury. For bulk gold surfaces, saturation occurs upon a monolayer coverage ($\sim 4.6 \times 10^{15} \text{ atoms Hg/cm}^2 \text{ Au}$) [158]. This is equivalent to about 0.3 \mu g/cm^2 . The absorption area available in films is 10 to 100 times greater than in bulk [159] so that using films for this application is more efficient and economical. Upon immersion in water it was found that the thick ($\sim 5000 \text{ \AA}$) gold coated silver contacts peeled off whereas the main film ($\sim 200 \text{ \AA}$ thick) was not affected. The thin films of gold in this thickness range might,

therefore, be useful in accelerating the recovery of the victims of mercury poisoning [161].

6.4.4 Gold coated glass wool

Gold coated glass wool has been found effective in eliminating mercury from the reference arm of the bridge. It may also find other applications, for example, in

- (a) Sample collecting for monitoring elemental mercury pollution in the atmosphere,
- (b) Breathing masks for protecting personnel working in mercury mines or industries employing mercury, and
- (c) Eliminating mercury from the flue gases of coal burning plants. This particular application, admittedly, is exorbitant in cost. However, in the not so remote future, as the known reserves of mercury decline [155], this cost, to some extent may be offset by the recovery of mercury. This is notwithstanding the environmental benefits.

In any of the above applications, the mercury may be desorbed by heating at 175°C. The basic material is then reusable an indefinite number of times. One gram of gold yields about 5 m² of 100 Å thick adsorbing surface - without considering the increased area in films as compared to an ideally flat surface [161]. The high cost of initial investment may be justified on this ground also. Large scale units already exist for continuously coating surfaces (~ 10 ft x 14 ft) using electron beam evaporators [21].

CHAPTER VII

CONCLUSION AND SUGGESTIONS FOR FURTHER WORK

7.1 Conclusion

The following conclusions are made from results in this thesis:

The method of monitoring mass thickness has an overall accuracy of $\pm 3\%$ $\pm 0.25 \text{ \AA}$ for gold or platinum. Employing a 5 MHz AT ($\phi = 35^\circ 13' \pm 2'$) cut quartz crystal plate, a simple oscillator circuit with water cooled crystal mount gives a frequency stability within ± 2.5 Hz over a 12 hour period.

Microwave measurement of sheet resistivity is advantageous in that (1) the cleavage defects of the substrate surfaces do not affect the resistivity measurements, and (2) annealing studies can be made on the same films. The method is then particularly suitable for thin films deposited on mica sheets cleaved in ultra-high vacuum where examination of the surfaces for scratches etc., is not possible.

Thin films of gold, between 5 and 40 \AA thick and deposited on 3 to 10 \AA thick platinum nucleating layers on air-cleaved mica substrates, have been found highly conducting. Comparison with theoretical results showed that these films may be continuous with a maximum surface roughness parameter of $\sim 3 \text{ \AA}$. It has been possible to obtain such films of thicknesses below 50 \AA for the first time. Owing to the decreasing sticking coefficients for thinner films, the actual thickness of the thinnest Au-Pt film

($\sim 10.8 \text{ \AA}$) may be only a few monolayers. This suggests a Frank-van der Merwe type of growth mechanism, avoiding the agglomerate structure. The island formation is thus considerably inhibited, if not altogether eliminated.

The conclusion that the films may be continuous has been further supported by the annealing results. The films showed improved conductivity on annealing up to about 175°C ; the resistance increased on heating to an even higher temperature.

In application to mercury detection, it was found that the composite (Au-Pt or Au-Ag) films on glass, although highly conducting, displayed reduced sensitivity on aging and/or annealing. The phenomenon can be attributed to the desensitization of the film surface to mercury adhesion as a result of alloying.

In the case of pure gold films, optimum parameters can be obtained by:

- (1) Evaporating the films from an electron beam heated source to obtain better adhesion and avoid source contamination,
- (2) Maintaining the film thickness $\sim 100 \text{ \AA}$, and
- (3) Annealing the films at a temperature in the region of $\sim 175^{\circ}\text{C}$ for improving film structure and causing stress relief.

Upon saturation due to mercury adsorption, the films can be prepared for further use by heating at 175°C to evaporate mercury.

Gold films coated on glass wool remove elemental mercury contained in an airstream. With optimum parameters as above, gold

films coated on glass wool have application in the protection of personnel working in a mercury-laden atmosphere and the removal and recovery of mercury from air, as caused by fossil-fuel combustion.

Thin gold films on glass can also extract mercury from weak solutions of inorganic mercury compounds. A possible application is in the removal of mercury from the bloodstream of victims of mercury poisoning.

7.2 Suggestions for Further Work

A number of the phenomena observed warrant further investigation; some of these are suggested.

7.2.1 Work on ultra-thin films

In order to confirm the growth process of the films deposited on suitable nucleating layers, these must be deposited on ultra-high vacuum cleaved surfaces. Since the films are conducting both at d.c. and at microwave frequencies, in-situ d.c. measurements are possible. Also, in-situ determination of the sticking coefficient, the actual film thickness, and the film structure will help in further understanding the nucleation and growth mechanisms.

Some of the difficulties encountered in this work and their possible remedies are suggested below:

- (1) The pressure rise on commencing evaporation from an electron beam heated source will cause contamination of the ultra-high vacuum cleaved surfaces. Adequate

pumping speeds should, therefore, be provided. The ion pump, as an example, appeared incapable of handling a sudden rise in gas load.

- (2) It was extremely difficult to control the film thicknesses at small values ($\sim 10 \text{ \AA}$ or less) using the e-beam evaporator. To some extent a longer source-to-substrate distance will help; this would need a larger system than used in this work. Alternatively, predetermined quantities of wire may be flash-evaporated by Faraday's method.
- (3) The ion-effects in electron beam evaporation could be influencing the mechanism of film growth. Resistance heated sources cause contamination, and so Faraday's method of flash evaporation of wires could be investigated as an alternative in this regard.
- (4) Modern surface analysis techniques, including Auger-electron spectroscopy (A.E.S.), reflection electron diffraction (R.E.D.), soft X-ray emission spectroscopy, etc., can be used to study diffusion in thin films.
- (5) Theoretical models for the analysis of size effects on electrical conductivity need to be developed further for application to ultra-thin, composite films, especially to account for the individually varying electron mean-free paths.
- (6) Investigations need to be made to determine a critical nucleating layer thickness, ℓ_c , at which the structure of composite films attains optimum perfection. ℓ_c

will, in all probability, be different for various substrates. Hence, a correlation between λ_c and the surface and/or crystal binding energy will augment the studies of surface phenomena. Epitaxy can also be studied.

- (7) It may be possible to investigate other suitable nucleating materials which do not cause problems due to alloying. Some oxides (Al_2O_3 , Y_2O_3 , etc.) are specially promising.

7.2.2 Mercury detection experiments

- (1) Mercury detection sensitivity of the films is shown to be affected by (a) surface composition, (b) structure of the film, and (c) the stress pattern. An integrated system including A.E.S., R.E.D., and stress monitoring techniques may be built to determine the sticking coefficient of mercury and the manner in which it is affected by the above parameters. Since mercury amalgamates with all metals except platinum and certain steels, the results can, in turn, be applied to investigate the above parameters.
- (2) Further work is involved in developing a commercial, portable apparatus to monitor mercury and incorporate a warning system for excessive mercury pollution, particularly in air.
- (3) Development of a breathing apparatus to protect personnel working in a mercury laden atmosphere may

be undertaken. Finally,

- (4) A large amount of work involving the possible medical use of thin films will have to be undertaken to investigate a method of applying gold films on glass to the treatment of victims of mercury poisoning.

REFERENCES

1. R. Bunsen, "Vulkanische Exhalationen", J. Prakt. Chem., 56, 53 (1852).
2. W.R. Grove, "On the electro-chemical polarity of gases", Phil. Trans. Roy. Soc. London, 142, 87 (1852).
3. M. Faraday, "Experimental relations of gold (and other metals) to light", Phil. Trans. Roy. Soc. London, 147, 145 (1857).
4. R. Nahrwold, "Über Luftelectricität", Ann. Physik Chemie, 31, 448 (1887).
5. R. Pohl and D. Pringsheim, "Über einige lichtelektrische Beobachtungen an Al und Mg", Verhandl. Deut. Physik. Gesel., 14, 546 (1912).
6. I. Langmuir, "The vapour pressure of metallic tungsten", Phys. Rev. 2, 329 (1913).
7. - "The condensation and evaporation of gas molecules", Proc. Nat. Acad. Sci. U.S., 3, 141 (1917).
8. L. Holland, "The production, properties, and uses of thin films condensed in vacuo", Vacuum, 1, 23 (1951).
9. V. Vand, "A theory of irreversible electrical resistance changes of metallic films evaporated in vacuum", Proc. Phys. Soc. London, 55, 222 (1943).
10. J.J. Thomson, "On the theory of metallic conduction in thin metallic films", Proc. Cambridge Phil. Soc., 11, 120 (1901).
11. K. Fuchs, "The conductivity of thin metallic films according to the electron theory of metals", Proc. Cambridge Phil. Soc., 34, 100 (1938).
12. E.H. Sondheimer, "The mean free path of electrons in metals", Advan. Phys., 1, 1 (1952).
13. V. Halpern, "Electron transport in isotropic thin metal films", J. Phys. F: Metal Phys., 1, 608 (1971).
14. Y. Namba, "Resistivity and temperature coefficients of thin metal films with rough surfaces", Japan. J. Appl. Phys., 9, 1326 (1970).
15. L. Holland, "Current and future uses of vacuum deposition", Electronic Components, Aug. 1972, p. 761.

16. E.J. Gillham, J.S. Preston, and D.W. Williams, "Transparent, conducting films", *Phil. Mag.*, 46, 1051 (1955).
17. L. Holland and G. Siddal, "Heat reflecting windows using gold and bismuth oxide films", *Brit. J. Appl. Phys.*, 9, 113 (1958).
18. W.G. Egan, "Eye protection in radar field", *Elect. Engrg.*, 76, 126 (1957).
19. B.M. Schiffman, L. Young, and R.B. Larrick, "Thin film waveguide bolometers for multimode power measurements", *IEEE Trans. Microwave Theory Tech.*, MTT-12, 155 (1964).
20. G. Keinel and H. Walter, "Sputtering optical thin films on large surfaces", *Res./Dev.*, 24, 49 (1973).
21. A.D. Grubb, "Design and operation of a large scale semi-continuous electron beam evaporator", *J. Vac. Sci. & Technol.*, 10, 53 (1973).
22. S.F. Lin and W.F. Leonard, "Thermoelectric power of thin gold films", *J. Appl. Phys.*, 42, 3634 (1971).
23. A.B. Meinel and M.P. Meinel, "Physics looks at solar energy", *Physics Today*, 24, 44 (1972).
24. J.J. McNerney, P.R. Buseck, and R.C. Hansen, "Mercury detection using thin films of gold", *Science*, 173, 611 (1972).
25. H.K. Chaurasia, A. Huizinga, and W.A.G. Voss, "Optimum gold films for mercury detection", *J. Phys. D: Appl. Phys.*, to be published.
26. O.S. Heavens, Thin Film Physics, London: Mathuen 1970, pp. 2-3.
27. G.A. Somorjai, Structure and Chemistry of Solid Surfaces, New York: Wiley 1970.
28. D.W. Pashley, in Recent Progress in Surface Sciences, vol. 3, eds. J.F. Danielli, A.C. Riddiford, and M.D. Rosenberg, New York: Academic Press 1970, pp. 26-69.
29. P. Estrup, in Modern Diffraction and Imaging Techniques, eds. S. Amelinckx, R. Gerver, G. Remaut, and J. van Landuyt, Amsterdam: North Holland 1970, p. 377.
30. A.R. Moon, and J.M. Cowley, "Medium energy electron diffraction", *J. Vac. Sci. & Technol.*, 9, 649 (1972).
31. P. Auger, "Sur l'effet photoelectrique compose", *J. Phys. Radium*, 6, 205 (1925).

32. L.A. Harris, "Some observations of surface segregation by Auger electron emission", J. Appl. Phys., 39, 1428 (1969).
33. - "Analysis of materials by electron excited Auger electrons", J. Appl. Phys., 39, 1419 (1969).
34. - "Miscellaneous topics in Auger electron spectroscopy", J. Vac. Sci. & Technol., 11, 23 (1974).
35. J.F. Ziegler and J.E.E. Baglin, "Determination of surface impurity concentration profiles by nuclear backscattering", J. Appl. Phys., 42, 2031 (1971).
36. J.W. Mayer and K.N. Tu, "Analysis of thin film structure with nuclear backscattering and x-ray diffraction", J. Vac. Sci. & Technol., 11, 86 (1974).
37. H. Poppa, R.D. Moorhead, and K. Heinemann, "Experimental approaches to controlled studies on thin film nucleation and growth", Nucl. Instrum. Methods, 102, 521 (1972).
38. C.A. Neugebauer, "Structural disorder phenomena in thin metal films" in Physics of Thin Films, vol. 2, eds. G. Hass and R.E. Thun, New York: Academic Press 1964, pp. 1-62.
39. T.N. Rhodin, "Nucleation and growth on solid surfaces: theory and application" in The Use of Thin Films in Physical Investigations, ed. J.C. Anderson, London: Academic Press 1966, pp. 187-202.
40. J.P. Hirth and K.L. Muazed, "Nucleation processes in thin film formation" in Physics of Thin Films, vol. 4, eds. G. Hass and R.E. Thun, New York: Academic Press 1967, pp. 79-136.
41. B. Lewis and D.S. Campbell, "Nucleation and initial growth behaviour of thin film deposits", J. Vac. Sci. & Technol., 4, 209 (1967).
42. O.S. Heavens, "Growth and structure of films" in Thin Film Physics, London: Mathuen 1970, pp. 39-52.
43. H. Sato, "Film growth", Annual Rev. Materials Sci., 2, 217 (1972).
44. E. Bauer and H. Poppa, "Recent advances in epitaxy", Thin Solid Films, 12, 167-185 (1972).
45. F.C. Franck, "An outline of nucleation theory", J. Crystal Growth, 13/14, 154 (1972).

46. M.J. Stowell, "Thin film nucleation kinetics", *Phil. Mag.*, 26, 361 (1972).
47. R.A. Sigsbee, "Adatom capture and nuclei growth", *J. Crystal Growth*, 13/14, 135 (1972).
48. R.C. Sundahl, "Relationship between substrate surface chemistry and adhesion of thin films", *J. Vac. Sci. & Technol.*, 9, 181 (1972).
49. L.C.A. Stoop and J.H. Van der Merwe, "A simple model for layered growth in small epitaxial islands", *Thin Solid Films*, 17, 291 (1973).
50. D. Robertson, "Coalescence kinetics of migrating crystallites", *J. Appl. Phys.*, 44, 3924 (1973).
51. R.F. Adamsky, "Nucleation and growth of metal films" in The Use of Thin Films for Physical Investigation, ed. J.C. Anderson, London: Academic Press 1966, p. 256.
52. K.L. Chopra, Thin Film Phenomena, New York: McGraw Hill 1969, p. 173.
53. A.E. Ennos, "Highly conducting gold films prepared by vacuum evaporation", *Brit. J. Appl. Phys.*, 3, 359 (1957).
54. K.L. Chopra and L.C. Bobb, "Electrical conduction in epitaxially grown gold films" in Single Crystal Films, eds. M.H. Francombe and H. Sato, New York: Macmillan 1964, pp. 373-381.
55. R. Cornelly and N. Fuschillo, "Electrical conductivity, structure, and optical properties of r.f. sputtered Au films", *Bull. Am. Phys. Soc.*, 18, 16 (1973).
56. H.K. Chaurasia, "Studies on Thin Films of Gold", M.A.Sc. Thesis, Univ. of British Columbia, Vancouver, 1964.
57. C.A. Neugebauer and M.B. Webb, "Electrical conduction in ultrathin, evaporated metal films", *J. Appl. Phys.*, 33, 74 (1962).
58. T.E. Hartmann, "Electrical conduction in discontinuous thin metal films", *J. Appl. Phys.*, 34, 943 (1963).
59. N.B. Bashara, "A survey of conduction mechanism in very thin films", *IEEE Trans. Comp. Parts.*, CP-11, 4 (1964).
60. J.E. Morris, "Calculation of activation energy in discontinuous thin metal films", *J. Appl. Phys.*, 39, 6107 (1969).

61. B.R. Cooper, "Theory of electronic properties of ultra-thin films of transition and noble metals", *Bull. Am. Phys. Soc.*, 17, 257 (1972).
62. H.K. Chaurasia and W.A.G. Voss, "Ultra-thin conducting films of gold on platinum nucleating layers", *Nature*, 249, 28 (1974).
63. M.P. Lepselter, "Beam-lead technology", *Bell System Tech. J.* 45, 233 (1966).
64. W.B. Novak and R.N. Dyre, "Diffusion in thin film couples of platinum-gold", *J. Vac. Sci. & Technol.*, 9, 279 (1972).
65. H.E. Culver, H. Schilling, and R.E. Thun, "Advanced thin film metallurgy for beam leaded integrated circuits", *J. Vac. Sci. & Technol.*, 10, 170 (1973).
66. L. Holland, Vacuum Deposition of Thin Films, London: Chapman & Hall 1963, pp. 220-231.
67. K.H. Behrndt, "Film thickness and deposition rate monitoring devices and techniques for producing films of uniform thickness" in Physics of Thin Films, vol. 3, eds. G. Hass and R.E. Thun, New York: Academic Press 1966, pp. 1-59.
68. K.L. Chopra, Thin Film Phenomena, New York: McGraw Hill 1969, pp. 83-107.
69. W.A. Pliskin and S.J. Zanin, "Film thickness and composition" in Handbook of Thin Film Technology, eds. L.I. Maissel and R. Glang, New York: McGraw Hill 1970, pp. 11-1 to 11-34.
70. C. Greaves, "Film thickness measurement by monitoring methods", *Vacuum*, 20, 332 (1970).
71. S. Tolansky, Multiple Beam Interferometry, Oxford: Clarendon Press, 1948, pp. 8-73.
72. S. Tolansky, Surface Microtopography, London: Longmans 1960, pp. 62-68.
73. B.J. Stern, "Thin film thickness measurements using silver modified Newton's rings", *Rev. Sci. Instrum.*, 34, 874 (1963).
74. S. Tolansky, Microstructure of Surfaces Using Interferometry, New York: American Elsevier 1968, pp. 4-17.
75. H. Friedman and L.S. Birks, "Thickness measurement of thin films by x-ray absorption", *Rev. Sci. Instrum.*, 17, 874 (1946).

76. L.E. Preuss, "A study of the propagation mode for metal vapour in shado casting by vacuum evaporation of Au(198) and Cr(51)", J. Appl. Phys., 24, 1401 (1953).
77. T.N. Rhodin, "Oriental arrangement of thin aluminium films formed on ionic substrates", Disc. Faraday Soc., 5, 215 (1949).
78. R.W. Dudding, "Aluminium backed screens for cathode ray tubes", Britt. Instt. Radio Engrs., 11, 455 (1951).
79. G.Z. Saurbrey, "Use of quartz oscillators for weighing thin layers and microweighing", Z. Physik, 155, 206 (1959).
80. C.D. Stockbridge, "Resonance frequency versus mass added to quartz crystals", in Vacuum Microbalance Techniques, vol. 5, ed. K. Behrndt, New York: Plenum Press 1966, pp. 193-205.
81. A.W. Warner, "Microweighing with quartz crystal oscillator - theory and design" in Ultra Microweight Determination in Controlled Environment, eds. S.P. Wolsky and E.J. Zdanuk, New York: Interscience 1969, pp. 137-161.
82. N. Niedermayer and D. Hillecke, "Mass-thickness determination in ultra-high vacuum", *ibid*, pp. 260-266.
83. D.R. Denison, "Linearity of a heavily loaded quartz crystal microbalance", J. Vac. Sci. & Technol., 10, 126 (1973).
84. C. Lu, "Improving the accuracy of quartz crystal monitors", Res./Dev., 25(3), 45 (March 1974).
85. J.C. Slater, Microwave Electronics, Princeton N.J.: Van Nostrand 1950, pp. 34-35.
86. H.K. Chaurasia and W.A.G. Voss, "Resistivity of thin metal films", IEEE Trans. Microwave Theory Tech., MTT-21, 51 (1973).
87. F.W. Karasek and R.J. Laub, "Limits of Detection", Res./Dev., 25, 36 (June 1974).
88. A. Huizinga, H.K. Chaurasia, and W.A.G. Voss; U.S. patent application No. 490,322 dated July 22, 1974.
89. E.B. Graper, "Distribution and apparent source geometry of electron beam heated evaporation sources", J. Vac. Sci. & Technol., 10, 100 (1973).

90. S. Komiza, T. Narusawa, and C. Hagashi, "Effect of gold coating on sorption characteristics of CO, sulphur, and other gases on stainless steel", *J. Vac. Sci. & Technol.*, 9, 302 (1972).
91. L. Holland, Vacuum Deposition of Thin Films, London: Chapman & Hall 1963, p. 145.
92. H. Poppa, K. Heinemann, and A.G. Elliot, "Epitaxial orientation studies of gold on ultra-high vacuum cleaved mica during early stages of nucleation and growth", *J. Vac. Sci. & Technol.*, 8, 471 (1971).
93. J.J. Gilman, "Deformation and fracture of ionic crystals" in Progress in Ceramic Science, vol. 1, ed. J.E. Burke, New York: Pergamon 1961, p. 145.
94. L.I. Meissel, "Electrical properties of metallic thin films", in Handbook of Thin Film Technology, eds. L.I. Meissel and R. Glang, New York: McGraw Hill 1970, p. 13-7.
95. H. Poppa and A.G. Elliot, "The surface composition of mica substrates", *Surface Sci.*, 24, 149 (1971).
96. K.L. Chopra, Thin Film Phenomena, New York: McGraw Hill 1969, pp. 62-63.
97. D.I. Gaffee, "The layout of microcircuits, masking and etching techniques" in Thin Film Microelectronics, ed. L. Holland, New York: Wiley 1965, pp. 276-277.
98. E.B. Graper, "Charge flux generated by an electron beam deposition source", *J. Vac. Sci. & Technol.*, 7, 282 (1970).
99. W.R. Chase and E.L. King, "Self induced sputtering in electron beam evaporation of Ta", *J. Appl. Phys.*, 42, 5856 (1971).
100. F.L. Schuermeyer, W.R. Chase and E.L. King, "Ion effects during electron beam deposition of metals", *J. Vac. Sci. & Technol.*, 9, 330 (1972).
101. D. Hoffman and D. Leibowitz, "Effect of substrate potential on Al₂O₃ films prepared by electron beam evaporation", ibid, p. 326.
102. K.L. Chopra, Thin Film Phenomena, New York: McGraw Hill 1969, p. 53.
103. H.S. Story and R.W. Hoffman, "Stress annealing in vacuum deposited copper films", *Proc. Phys. Soc. London*, B-70, 950 (1957).

104. IRE Standards on Piezoelectric Crystals, 49 IRE 14.51, Proc. IRE, 37, 1379 (1949)
105. W.P. Mason, Piezoelectric Crystals and Their Application in Ultrasonics, New York: Van Nostrand 1950, pp. 78-113.
106. D. King and G.R. Hoffman, "Observations on a quartz crystal monitor", J. Phys. E: Scientific Instruments, 4, 993 (1971).
107. H.L. Eschbach and E.W. Kruidhof, "A direct calibration method for a crystal oscillator film thickness monitor" in Vacuum Microbalance Techniques, vol. 5, ed. K. Behrndt, New York: Plenum Press 1966, pp. 207-216.
108. J.J. Nagle, "Crystal stabilized tunnel diode oscillators", Electronics, 34(35), 40 (1 Sept. 1961).
109. W.F. Chow, Principles of Tunnel Diode Circuits, New York: Wiley 1964, pp. 163-172.
110. K.K. Clarke and D.T. Hess, Communication Circuits: Analysis and Design, New York: Addison Wesley 1971, pp. 262-267.
111. C.D. Stockbridge and A.W. Warner, "A vacuum system for mass and thermal measurements with resonating crystalline quartz" in Vacuum Microbalance Techniques, vol. 2, ed. R.F. Walker, New York: Plenum Press 1962, pp. 93-113.
112. M.S. Blois, Jr., and C.M. Riesser, Jr., "Apparent density of evaporated thin films", J. Appl. Phys., 25, 338 (1954).
113. A.R. Walter, "Measurement of metallic film densities by an optical technique", J. Appl. Phys., 36, 2377 (1965).
114. T.E. Hartman, "Density of thin evaporated aluminum films", J. Vac. Sci. & Technol., 2, 239 (1965).
115. J. Edgecumbe, "Thin film densities", J. Vac. Sci. & Technol., 3, 28 (1966).
116. S. Chandra and G.D. Scott, "Condensation coefficients of silver, gold and copper in vacuum", Canad. J. Phys., 36, 1148 (1958).
117. D.E. Clark, "The resistivity of thin metallic films", Brit. J. Appl. Phys. 6, 158 (1955).

118. K.J. Champlin, J.D. Holm, and G.H. Glover, "Electrodeless determination of semiconductor conductivity from TE_{01}^0 -mode reflectivity", J. Appl. Phys. 38, 96 (1967).
119. R.L. Ramey and T.S. Lewis, "Properties of thin metal films at microwave frequencies", J. Appl. Phys. 39, 1147-1152 (1968).
120. H.H. Wieder, Intermetallic Semiconductor Films, London: Pergamon 1970, pp. 180-187.
121. R.H. Havemann and L.E. Davis, "Conductivity and the microwave properties of 81-permalloy thin films", IEEE Trans. Microwave Theory Tech., (Corresp.), MTT-19, 113-116 (1971).
122. T. Moreno, Microwave Transmission Design Data, New York: Dover 1958, p. 170.
123. Microwave Measurements for Calibration Laboratories, Hewlett-Packard Application Note 38, Section 4, p. 11, 1962.
124. W.A. Ament, "Toward a theory of reflection by a rough surface", Proc. IRE, 41, pp. 142-146 (1953).
125. R.L. Ramey, H.S. Landes, and E.A. Manus, "Microwave properties of thin films with apertures", IEEE Trans. Microwave Theory Tech., MTT-18(4), pp. 196-204 (1970).
126. R.E. Collin, Foundations for Microwave Engineering, New York: McGraw Hill, 1966, pp. 218-220.
127. E.M. Hörl and K.H. Rieder, "Diffusion of metals in thin metal films", J. Vac. Sci. & Technol., 9, 276-278 (1972).
128. R.C. Chambers, "Transport properties: surface and size effects" in The Physics of Metals 1. Electronics, ed. J.M. Ziman, Cambridge, U.K: Cambridge Univ. Press 1969, pp. 175-249.
129. D. Schoenberg, "Electronic structure: the experimental results", ibid., p. 83.
130. A. Heiman and V. Halpern, "A calculation of the electrical conductivity of thin films of potassium and sodium", J. Phys. F: Metal Phys., 4, 107 (1974).
131. C.A. Neugebauer, "Electrical resistivity of ultra-thin metal films" in AVS Trans. 9th Vacuum Symposium, ed. G.C. Bancroft, New York: McMillan 1962, pp. 45-51.

132. C. Weaver, "Diffusion in metallic films" in Physics of Thin Films, vol. 6, eds. M.H. Francombe and R.W. Hoffman, New York: Academic Press 1971, pp. 301-347.
133. A.K. Sinha, T.E. Smith, and T.T. Sheng, "Thin film diffusion of platinum in gold", Thin Solid Films, 22, 1 (1974).
134. M. Hansen, Constitution of Binary Alloys, Second Edition, New York: McGraw Hill 1958, pp. 226-229.
135. R.E. Elliot, Constitution of Binary Alloys, First Supplement, New York: McGraw Hill 1965, p. 98.
136. F.A. Shunk, Constitution of Binary Alloys, Second Supplement, New York: McGraw Hill 1969, p. 77.
137. K.L. Chopra, Thin Film Phenomena, New York: McGraw Hill 1969, p. 353.
138. J.R. Putman, "Quick silver and slow death", National Geographic, vol. 142, no. 4, 507-527 (Oct. 1972).
139. J. Vostal, "Transport and transformation of mercury in nature and possible routes of exposure" in Mercury in the Environment, an Epidemiological and Toxicological Appraisal, eds. L. Friberg and J. Vostal, Cleveland, Ohio: C.R.C. Press 1972, pp. 15-27.
140. G.M. Glidden, "Recovery and filtering apparatus and method", U.S. Patent No. 2,785,767 (March 19, 1957).
141. A.M. Fraser, K.I. Melville, and R.L. Stehle, "Mercury laden air: the toxic concentration, the proportion absorbed, and the urinary excretion", J. Industr. Health, 16, 77 (1934).
142. L. Friberg and G.F. Norberg, "Inorganic mercury - relation between exposure and effects" in Mercury in the Environment, an Epidemiological and Toxicological Appraisal, eds. L. Friberg and J. Vostal, Cleveland, Ohio: C.R.C. Press 1972, pp. 113-139.
143. T. Takeuchi, "A pathological study of Minamata disease in Japan", Proc. III Intern. Conf. Neurol., Rome 1961, p. 1.
144. M. Saito, T. Osono, J. Watanabe, T. Yamamoto, M. Takeuchi, Y. Ohyagi, and H. Katsunuma, "Studies on Minamata disease, establishment of criterion of etiological research in mice", Jap. J. Exp. Med., 31, 277 (1961).
145. S. Jensen and A. Jernelov, "Biological methylation of mercury in aquatic organisms", Nature, 223, 753 (1969).

146. A. Jernelöv, "Conversion of mercury compounds" in Chemical Fallout. Current Research on Persistent Pesticides, eds. M.W. Miller and G.G. Berg, Springfield, Ill: C.C. Thomas 1969, p. 68.
147. N. Fimreite, "Mercury uses in Canada and their possible hazards as sources of mercury contamination", Environ. Pollut., 1, 119 (1970).
148. M.A. Benarde, Our Precarious Habitat, New York: W.W. Norton 1973, p. 81.
149. L.J. Goldwater, "Mercury in the environment", Scientific American, 224(5), 15 (May 1971).
150. H.V. Weiss, M. Koide, and E.D. Goldberg, "Mercury in a Greenland ice sheet: Evidence of recent input by man", Science, 174, 692 (1971).
151. O.I. Joensuu, "Fossil fuels as a source of mercury pollution", Science, 172, 1027 (4 June 1971).
152. C.E. Billings and W.R. Matson, "Mercury emission from coal combustion", Science, 176, 1232 (16 June 1972).
153. N. Berkowitz, "An energy blueprint for the '70s", Reader's Digest p. 31 (June 1974).
154. K.J. Constable, "Alberta Coal Resources: Economic Relations and Problems" dissertation, Faculty of Bus. Admin. and Commerce, The Univ. of Alberta, Edmonton, Jan. 1974.
155. K. Dunham, "How long will our minerals last", New Scientist, p. 129 (17 Jan. 1974).
156. G. Lindstedt and S. Skerfving, "Methods of analysis" in Mercury in the Environment, an Epidemiological and Toxicological Appraisal, eds. L. Friberg and J. Vostal, Cleveland, Ohio: C.R.C. Press 1972, pp. 3-13.
157. J.K. Hirnovern, W.H. Weisenberger, J.E. Westmoreland, and R.A. Meussner, "Backscattering investigation of low temperature migration of chromium through gold", J. Appl. Phys. Lett., 21, 37-39 (1972).
158. R.W. Joyner and M.W. Roberts, "Auger electron spectroscopy studies of clean polycrystalline gold and the adsorption of mercury on gold", J. Chem. Soc. Faraday Trans. I, 69, 1242-1250 (1973).
159. B. DeLaughter, "Mercury determination in industrial plant atmosphere by atomic absorption spectroscopy", Atomic Abs. Newslett., 9, 49 (1970).

160. F.M. d'Heurle and R. Rosenberg, "Electromigration in thin films" in Physics of Thin Films, vol. 7, eds. G. Hass, M.H. Francombe, and R.W. Hoffman, New York: Academic Press 1973, pp. 257-310.
161. Dr. H.D. Baillie, Crumpsall Hospital, Machester, U.K., private communication.
162. H. Peterson and W.K. Chen, "Mass transport in solids" in Annual Review of Materials Science, vol. 3, eds. R.H. Huggins, R.H. Bule, and R.W. Roberts; Palo Alto: Annual Reviews Inc., 1973, pp. 75-109.
163. D. Gupta, "Grain boundary self-diffusion in evaporated Au films at low temperatures", Thin Solid Films, 22, 121 (1974).
164. M. Hansen, Constitution of Binary Alloys, New York: McGraw Hill 1958, p. 227.
165. S. Thomas, "Surface enrichment of In in evaporated Au-In films", Appl. Phys. Lett., 24, 1 (1974).
166. R.E. Schlier and H.E. Farnsworth, "Low energy electron diffraction studies on oxygen adsorption and oxide formation on a (100) face of nickel cleaned under high vacuum condition", Advances in Catalysis IX, 434 (1957).
167. J. Bardeen, "Electrical conductivity of metals", J. Appl. Phys., 11, 88 (1939).
168. L.A. Maissel, "Electrical properties of metallic thin films" in Handbook of Thin Film Technology, eds. L.A. Maissel and R. Glang, New York: McGraw Hill 1970, pp. 13-1,2.
169. A. Kinbara and H. Hakari, "Internal stress of evaporated thin gold films", Jap. J. Appl. Phys., 4, 243 (1965).
170. P. Chaudhary, "Grain growth and stress relief in thin films", J. Vac. Sci. & Technol., 9, 520 (1972).
171. J.R. White, "Annealing behaviour of thin evaporated gold films", Thin Solid Films, 22, 23 (1974).
172. K.L. Chopra, Thin Film Phenomena, New York: McGraw Hill 1969, p. 311.
173. R.W. Hoffman, "The mechanical properties of thin films" in The Use of Thin Films for Physical Investigations, ed. J.C. Anderson, London: Academic Press 1966, pp. 261-280.

174. E. Klokholm and B.S. Berry, "Intrinsic stress in evaporated metal films", J. Electrochem. Soc., 115, 823 (1968).
175. K. Kinoshita, "Recent developments in the mechanical properties of thin films", Thin Solid Films, 12, 17 (1972).
176. K.L. Chopra, Thin Film Phenomena, New York: McGraw Hill 1969, p. 185.

B30102